AD-A131 291 CW (CONTINUOUS WAVE) ANTENNA DESIGN AND TESTING(U) IRT 1/2
CORP SAN DIEGO CA T BUCKMAN ET AL. 01 AUG 82 DNA-6188F
DNA001-79-C-0210

UNCLASSIFIED F/G 9/5 NL

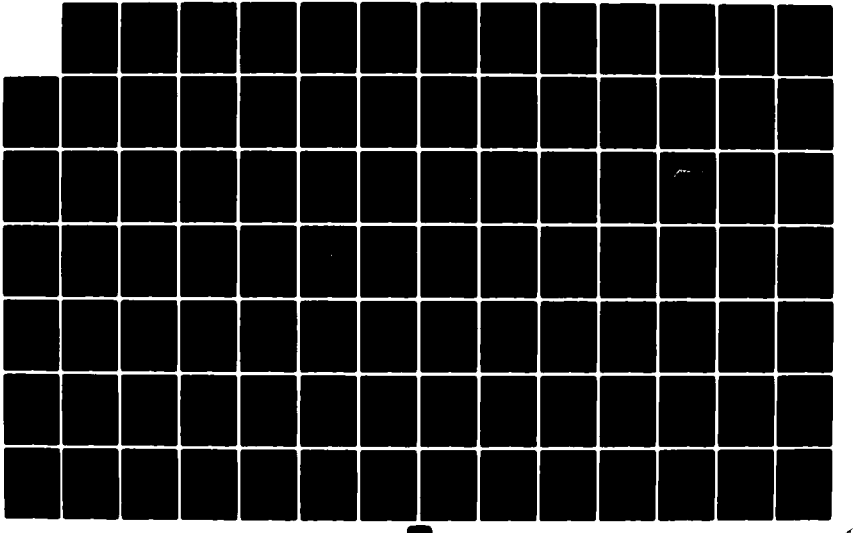

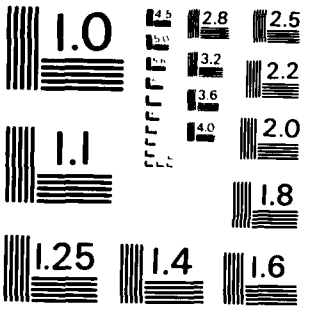


MICROCOPY RESOLUTION TEST CHART
NATIONAL BUREAU OF STANDARDS - 1963 - A

(12)

DNA 6188

AD A131291

# CW ANTENNA DESIGN AND TESTING

IRT Corporation
P.O. Box 80817
San Diego, California 92138

1 August 1982

Final Report for Period 15 January 1979—1 August 1982

CONTRACT No. DNA 001-79-C-0210

APPROVED FOR PUBLIC RELEASE;
DISTRIBUTION UNLIMITED.

THIS WORK WAS SPONSORED BY THE DEFENSE NUCLEAR AGENCY
UNDER RDT&E RMSS CODE B363079462 G52AAXEX40402 H2590D.

DTIC FILE COPY

Prepared for
Director
DEFENSE NUCLEAR AGENCY
Washington, DC 20305

DTIC
ELECTE
AUG 11 1983
S
B

83 08 3 089

Destroy this report when it is no longer needed. Do not return to sender.

PLEASE NOTIFY THE DEFENSE NUCLEAR AGENCY, ATTN: STTI, WASHINGTON, D.C. 20305, IF YOUR ADDRESS IS INCORRECT, IF YOU WISH TO BE DELETED FROM THE DISTRIBUTION LIST, OR IF THE ADDRESSEE IS NO LONGER EMPLOYED BY YOUR ORGANIZATION.

UNCLASSIFIED

SECURITY CLASSIFICATION OF THIS PAGE (When Data Entered)

| REPORT DOCUMENTATION PAGE | | READ INSTRUCTIONS BEFORE COMPLETING FORM |
|---|---|---|
| 1. REPORT NUMBER<br>DNA 6188F | 2. GOVT ACCESSION NO.<br>AD A131291 | 3. RECIPIENT'S CATALOG NUMBER |
| 4. TITLE (and Subtitle)<br>CW ANTENNA DESIGN AND TESTING | | 5. TYPE OF REPORT & PERIOD COVERED<br>Final Report for Period<br>15 Jan 79—1 Aug 82 |
| | | 6. PERFORMING ORG. REPORT NUMBER |
| 7. AUTHOR(s)<br>T. Buckman<br>R. W. Stewart | | 8. CONTRACT OR GRANT NUMBER(s)<br>DNA 001-79-C-0210 |
| 9. PERFORMING ORGANIZATION NAME AND ADDRESS<br>IRT Corporation<br>P.O. Box 80817<br>San Diego, California 92138 | | 10. PROGRAM ELEMENT, PROJECT, TASK AREA & WORK UNIT NUMBERS<br>Subtask G52AAXEX404-02 |
| 11. CONTROLLING OFFICE NAME AND ADDRESS<br>Director<br>Defense Nuclear Agency<br>Washington, DC 20305 | | 12. REPORT DATE<br>1 August 1982<br>13. NUMBER OF PAGES<br>102 |
| 14. MONITORING AGENCY NAME & ADDRESS(if different from Controlling Office) | | 15. SECURITY CLASS (of this report)<br>UNCLASSIFIED<br>15a. DECLASSIFICATION/DOWNGRADING SCHEDULE<br>N/A since Unclassified |

16. DISTRIBUTION STATEMENT (of this Report)

Approved for public release; distribution unlimited.

17. DISTRIBUTION STATEMENT (of the abstract entered in Block 20, if different from Report)

18. SUPPLEMENTARY NOTES

This work was sponsored by the Defense Nuclear Agency under RDT&E RMSS Code B363079462 G52AAXEX40402 H2590D.

19. KEY WORDS (Continue on reverse side if necessary and identify by block number)

| | |
|---|---|
| EMP | Antenna Design |
| Field Mapping | CW Testing |

20. ABSTRACT (Continue on reverse side if necessary and identify by block number)

This report presents details of the development of HEMP relatable portable antenna for use with the existing DNA CW system.

The rationale leading to the choice of a dielectric pre-stressed support tower and wire cage structure for the antenna arms is presented.

Calculations of the antenna electromagnetic and mechanical performance

DD FORM 1 JAN 73 1473 EDITION OF 1 NOV 65 IS OBSOLETE

UNCLASSIFIED

SECURITY CLASSIFICATION OF THIS PAGE (When Data Entered)

20. ABSTRACT (Continued)

parameters are given and confirmed by the presentation of preliminary measured operating data.

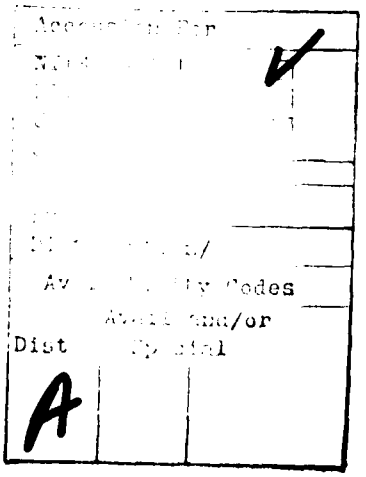


## TABLE OF CONTENTS

## LIST OF ILLUSTRATIONS

## LIST OF ILLUSTRATIONS (Cont'd)

## LIST OF ILLUSTRATIONS (Cont'd)

# 1. INTRODUCTION

## 1.1 BACKGROUND

This document records the process involved in designing and producing a new antenna for the DNA Continuous Wave (CW) measurement system. This process was closely linked with several DNA programs, the most notable being the test program conducted at the Naval Communications Area Master Station Eastern in Pacific (NAVCAMS EASTPAC) on the island of Oahu, Hawaii.

The NAVCAMS EASTPAC test provided a considerable amount of information that had a direct bearing on the antenna design and in some ways was responsible for the antenna development program itself.

The NAVCAMS test includes CW response measurements made on the communications facility. Measurements were made with two types of antennas. The first was a portable top-loaded monopole which produced dominate vertical E fields; the second was the TEMPS antenna modified for CW drive which produced a dominate horizontal E field. Initial calculations made with data from both antennas showed a larger difference in the predicted values of the induced responses than had been initially estimated. This finding lead to a commitment on DNA's part to develop a highly portable CW antenna system that produced a dominate horizontal E field. This commitment was part of a larger program to upgrade the existing DNA CW system.

In addition to the above data, the NAVCAMS EASTPAC program also produced limited field map data on a third antenna. This antenna represented a prototype design to meet the requirement of a portable CW antenna with a dominate horizontal E field. This data proved to be important in evaluating candidate designs and, as it turned out, also provided design data since that basic design was the one finally selected for construction.

## 1.2 DOCUMENT OVERVIEW

The remainder of the document is divided into three sections and an appendix.

The first section, Program Specifications, discusses the objectives and constraints associated with the antenna development program. The objectives specify the desired characteristics for the antenna while the constraints represent characteristics that the antenna required to make it compatible with operation requirements. The next section, titled Specification of the Design, explains the procedure followed in arriving at the final design. The final section, Antenna Checkout, discusses the initial field test with the new antenna. Various measurements were made during this test to confirm predicted behavior. In addition, parametric studies were done to gather data for finalizing the antenna design. The Appendix contains antenna drawings and design specifications and the results of a structural analysis done on the dielectric support structure used with the CW antenna.

# 2. PROGRAM SPECIFICATIONS

## 2.1 INTRODUCTION

The following section discusses the design objectives and the design constraints that guided the DNA CW antenna development program. The discussion in this section is divided into two main parts: design objectives and design constraints, with each part considering the electromagnetic and mechanical aspect of the topic.

From an electromagnetic standpoint, the primary objective was to produce a HEMP relatable simulator, specifically designed for application to ground-based $C^3$ facilities. From a mechanical perspective, the primary objective was to produce a highly portable antenna system that could be easily assembled and erected by three men in a few hours.

## 2.2 DESIGN OBJECTIVES

### 2.2.1 Electromagnetic Objectives

The prime objective of the antenna development program was to produce a HEMP relatable simulator. Due to constraints of time and cost, the design was to be selected from generic designs available at that time. The antenna was to be energized by a CW source and produce fields with a dominate horizontal E field component. If the form of the final design permitted, the antenna design was to include provisions to change the field characteristics of the antenna to produce fields with a dominate vertical E field relative to a test object.

The only other objective specified for the program was one relating to the interface between the antenna and the CW system output power amplifier. The antenna design process was to include the design of the antenna feed. The object of this design was to allow the antenna to be fed from an unbalanced source. The ability to feed the antenna from an unbalanced source greatly simplifies the use of the entire CW system in normal field operations.

### 2.2.2 Mechanical Objectives

As the introduction to the document stated, the motivating force behind the antenna development program was the desire to create a horizontal "polarized" antenna system which was much more portable than any antenna in the DNA inventory at that time. This objective resulted in the formulation of the following requirements. The design of the antenna was to include the design of all supporting structures and rigging. The entire antenna plus support structure and rigging was to weigh less than 450 lbs. The maximum length of any single component of antenna or antenna support structure, when disassembled and made ready for shipping, was to be no greater than 10 feet. The antenna system was to be designed so that it could be assembled and erected or lowered and disassembled by three men, in four hours, using only hand tools and small power tools. Finally, the design was to be either small enough or flexible enough to adapt to the demands of local geography and site configuration.

Thus, even though the prime objective of the program was to build an EMP simulator antenna suitable for application to ground-based $C^3$ facilities, it was a prime objective that had to meet the simultaneous demands of weight, transportability and ease of erection.

## 2.3 DESIGN CONSTRAINTS

In formulation of the program specifications, it was necessary to put constraints on the methods used to meet the design objectives. These constraints were necessary in order to achieve certain operational capabilities established for the new CW system. These operational requirements were primarily developed from consideration of operational costs.

The program emphasis on portability and ease of erection was an outgrowth of a broader emphasis on reducing the overall cost of testing. A key part of reducing these costs is minimizing the impact of the test system on the daily operation of the test facility as well as minimizing its impact on the environment. For example, if the antenna system requires a large amount of dedicated real estate for its use, it drives up labor cost significantly due to such things as negotations for use of the land and cost of returning the land to its original configuration after the test. The less impact the test system has on the operations of the facility under test and on the daily activities of people living or working in the immediate vicinity of the facility, the less coordination is required in arranging the tests and in arranging for the reconfiguration of the test site.

### 2.3.1 Electromagnetic Constraints

From an electromagnetic point of view, the primary constraint on the design of the antenna system arose out of a decision to operate the antenna in close physical proximity to the system under test.

This decision to operate in the near field of the antenna was made in order to enhance the site compatability of the CW system. If, for example, the antenna designed required separation between test site and antenna of several hundred feet or more, this would, in most cases, put the antenna on property that is not under control of the site being tested and may or may not be available for use during a test. In addition, such separations will often result in other structures being located between the antenna and the test object, creating an undesirable shadowing effect on the antenna fields. The only other choice for achieving large physical separation between antenna and test object would require support from an airborne vehicle which automatically requires a level of support and sophistication that is incompatible with the operational concept laid out for the CW system.

The decision to operate the antenna in close physical proximity to the system under test proved to be the key decision in the antenna development program. It, more than any other single requirement, was the deciding factor in selecting the final design.

### 2.3.2 Mechanical Constraints

The primary constraints on the mechanical aspect of the antenna design arose from the goal of minimizing the environmental impact of the antenna system on the test site and from a need to build an antenna system that could withstand wind loadings of 80 kmph (50 mph) or better. The severity of these constraints could not be assessed until the antenna design itself was selected. The antennas that one might look at for this application vary over a considerable range of sizes, as well as having sail areas that vary widely. Some designs provide a degree of structural self-support while others do not. As an example of how these factors impact system design, some antenna designs present structural loading in a 80 kmph (50 mph) wind that require a concrete footing or a partially buried post for the antenna support structure. The impact of such needs on the test site environment is an undesirable penalty on a system with the operational requirements of the CW system. The actual impact of these constraints will be assessed in Section 3.3 after a more definite idea of the antenna design has been formulated.

# 3. SPECIFICATION OF THE DESIGN

## 3.1 INTRODUCTION

The previous section listed the objectives and constraints from which design specifications were developed. This section goes on to explain how these specifications determined the details of the final antenna system design.

The section begins with electromagnetic considerations, which is in keeping with the actual process used to select the antenna design. The selection process began by reviewing existing classes of EMP simulators and selecting those classes which were suitable for the task at hand. The result of this screening lead to the selection of hybrid and dipole classes of simulators for further study. Further consideration of operational requirements lead to the selection of two representative designs, one in each area, which were further evaluated. The final outcome of this process was the choice of a hybrid class simulator.

The choice of a large antenna structure, like a hybrid class simulator, made meeting the mechanical requirements fairly difficult. This leads to the next subsection and the next step in the design process, Mechanical Considerations.

The subsection on mechanical considerations outlines the rationale used in selecting the final mechanical configuration for the antenna design. The final subsection, The Final Design, in conjunction with Appendix A, gives a concise description of the design that was finally fabricated and put into use with the DNA CW measurement system.

## 3.2 ELECTROMAGNETIC CONSIDERATIONS

A useful review of classes of EMP simulators is found in Sensor and Simulation Note 240, "EMP Simulators for Various Types of Nuclear EMP Environments: An Interim Categorization." This paper was one of the key articles reviewed in performing an initial review of EMP simulators.

### 3.2.1 PxM Antenna

The first simulator class that qualified for limited consideration was the dipole simulator class. This class of simulator which is basically a dipole is useful for EMP simulation in cases where the simulator is to be far from the system under test compared to the size of the dipole structure. In view of the constraint of operating the antenna in close physical proximity to the test object, this would imply that the antenna itself should be quite small physically. In view of this requirement, the only antenna type out of the dipole class that would be suitable is the PxM type antenna.

The PxM antenna, unlike most other "radiating" antennas, can produce fields which are transverse electric and magnetic (TEM) at all frequencies for which the dipole moments give the only significant contribution to the fields at the test object. This feature makes the antenna almost ideal for applications where one is trying to simulate HEMP and operate in close proximity to the test object. The dimensions of the antenna are also required to be small with respect to a wavelength in order to have the dipole moments dominate the field. Since the highest frequency of interest is 100 MHz, and one would like to operate at 20 or 25 meters from the test object, this implies that the antenna would have to have a maximum linear dimension on the order of two meters or less.

The small physical size required for the PxM has many advantages, but is also the source of the major disadvantage of the PxM. Due to the small size of the PxM in this application, it is difficult to achieve reasonable field levels at low frequencies at distances which are large with respect to the simulator dimensions. In addition, since the field levels at low frequencies are dominated by the $1/r^3$ dipole term, the fields fall off very rapidly as a function of distance leading to nonuniform illumination of the test object. The following table shows how the amplitude of the various terms in a dipole field falls off as a function of distance. It is assumed that the simulation volume is 80 meters deep and the distances on the left hand side of the table is the distance of the dipole from the front of the simulation volume.

As one can see from Table 3.1, the fields fall off very rapidly from the front to the back side of the simulation volume when operating a dipole antenna in close proximity to the simulation volume. This is especially true for the $1/r^3$ component which is the one that dominates at low frequencies. It will be seen in 3.2.2, when hybrid simulators are considered, that this problem is not as severe for this antenna class due to the relatively large physical size of the antenna with regard to the size of the simulation volume.

**Table 3.1. The Attenuation of Dipole Field Components Across A Simulation Area 80 Meters Wide, As A Function of Dipole Distance From Side of Simulation Area**

| Distance (meters) | $1/r$ | $1/r^2$ | $1/r^3$ |
|---|---|---|---|
| 20 | 14 | 28 | 42 |
| 40 | 9 | 18 | 27 |
| 60 | 7 | 14 | 21 |
| 80 | 6 | 12 | 18 |
| 100 | 5 | 10 | 15 |
| 200 | 3 | 6 | 9 |
| 300 | 2 | 4 | 6 |

The values given in Table 3.1 are valid for a dipole located in free space, but not for a PxM located over a ground plane. In order to estimate the magnitude of such variations across a simulation volume, additional calculations are necessary. The details of these calculations are presented in Appendix C and only the results of those efforts are presented here.

The calculations made in Appendix C assume an antenna with maximum linear dimensions of 2 meters located at a height of h meters above an ideal ground plane. Note that it is possible to build a PxM using a ground plane as part of the antenna structure, however, one can only obtain vertically polarized fields using this approach while the requirements specify horizontally polarized fields.

The calculations assumed that the PxM was oriented to produce horizontally polarized fields along the TEM axis, and the axis was oriented so that it intersected the ground plane in the center of the simulation area (Figure 3.1).

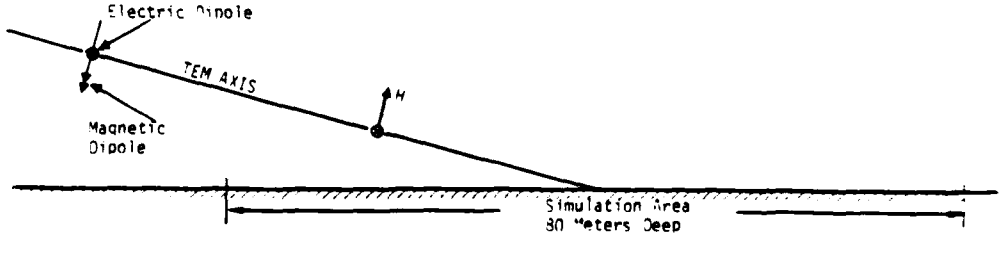


**Figure 3.1. Orientation of PxM antenna to simulation volume**

The calculations were broken into low frequency and high frequency approximations with only the H field on the surface of the ground plane being computed. The amplitude variation of this quantity provides sufficient insight into the antenna propertities to decide if more detailed calculations are called for. The results of calculations for a PxM antenna located over an ideal ground plane are shown in Figure 3.2. Note that only $H_x$ was calculated, since this would be the only field component present on the surface of the conductor from an incident horizontally-polarized planewave with a direction of propagation in the x-y plane. For the plane wave case, the amplitude of $H_x$ would be constant throughout the simulation area yielding a 0 dB variation in amplitude. Thus, the numbers given in Figure 3.2 indicate directly the amplitude variation between the PxM and the analogous plane wave case.

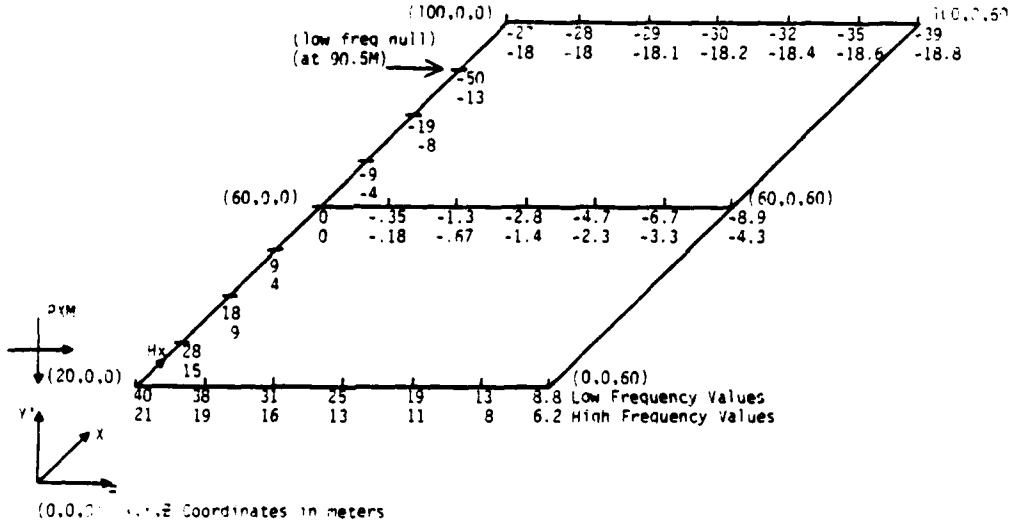


**Figure 3.2. Magnitude of $H_x$ field component in dB relative to $H_x$ at (60,0,0) for the low frequency and high frequency approximations. The antenna is located at (0,10,0) in this example.**

The amplitude variations shown in Figure 3.2 are too large to make the antenna useful as an EMP simulator for simulation areas of the dimensions shown. The only method available for reducing these amplitude variations is to move the antenna away from the simulation volume. Table 3.2 shows the effect of varying the distance from, and the height above the simulation area. The table indicates that this variation can be reduced considerably by moving the antenna to a location 100 meters from the simulation area, however further reductions come much more slowly after that.

**Table 3.2. Low Frequency Amplitude Variation in $H_x$ Field Component From Front to Back of Simulation Area 80 Meters Deep**

| Distances (meters) | Height Above (meters) | Low Frequency Variation In Amplitude From Front to Back Simulation Volume (dB) |
|---|---|---|
| 20/100 | 10.0 | 67.0 |
| 20/100 | 25.5 | 55.0 |
| 100/180 | 23.0 | 30.7 |
| 100/180 | 59.5 | 26.2 |
| 200/280 | 40.0 | 17.2 |
| 200/280 | 102.0 | 14.9 |
| 300/380 | 56.7 | 12.0 |
| 300/380 | 144.0 | 10.5 |

Another matter which must be taken into consideration when using this or any other antenna is the field levels that can be achieved with a given power source. Ultimately, these fields must induce signals large enough to be detected by the receiver instrumentation. As an aid in addressing these matters, the magnitude of the incident E field and the total H field at the center of the simulation area was calculated assuming a 500 watt power amplifier for the power source. (This power amplifier size is the size of the unit used with the CW system.) The details of these calculations are given in Appendix C; the key results are displayed in Table 3.3.

The numbers shown in Table 3.3 will become more meaningful in Subsection 3.4 when a comparison between these values and representative hybrid simulator numbers will be made. However as a general observation, one can note that the low to high frequency variation in field levels is very large (at least 90 dB). This large a variation can generate a problem in terms of keeping the received signal within the dynamic range of the receiver system, and may result in inadequate signal-to-noise ratio at low frequencies.

### 3.2.2 Hybrid Simulator

The second and last simulator class that qualified for consideration in this application was the Hybrid simulator.. These simulators are formed by combining various features of radiating simulators and static simulators. For this simulator concept to apply, the system under test should be within or quite near the simulator structure. The basic concept of this class of hybrids can be summarized in three basic characteristics.

**Table 3.3. Fields Produced By A PxM of One Meter Radius Driven By A 500 Watt Power Amplifier**

| Distance From Antenna to Center of Simulation Area (meters) | Antenna Height Above Ground (meters) | Incident E Field at Center of Simulation Area (V/M) | | | |
|---|---|---|---|---|---|
| | | 100 kHz | 1 MHz | 10 MHz | 100 MHz |
| 60 | 10.0 | $6.75\ 10^{-3}$ | $22.9\ 10^{-3}$ | 2.9 | 219.0 |
| 140 | 23.0 | $.54\ 10^{-3}$ | $9.4\ 10^{-3}$ | .94 | 93.9 |
| 240 | 40.0 | $.105\ 10^{-3}$ | $5.47\ 10^{-3}$ | .55 | 54.7 |
| 340 | 56.7 | $.054\ 10^{-3}$ | $3.86\ 10^{-3}$ | .39 | 38.6 |
| | | Total H Field at Center of Simulation Area (A/M) | | | |
| 60 | 10.0 | $35.8\ 10^{-6}$ | $121\ 10^{-6}$ | $154\ 10^{-3}$ | 1.16 |
| 140 | 23.0 | $2.86\ 10^{-6}$ | $49.9\ 10^{-6}$ | $49.8\ 10^{-3}$ | .498 |
| 240 | 40.0 | $.56\ 10^{-6}$ | $29.0\ 10^{-6}$ | $29.0\ 10^{-3}$ | .290 |
| 340 | 56.7 | $.28\ 10^{-6}$ | $20.5\ 10^{-6}$ | $20.5\ 10^{-3}$ | .205 |

1. The early-time (high frequency) portion of the waveform reaching the system is radiated from a relatively small source region compared to the major simulator dimensions.

2. The low-frequency portions of the waveform are associated with currents and charges distributed over the major dimensions of the simulator structure. This structure either surrounds the system or is very close to it.

3. The structure is sparse so that most of the high-frequency energy radiates out of the simulator without reflecting off the simulator structure. The structure is also impedance loaded to further reduce unwanted reflections in the simulator.

An important example of a hybrid-type simulator is the TEMPS antenna. This antenna was used in the NAVCAMS EASTPAC test primarily as a threat-level time domain simulator, but was modified so that it could be driven by a CW source and thus irradiate the test site with CW fields. Data gathered and processed from the antenna demonstrated the practicality of predicting responses of a facility to a high-level transient signal using low-level CW signals.

The TEMPS antenna is a large, horizontal dipole with a biconical feed, resistively terminated to earth. The structure is representative of the type of hybrid simulator that is reasonable to erect and use at a large $C^3$ facility.

The experience with the TEMPS antenna as a CW simulator provided much useful data, not the least of which was the field levels necessary to achieve adequate signal-to-noise ratios when using the DNA CW measurement system. In terms of making comparisons, the key value to establish is the low-frequency H field level associated with the antenna. The magnitude of the low-frequency fields is the area where the PxM is most lacking. If the PxM can obtain adequate field levels in this frequency regime, it will have no problem at higher frequencies. The H field was selected because it was routinely measured during the NAVCAMS EASTPAC test and provided the most readily available CW measurement on the TEMPS antenna.

The TEMPS CW H field measurement that will be used as a reference value was measured at a position 15.9 meters out on the center line of the antenna. A representative plot of a measurement made at this location shows a low frequency (i.e., approximately 100 kHz) field level of -49 dB A/M with the power amplifier set so that it would deliver 140 watts into a matched load. If the field level is referenced to a 500 watt setting on the power amplifier, the H field level becomes -37.9 dB A/M

or $12.7(10^{-3})$ A/M. Table 3.3. used in conjunction with Figure 3.2 indicates the same location and frequency for the PxM.

Another important value to establish is the low-frequency amplitude variation of the H field over the simulation volume to see how this compares with the computed values for the PxM. Since a CW field map of the TEMPS antenna was not available, it was necessary to use a simple model in order to obtain a rough estimate of this quantity. It was reasoned that at low frequencies where the antenna is small with respect to a wavelength, the antenna looks like a large current loop where the magnitude of the current is determined by the antenna terminator resistors, which had a value of 190 ohms. For the purpose of calculating the H field, the antenna was modified as a current filament over an ideal ground plane with a current magnitude established by the 500 watt power amplifier and the terminator resistors. The details of these calculations are shown in Appendix D.

The calculation technique shown in Appendix D yielded results which are shown in Table 3.4 along with the measured field level from TEMPS.

**Table 3.4. Field Levels and Field Variations for a Hybrid Antenna**

| | Low Frequency H Field At (0,20,0) (A/M) | Amplitude Variation From (0,20,0) to (0,100,0) |
|---|---|---|
| Temps Measured | $12.7(10^{-3})$ | |
| Current Filament Model | $14.3(10^{-3})$ | -29.0 dB |

The close agreement between the calculated and measured H field value gives one confidence in the current filament model as a tool for estimating amplitude variation over the simulation volume. In addition, the time domain field mapping on TEMPS indicated a 20 dB drop over the same distance with a gradual decrease in rise time from 12 to 6 nanoseconds. These results are consistant with the above calculations for the following reasons. The time domain results represent the combined amplitude attenuation effect of all frequency components; low, middle and high frequency. The high frequencies should attenuate less rapidly than the low, thus the combined effect should be less total attenuation over the simulation area for the time domain pulse than for the low frequency component. In addition, the gradual decrease in risetime as one goes out from the antenna along the center line indicates a gradual decrease in low frequency content which is consistent with the above remarks. Thus, for the purpose of making comparisons between the hybrid simulator concept and the PxM concept, a low frequency amplitude variation of 30 dB over the specified distance was used.

### 3.2.3 Selection of Simulator Class

The selection process involved comparing the ability of the two simulator classes to simulate the required fields, within the constraints placed on the design. This process is accomplished by comparing the amplitude of the various field components produced by the simulators, for a given polarization and angle of incidence, with the amplitude of the required fields. In the last two subsections, calculations were made for the simulators over an ideal ground plane, and comparisons based on a single H field component on the surface of the ground plane were made. These initial calculations indicated a large difference in the low frequency performance of the two antenna classes, a difference that was judged large enough to preclude the choice of the dipole class (PxM) simulator.

Figure 3.2 shows the variation in amplitude across a simulation volume 80 meters deep by 160 meters wide for both the low and high frequency case when the antenna is located 20 meters from the side of the simulation volume. These dimensions are thought to be representative of ones required in actual operation, and it reveals that at the low frequency end of the spectrum a front-to-back amplitude variation of 67 dB can be expected. This number compares with 30 dB calculated for the hybrid class simulator.

Although both numbers are larger than one would like, 67 dB is much worse than 30 dB. The impact of this nonuniform illumination, when using the antenna to predict EMP responses, is to imply a variation in signal amplitude that is not actually there. When using the antenna as part of a CW system this property can lead to over or under prediction of induced responses depending on how the measurements are referenced. When a signal close to the antenna is used as a reference, it tends to underpredict the induced response. In order to have a conservative predictor (one that tends to over estimate the induced response) a signal that is farther from the antenna than the test object should be used or the response scaled to account for the variation.

Based on the ideas just presented, antennas with larger signal amplitude variations over the simulation volume will tend to have larger variations between the predicted responses and the true EMP response in an average sense. Thus, in a statistical sense, the larger the amplitude variations over the simulation volume the less accurate the antenna as an EMP simulator. It should be kept in mind that the comparisons made between the hybrid and dipole class antennas have only been made for one field component at a few selected locations when, in fact, there are six field components which should be considered. However, it is thought, based on physical reasoning, that

the results obtained for the one field component is representative of results that would be obtained with a more general formulation.

Another factor which came into play in selecting the hybrid class simulator was the magnitude of the fields which could be produced by the two antennas for a fixed power input level. The power level used was 500 watts, which is the size of the power amplifier available with the CW system. Using the numbers in Figure 2.3 and Tables 3.3 and 3.4, one can infer that the magnitude of the H field at the (0,20,0) location would be $3.56 \times 10^{-3}$ A/M for the PxM, and $12.7 \times 10^{-3}$ for the hybrid. Thus, the PxM has a signal which is 11 dB smaller at that location. From the same figure and tables, one can further deduce that the PxM would have a signal at the (0,100,0) location which is 48 dB smaller than that of the comparable signal from the hybrid antenna.

Experience with the hybrid TEMPS antenna used as a CW simulator has indicated that the signals produced by this antenna are sufficient, but certainly not excessive, in terms of obtaining adequate signal-to-noise ratio with the existing CW system instrumentation.

This implies that choosing an antenna which produces significantly smaller fields would most likely lead to a signal-to-noise ratio problem. Thus, not only is the hybrid simulator choosen because of amplitude variation over the simulation volume, it is also selected because of the magnitude of the fields generated by the antenna and its implication in terms of signal-to-noise ratio.

## 3.3 MECHANICAL AND FINAL DESIGN CONSIDERATIONS

Consideration of the electromagnetic requirements in the previous section lead to the choice of the hybrid class simulator. It was not necessary to do a comparative mechanical study in order to help make this choice. Thus, the thrust of this section is to discuss the impact of the mechanical design objectives and constraints on the formulation of a suitable hybrid simulator design.

The selection of a hybrid simulator was not an optimal choice from a mechanical standpoint. Hybrid simulators should be large with respect to the object being tested, which implies a physically large antenna (on the order of hundreds of meters) when the intended test object is a ground based $C^3$ facility. Constructing an antenna this size which meets the specified design objectives and design constraints was not an inconsequential task.

Attempting to meet the objective of keeping the overall weight of the antenna to 450 lbs. or less proved to be the driving consideration in developing the mechanical

design. It was decided that the antenna itself should be a wire framework like TEMPS, and many other hybrid class simulators, in order to minimize weight and sail area of the antenna. Preliminary calculations assuming a wire framework antenna in conjunction with a review of commerically available support structures, made it apparent that the majority of the weight budget would probably be consumed by the antenna support structure with associated rigging.

The review of commerically available support structures also revealed another problem which tended to focus much of the mechanical design effort into this one area. The original design objectives had called for a dielectric support structure to be used unless the support structure was actually part of the antenna itself, and was intended to serve as a radiator of electromagnetic signals. Since the general hybrid design does not use the support structure(s) as part of the antenna, a dielectric support was required. The review of the commerical literature revealed no suitable dielectric support structure, and very few conductive support structures which might prove to be suitable.

In view of the support problem, the design tended to separate into one effort which focused on funding a manufacturer to build a suitable dielectric support structure while another effort looked for methods to use a conductive support structure without perturbing the antenna fields. The weight objective, and the desire to use a conductive support structure argued for a single support located in the middle of a symmetric antenna with a balanced feed. Such an antenna should experience a minimum perturbance due to the conductive support. In addition, the weight budget would not allow more than one support structure since rough estimates of support structure weight required a minimum of several hundred pounds using conventional design approaches.

It became apparent at this point that a model for a new hybrid simulator tested at the end of the NAVCAMS EASTPAC test was ideally suited to the needs of the program. This antenna is best described as an inverted V antenna resistively terminated to earth at both ends. A two hundred meter version of this design had been tested using coaxial cable for the radiating structure. A limited set of parametric studies had been conducted where center height and terminating impedance had been varied, and the antenna design appeared to show a good deal of promise as a hybrid simulator. This design was well suited because it requires a single support structure in the center of the antenna. The basic configuration is also well suited to a design which could be rapidly assembled and erected by three or four men in three or four hours, thus meeting another of the design objectives. The antenna was thought to have field

patterns similar to the TEMPS antenna which was a hybrid class simulator in use at that time by DNA to test ground-based $C^3$ facilities. The limited measurements taken on the model antenna supported the idea that the fields were similar to TEMPS, and the similarity of physical shapes and construction of the two antennas also lead us to believe that the fields should be similar.

At this point in the program, the decision was made to build an inverted V antenna, and this fact, along with additional supporting data, was presented at a critical design review and approved for detailed design and construction.

The design of the antenna structure itself proceeded on the basis that a conductive support structure would be used. That is to say, the best commerically available metal tower was selected and its structural strength properties were used as input data to the antenna designed. It was then required that any dielectric support structure proposed for this application meet or exceed the structural strength of the metal tower.

The metal tower selected for this application was less than ideal since the minimum length of the tower was 22 feet, not 10 feet. The extended length of the antenna was 70 feet. This value had been selected based on the results of the parametric studies conducted on the prototype at NAVCAMS EASTPAC. A guyed tower was selected since it eliminated the need for concrete footing. The guyed tower can be held in place using only ground stakes. The tower and associated rigging weighted approximately 300 lbs. The tower was rated to support a 150 lb dead load with a seven square foot sail area. Thus, the design goal was established of 150 lbs. maximum weight for the antenna itself.

The basic inverted V design was taken and elaborated upon to try an improve its performance, while keeping the 120 lbs. design goal in mind. As mentioned earlier, a wire framework structure was decided upon to minimize weight and sail area. The desire was to use as many wires as weight permitted to create a cylindrical-shaped structure with a large effective diameter. In general, the larger the effective diameter of the cylinder, the better the broadband impedance characteristics (within certain limits). The large effective diameter also tends to lower the driving point impedance which usually simplifies the antenna feed design. From a weight standpoint, the design was limited to ten wires on each side. The total number of wires effectively established the maximum diameter for the cylindrical cross section of the antenna. If the wires are spaced too far apart around the perimeter of the cylinder, the structure no longer simulates a cylinder from an electromagnetic standpoint. Thus, it was

determined that ten wires limited the diameter to a maximum of approximately 3-1/2 ft.

The design of the antenna was further fixed when it was decided to slowly decrease the cross section diameter of the antenna arms as the antenna arms approached the ground plane. This was done to minimize localized impedance discontinuities which could set up undesirable resonances in the antenna. This in turn should lead to a more uniform distribution of current along the antenna arms and a more "uniform" illumination of the simulation volume.

With the above considerations in mind, an antenna was designed with a biconic feed to get from the fixed feed point out to a cylindrical cross section of 3-1/2 feet. The antenna structure then sloped down to the ground with a uniformly decreasing cross section which ended up at 9 inches at the ground termination point. Each antenna arm was designed to "hang" from the bicone in the shape of a catenary rather than being tensioned to the point that the arms would approach the ground with a constant slope. The catenary shape significantly decreased the compression loading on the tower while still providing enough tension to effectively "guy" the antenna support with the antenna arms, and thus increase the effective structural strength of the entire antenna structure.

At this point, the general design of the antenna was fixed. The sail area of the antenna was significantly larger than seven square feet, actually approaching 42 sq. ft. Rough order of magnitude wind loading calculations on the entire structure showed that the extra area could be tolerated due to the nature of the antenna design. The specific design choosen could be attached to the support structure in a manner which effectively eliminated shear loading on the tower, and tended to deliver the entire load as a compression load. Further calculations served to confirm the idea that the factory specifications were based on a mode of attachment that introduced significant shear loading into the tower, and that this was the primary failure mode. It was thought that the tower could handle significantly larger dead loads and sail areas if the antenna design/attachment could eliminate the majority of the shear loading.

While the antenna design was being finalized, progress had been made in finding a manufacturer for a dielectic tower. Bosch Laboratories of Fargo, North Dakota, had submitted a design for a dielectric tower which had been reviewed and accepted by IRT. The design used a truss-type structure as a tension compression device using a recently patented construction element called the captive columns for the compression members. The antenna was designed to have a total weight of 100 lbs. or less, and to

meet all of the requirements for erectability and maximum shipping dimension. Due to the unconventional nature of the Bosch tower, IRT had an independent analysis of the tower made by ABAM Engineering of Tacoma, Washington, to assure ourselves of the adequacy of the design. The results of the analysis are included in Appendix B. While the fabrication and initial testing of the tower was being conducted, the assembly and first fielding of the antenna was also being done. The first fielding of the antenna was to be done with a metal tower, while the final testing of the CW system (i.e., instrumentation system and antenna) was to be done with the dielectric tower. It was decided that a set of measurements would eventually be conducted which would determine it there was any difference between the field pattern of the antenna when supported by a metal versus a dielectric tower.

The remainder of the antenna design was detailed design work which will not be discussed here. The results of the design work are documented in Appendix A.

# 4. ANTENNA CHECKOUT

## 4.1 INTRODUCTION

The antenna design program called for an initial fielding of the antenna to demonstrate the adequacy of the design and to provide an opportunity to do limited experimental studies which would provide data to finalize certain aspects of the antenna design.

The antenna checkout involved both a mechanical, as well as electrical/electromagnetic evaluation. The mechanical portion of the checkout was simply a matter of making sure that the design functions in a practical environment. This effort was concerned not only with how the antenna went together and how it was erected, but also with its structural strength under realistic wind loading conditions. Summer thunderstorms in the area of the test site provided several opportunities to expose the antenna system to winds in excess of 50 mph. Experience gained with the antenna during this checkout period provided ideas for modifications that could be made to the basic design to improve the fieldability of the antenna system.

The other facet of the antenna checkout was the electrical/electromagnetic study. This portion of the work involved several parametric studies as well as a symmetry study. The parametric studies involved evaluating two different antenna feed systems, evaluating different values of terminating resistance for the antenna arms as well as determining the impact of different types of grounding systems. The symmetry study used B field measurements taken at a number of locations throughout the simulation volume to verify that the antenna fields were symmetric.

The details of the electrical/electromagnetic study are given in the remainder of Section 4. Subsection 4.2 considers the parametric studies while Subsection 4.3 presents the results of the symmetry study.

The antenna system was field tested at Kirtland AFB, New Mexico. The antenna system was evaluated without the use of the DNA CW instrumentation system, which

was being modified at the time. The instrumentation system used during the test consisted of an HP-8601A generator/sweeper, HP-8407A tracking receiver, and an HP-8412A phase-magnitude CRT display used in conjuction with a flat-bed plotter for generating hardcopy plots of the measured data.

## 4.2 PARAMETERIC STUDIES

When the antenna was fielded at Kirtland, the first task was to do an initial evaluation of the antenna feed system before proceeding to any of the other planned measurements.

The antenna was to be tested at Kirtland using two different antenna feed systems. The two techniques for feeding the antenna were referred to as the end-feed and the balun-feed. The end-feed was the one used at NAVCAMS EASTPAC when the TEMPS antenna was modified for CW drive and was considered a proven approach at the time of the Kirtland test. The end-feed consisted of isolating the transmitter power amplifier and associated power source along with the signal generator on a dielectric platform at one end of the antenna. A low-loss coaxial cable was then run from the output of the power amplifier to the bicone feed point inside and at the center of the antenna arm. The shield of the coax was grounded to one side of the bicone while the center conductor of the coax was connected to the other side of the bicone. This technique provides for a balanced feed to the antenna (i.e., equal current on each arm), but has the disadvantage of being physically quite awkward for general field use and results in considerable power loss at high frequency due to transmission loss. The balun feed, on the other hand, was quite simple to use, had a much shorter feed length (approximately 70 feet from the base of the antenna tower to the bicone), and did not require a dielectric platform to be constructed to isolate a large power amplifier, 10 kw generator and signal source from ground. The balun however, was not a proven approach. It is very difficult to build a single balun to operate from 100 kHz to 100 MHz even with a well-matched load. The CW antenna presents a driving point impedance which varies widely over the frequency range and the impact of this variation could not be easily anticipated.

The initial measurement sequence allows the balun feed system to be evaluated and to determine if there was any need to include this feed method in the subsequent testing. The success criterion for any feed system on this antenna was rather simple--it must provide currents of equal magnitude on each antenna arm. The word "equal" has to be used in light of the fact that some asymmetry was expected due to variations in

the local terrain, and one must also recognize that identical measurements made one right after the other can show 2 dB variations at some frequencies due to instrumentation effects.

The first measurements were of the current at the terminator resistors. A measurement would be made at one end of the antenna and then the fiber optic system would be moved at the other end of the antenna where the same measurement would be repeated. Figure 4.1 shows the results of this process. Note that the ratio of the current at the terminator resistors to the drive current is measured by the network analyzer. The graph represents the magnitude of the terminator as a function of the magnitude of the drive current (which is not constant). The graph shows the currents in the two terminations are nearly equal below approximately 45 MHz. At this point, the terminator current is 59 dB down from the drive current which indicates, as one would expect, that the ends of the antenna become relatively unimportant in terms of generating the antenna fields. At higher frequencies, it is the center region of the antenna which is primarily responsible for generating the fields. The largest variation in current (10 dB) occurred at approximately 54 MHz which was due in part to terrain variations which caused different parasitic loadings at the two ends of the antenna. The test side had a gentle slope to the ground which caused one antenna arm to be closer to the ground than the other.

Based on the success of the balun feed, as indicated by the measurement, it was decided to continue the test using the balun feed and to eventually take B field measurements using both feed approaches as a final demonstration of the adequacy of the balun feed.

The next phase of the field test was aimed at determining an optimal value of terminating resistance. The success criterion was to try and match the load to the source impedance as well as one could using only resistors. The idea was to try and minimize reflections from the ends of the antenna which causes unwanted standing wave patterns that detract from the broadband characteristics of the antenna.

Since the currents were balanced using the balun feed, the measurement shown in Figure 4.1 also provided a useable data point for the determination of a terminating resistance. A second measurement, identical to the first, was made using 100 ohm terminating resistors instead of the 50 ohm resistors used in the first sequence. The results are shown in Figure 4.2. Using the data in Figure 4.2 and 4.1 at approximately 1 MHz, one notes that the measured current is approximately 3 dB lower with the 100 ohm resistor than the 50 ohm resistor. Representing the source by a Norton

equivalent, the following two equations can be written for the current through the terminator resistor for the 50 and 100 ohm cases.

$$I_1 = \frac{R_s}{50 + R_s} \; I_T \tag{4.1}$$

$$I_2 = \frac{R_s}{100 + R_s} \; I_T \tag{4.2}$$

$$I_2 = .708 \, I_1 \tag{4.3}$$

where $R_s$ is the source resistance, $I_1$ is the terminator current with the 50 ohm resistor, $I_2$ is the terminator current with the 100 ohm resistor, and equation (4.3) is obtained from the measured data. Substituting (4.3) and (4.1) into (4.2), noting that $I_T$ cancels out, one can solve for $R_s$. The above calculations yielded a value for $R_s$ of 100 ohms which was the remainder of the test. However, prior to doing that, several additional measurements were made while varying the value of the terminating resistance. These measurements consisted of measuring the B field at position R (Figure 4.4) while varying the terminating resistance from 50 to 100 to 200 ohms. The main purpose for taking these measurements was to look for any signs of anomalous behavior in the B field which might be caused by changing the terminating resistance; none was observed.

The next sequence of measurements made were concerned with evaluating different grounding systems. The normal grounding approach for this type of antenna involves the use of ground rods located at both ends of the antenna to provide local grounds for the terminating resistors. In many cases, the installation of the ground system involves digging multiple holes several feet deep and "salting" the earth with copper sulfate to insure a low-impedance ground. Such procedures are not only time consuming, but are extremely difficult to implement at some test locations.

In an attempt to bypass the problems mentioned above, a ground system was incorporated into the design which used strips of chicken wire running from both terminators to the base of the antenna. Measurements were made during the field test to see if the chicken wire ground system was at least as good as the conventional ground rod system. Measurements were made of the current at the terminator resistor with the conventional ground system, the conventional ground with the chicken wire ground, and the chicken wire ground by itself. The measurements indicated that the chicken-wire ground performed as good or better than the conventional ground, and the chicken-wire ground became a permanent part of the antenna design.

At this stage in the field test, the design was essentially fixed. The feed system, the terminator resistance and the ground system had all been selected. However, two final checks were made to test the adequacy of the feed system. The first was to measure drive current as a function of drive voltage and compare it with the total coax current measured as a function of drive voltage. If the balun is performing as designed, the total current on the coax should be much smaller than the drive current. This condition insures the coax feed is not operating as part of the antenna, creating significant local fields of its own. The results of this measurement, shown in Figure 4.3, indicates that the total current on the coax is always 30 dB or smaller than the drive current. The final check on the balun feed is discussed in Section 4.3 and involved measuring the B field using both the balun and the end-feed.

## 4.3 FIELD MEASUREMENTS

During the preliminary fielding of the antenna, measurements of the antenna B field were made at fifteen different locations within the simulation area of the antenna (Figure 4.4). These measurements were made using both the balun feed and the end feed configuration. The intent of these measurements was threefold. The measurements were intended to show that the B field from the antenna was symmetric, that the balun feed produced fields that were essentially the same as the end feed, and to obtain a preliminary check on the amplitude variation of the B field over the simulation volume. No plans were made to do a detailed field map at the time. This type of mapping was to be done when the updated CW instrumentation system became available with all of its sophisticated data processing and data plotting capabilities. The preliminary check of the antenna fields provided data to meet the needs described above and also provided data to verify that the basic operating characteristics of the antenna were understood.

Figures 4.5 through 4.19 show measurements of B from 1 MHz to 100 MHz at the fifteen mapping locations. Measurements of B from 100 kHz to 1 MHz were also made, and proved to be quite uniform in nature. The 100 kHz - 1 MHz B measurements at seven of the fifteen locations are shown in Figures 4.24 through 4.30. The field mapping for the end feed configuration was also made at all fifteen locations and the results were just as suspected; the measured fields were essentially the same. The only real differences could be attributed to the power loss in the field line which was much longer for the end feed (100 meters) than the balun feed (21 meters). Since the data

provided no real surprises, only representative samples were reproduced in this document. The end-feed data are shown in Figures 4.20 through 4.23.

The data in Figures 4.8 through 4.19 can be reviewed to determine the symmetry of the measured B field component. (In all cases, the measured field was normal to the plane of the antenna.) The results of the comparison show that the variations in the 2 to 4 dB range which are approximately the limits of reproducibility. Figures 4.10(a)/(b) and 4.11(a)/(b) show representative results in trying to reproduce measured data. In both cases, the measurements were made within an hour of one another, and they both show the same 2 to 4 dB variations. It should also be noted that similar results were obtained with the antenna using the end-feed configuration.

The conclusion drawn from the field measurements, as well as the antenna current measurements, is that the fields are symmetric. The fact that the antenna is physically symmetric with respect to the field point, coupled with the fact that the current is also symmetric, requires that the fields produced by the antenna be symmetric. The B field measurements simply confirmed this fact and demonstrated that the minor asymmetry which did exist due to terrain etc., had no major impact on the field symmetry.

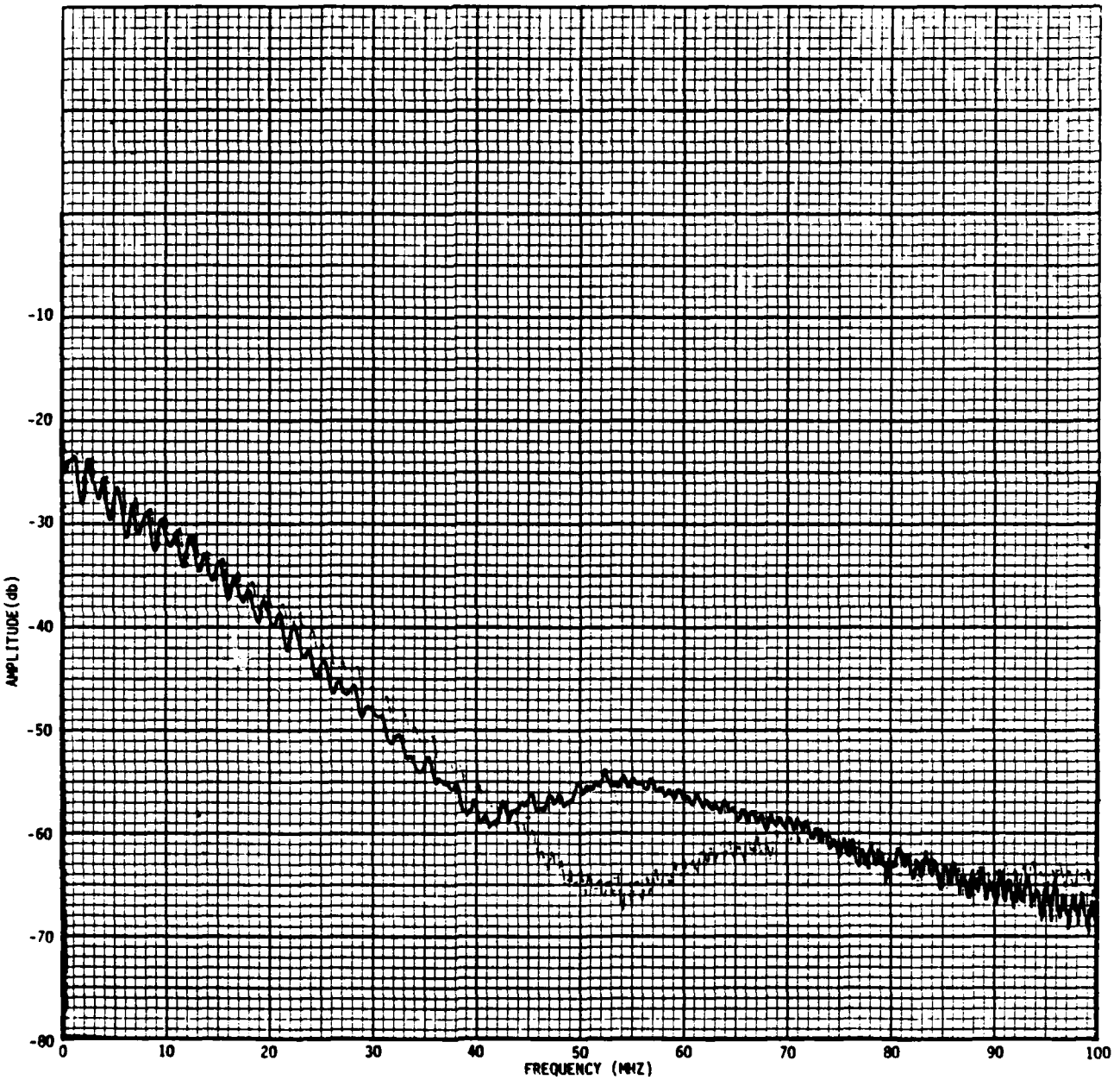


Figure 4.1. Current at terminating resistor, 50 Ω. chicken wire, no ground rods (Pv = 22)

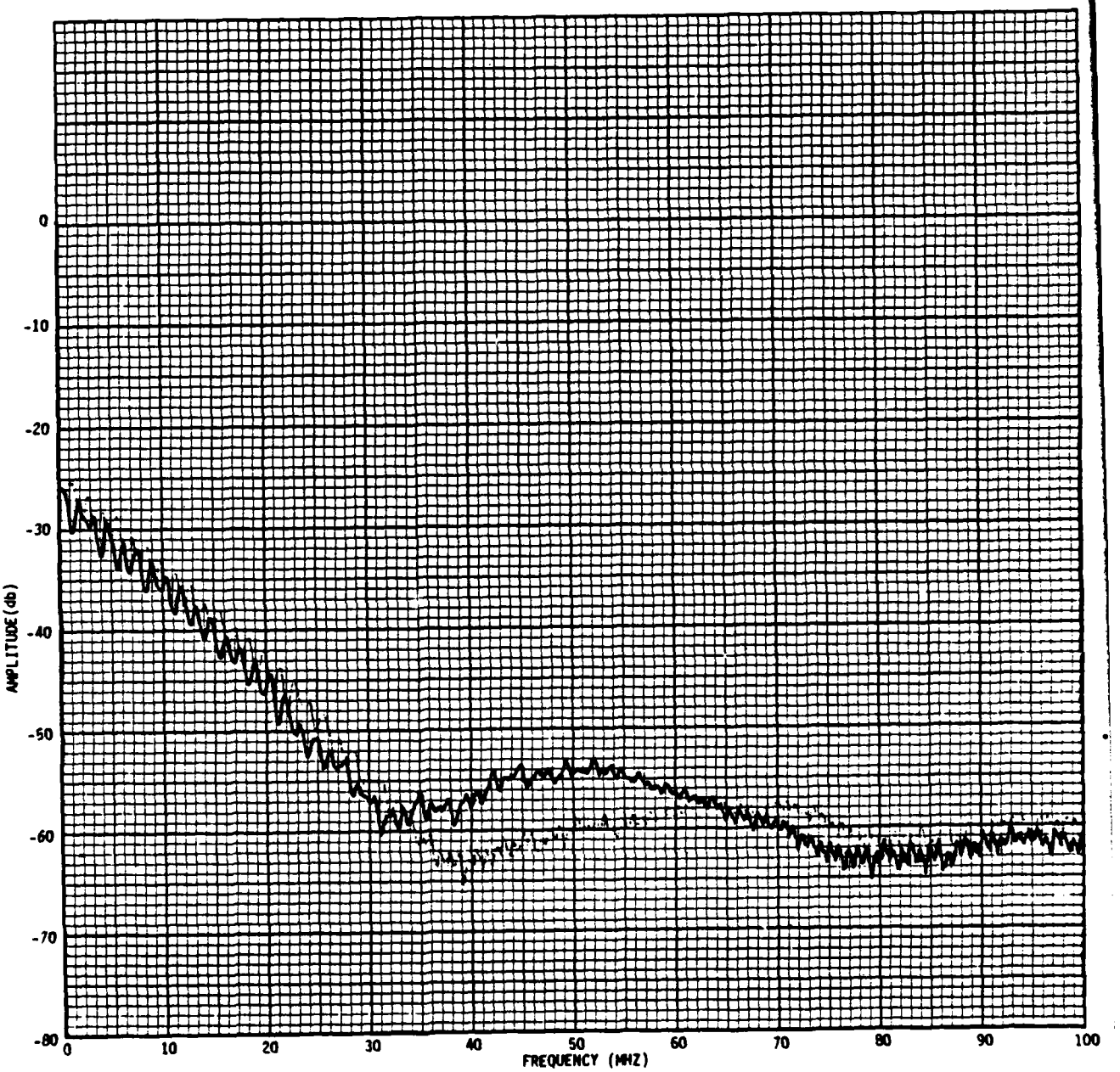


**Figure 4.2. Current at terminating resistor, 100Ω, chicken wire, no ground rods (Pv = 25)**

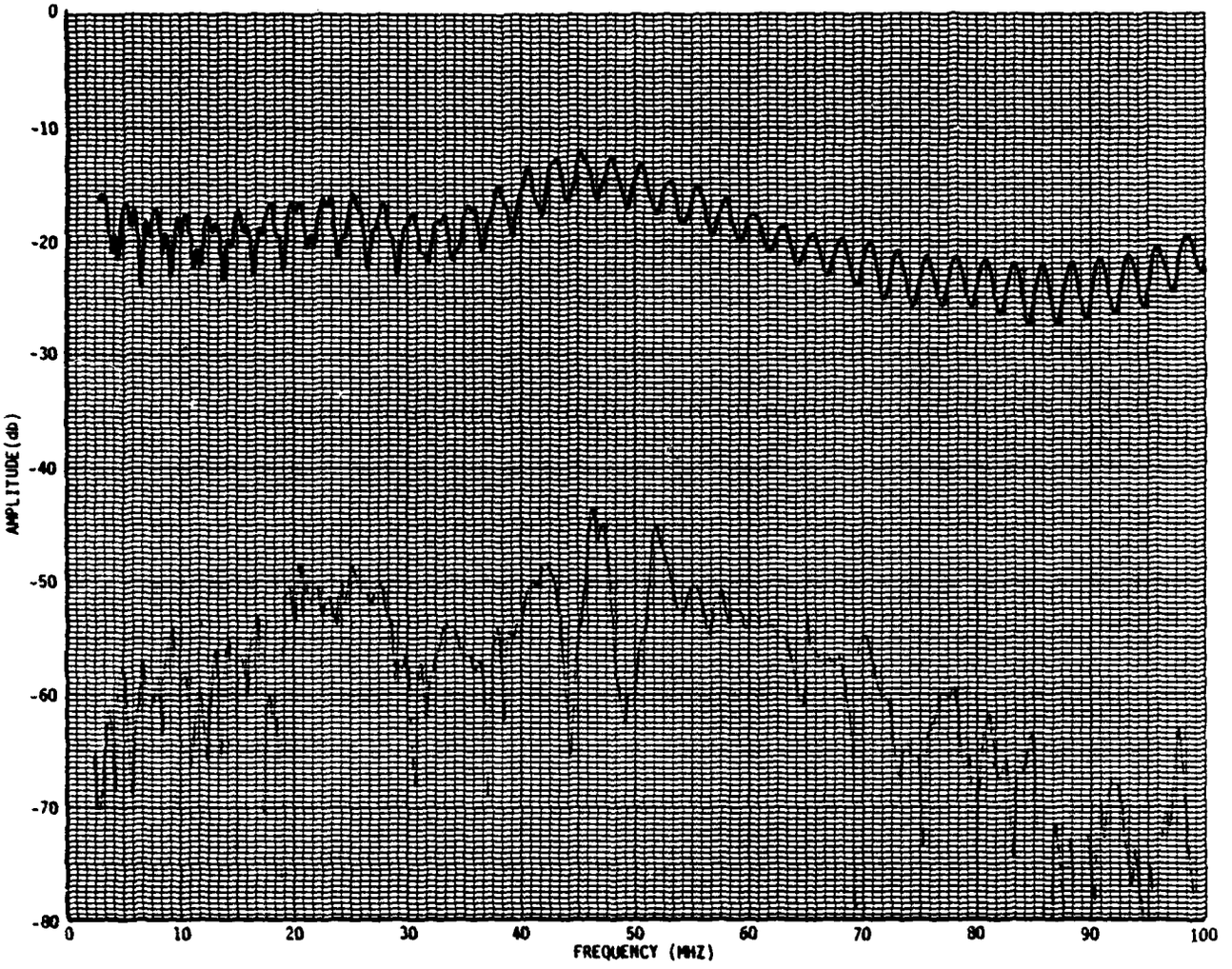


**Figure 4.3. Drive current and total coax current/drive voltage**

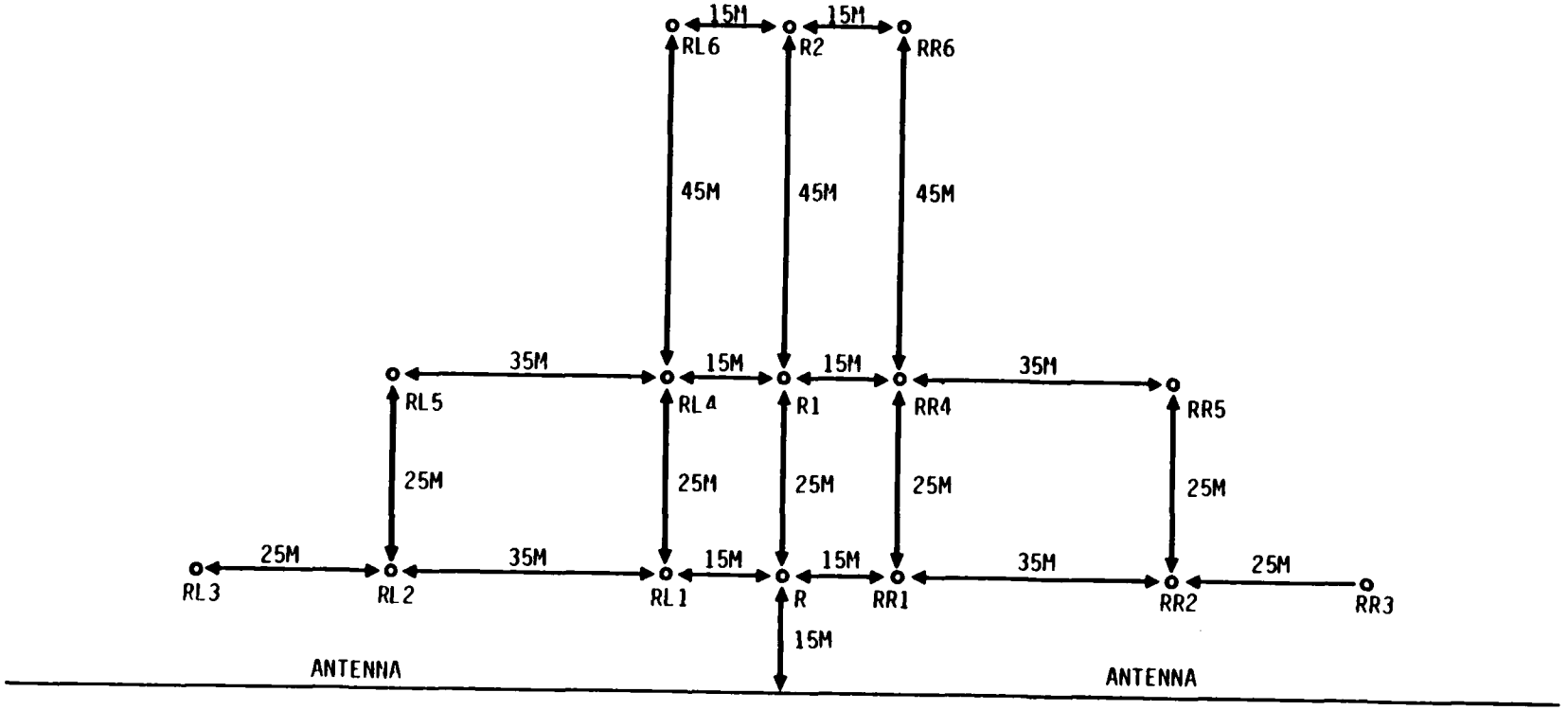


**Figure 4.4. Field Mapping Locations**

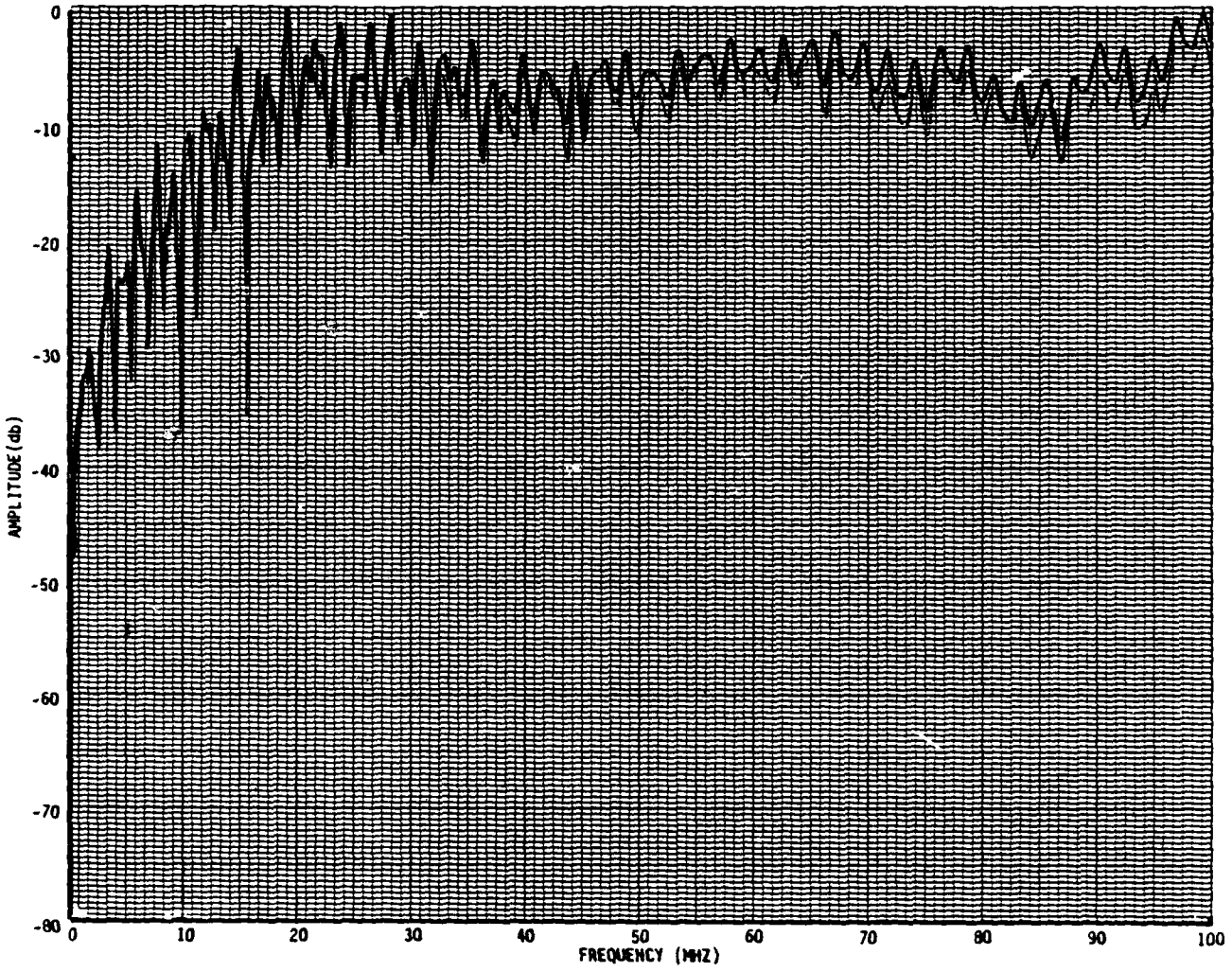


Figure 4.5. B 1-100 MHz at Position R, balun feed

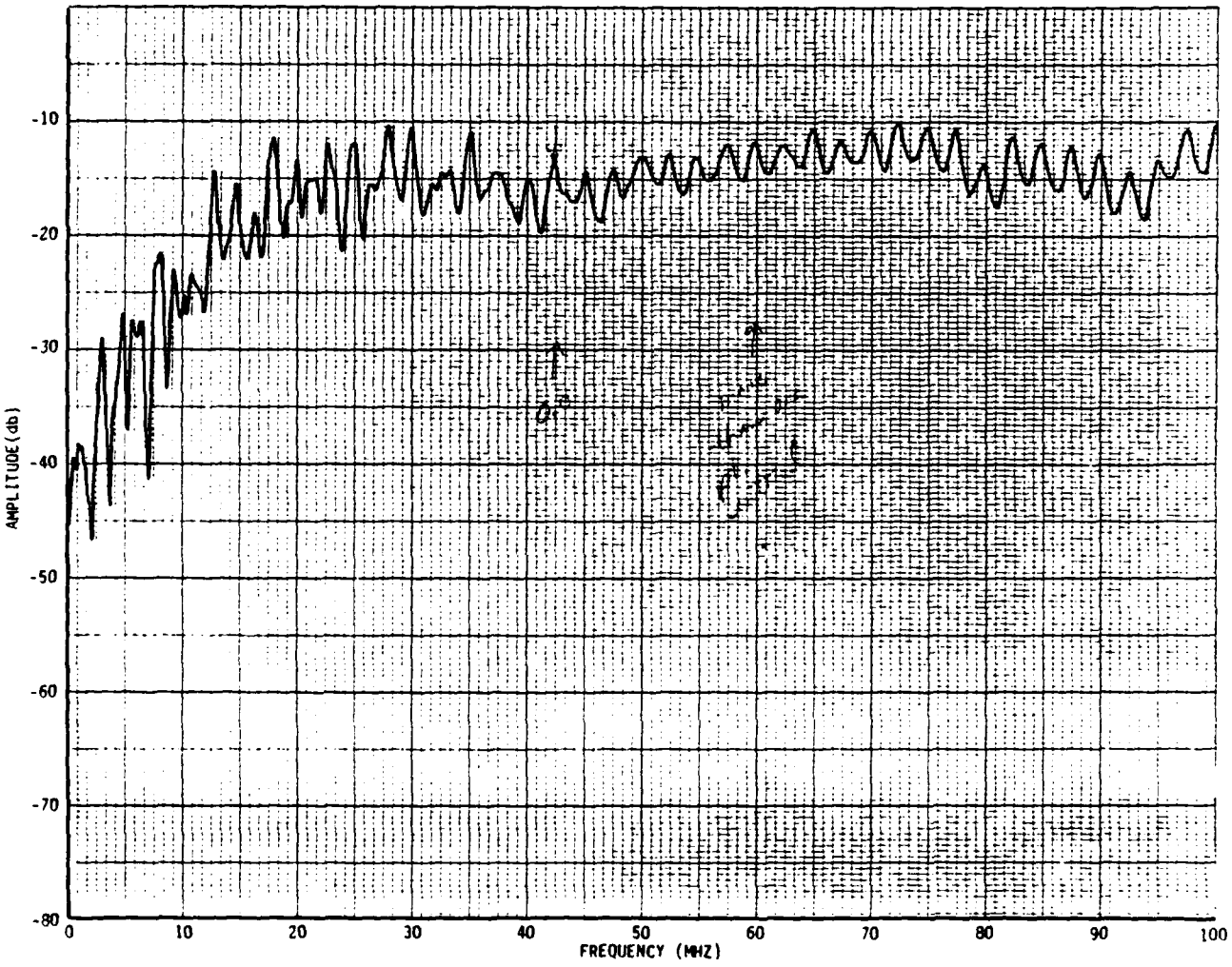


**Figure 4.6. B 1-100 MHz at Position R1, balun feed**

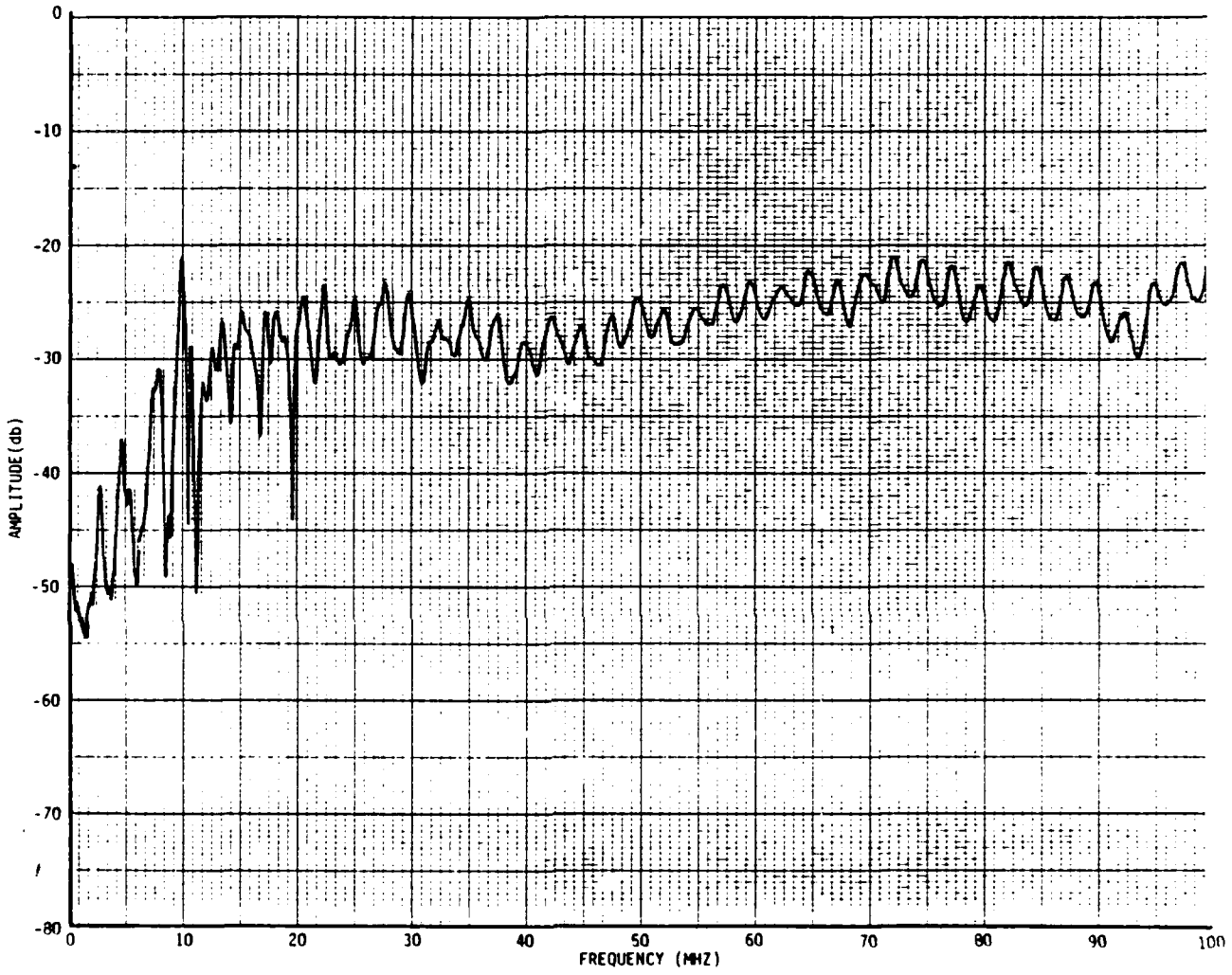


**Figure 4.7. B 1-100 MHz at Position R2, balun feed**

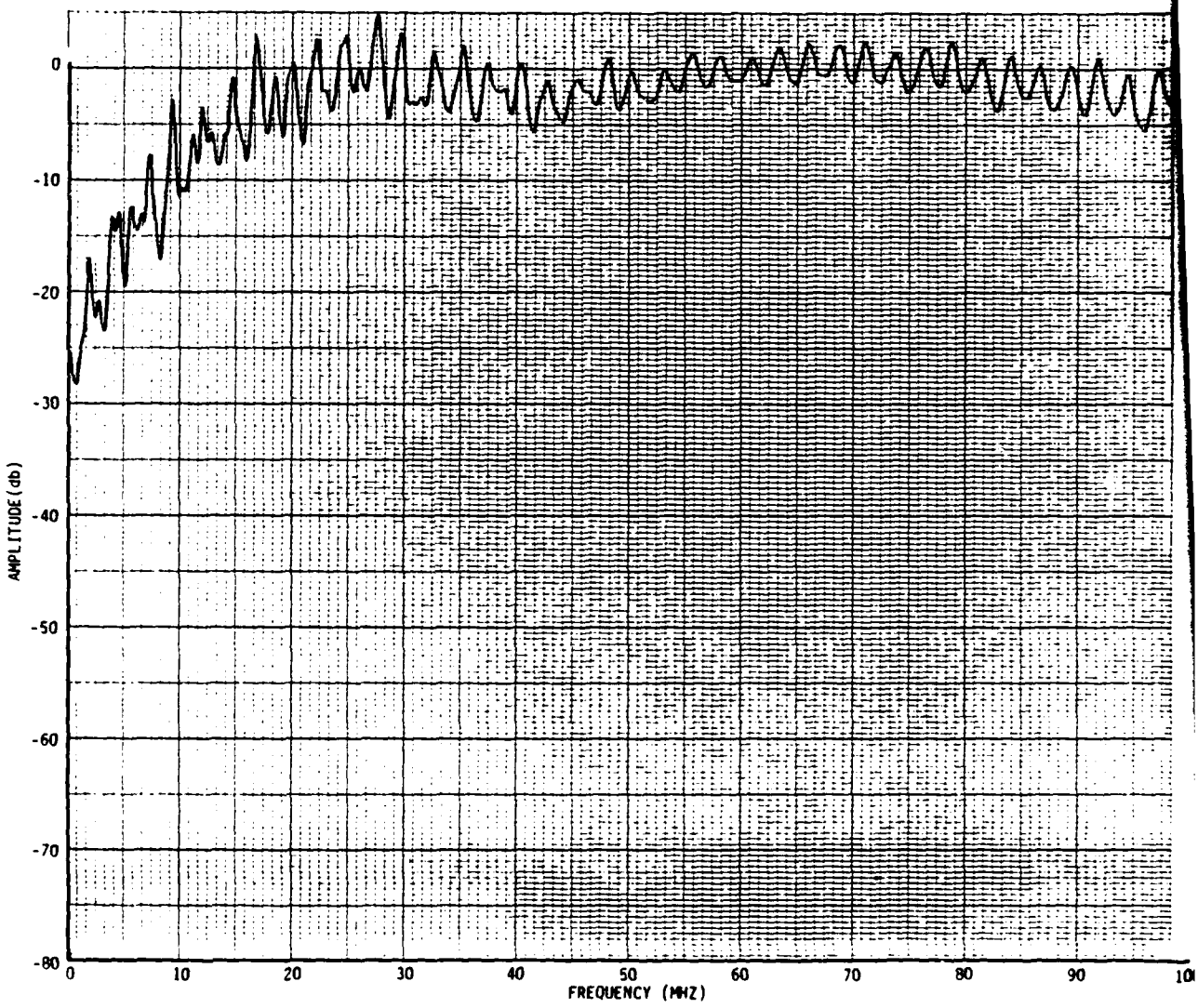


**Figure 4.8. B 1-100 MHz at Position RL1, balun feed**

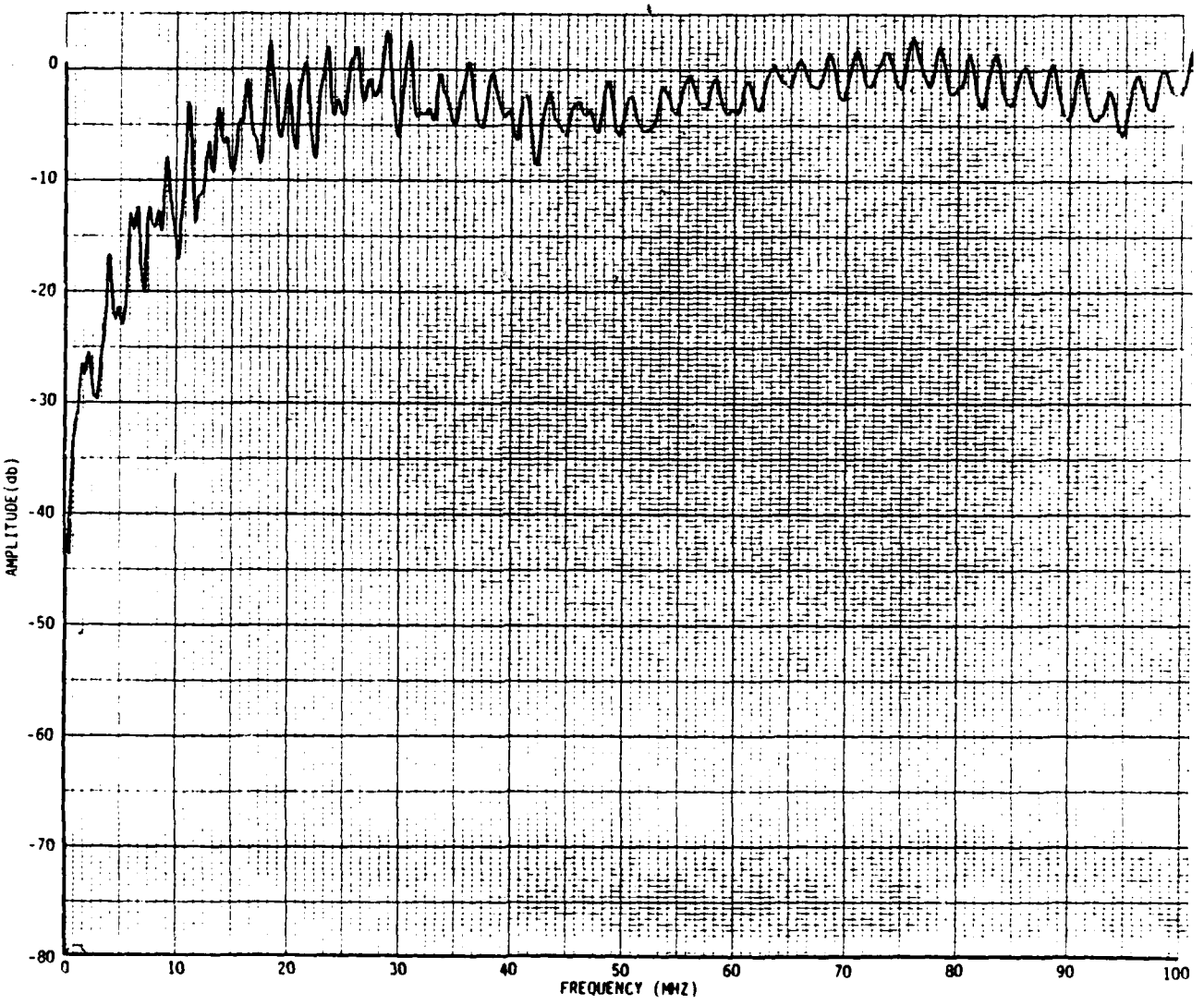


**Figure 4.9. B 1-100 MHz at Position RR1, balun feed**

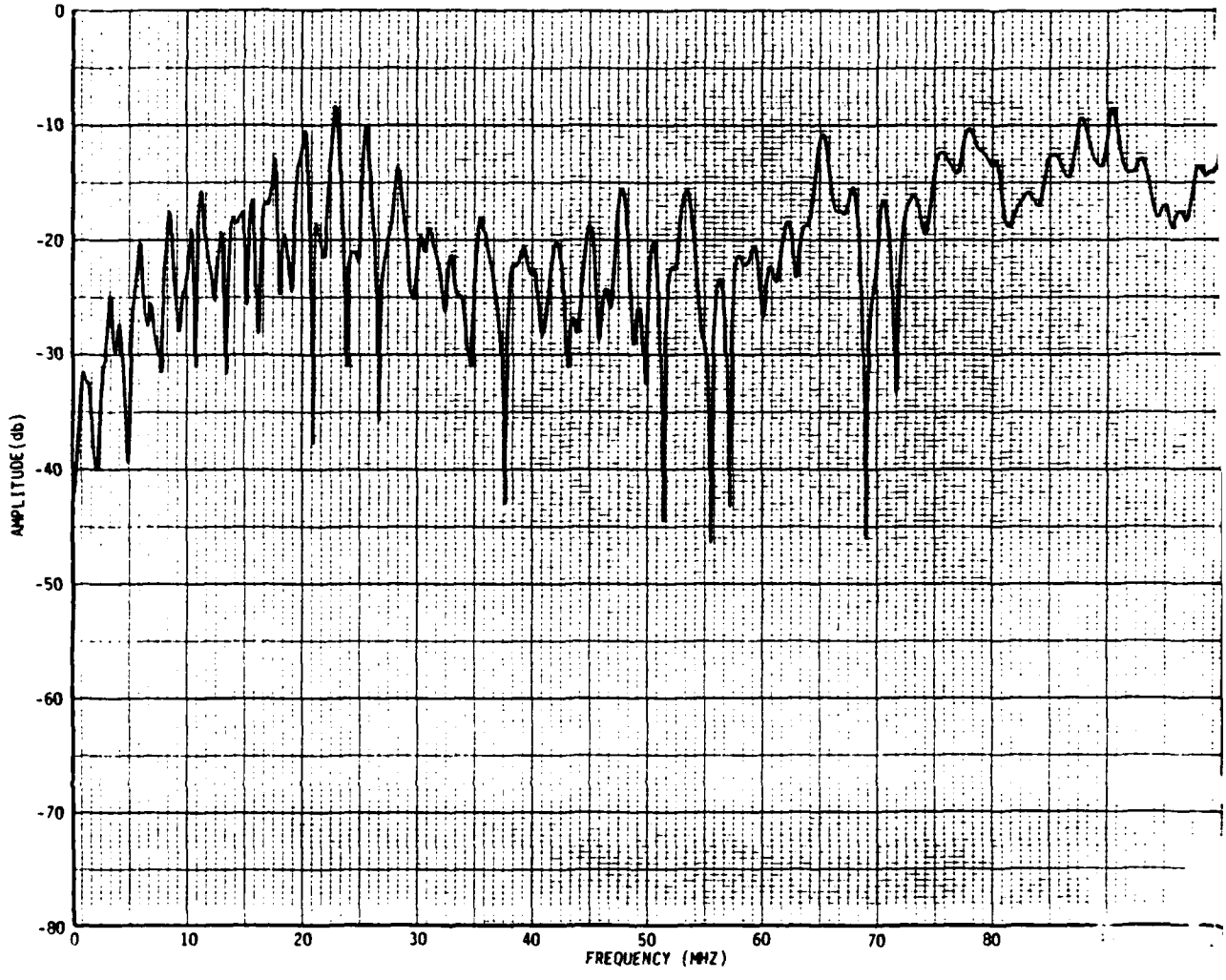


Figure 4.10(A). B 1-100 MHz at Position RL2, balun feed

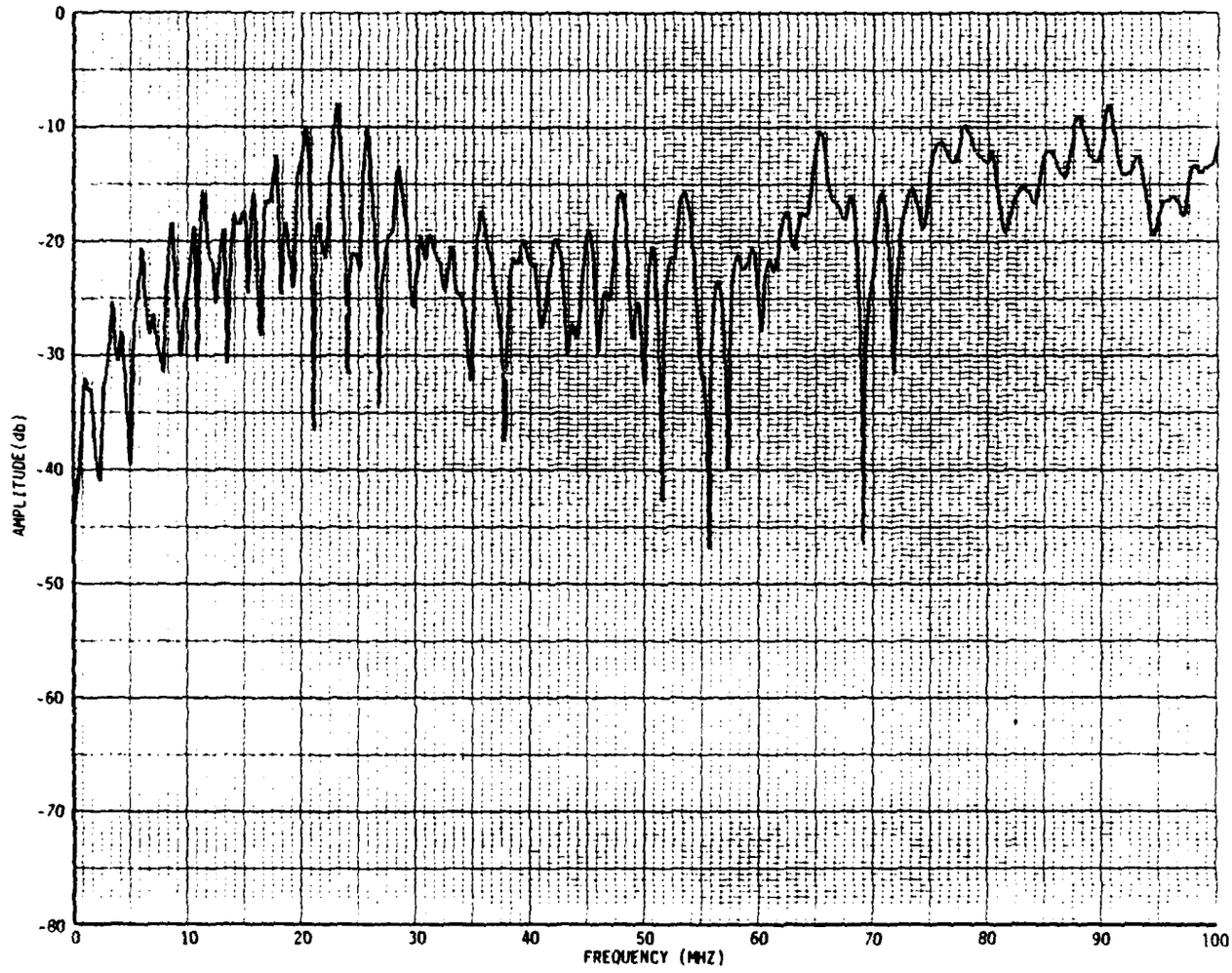


Figure 4.10(B). B 1-100 MHz at Position RL2, balun feed

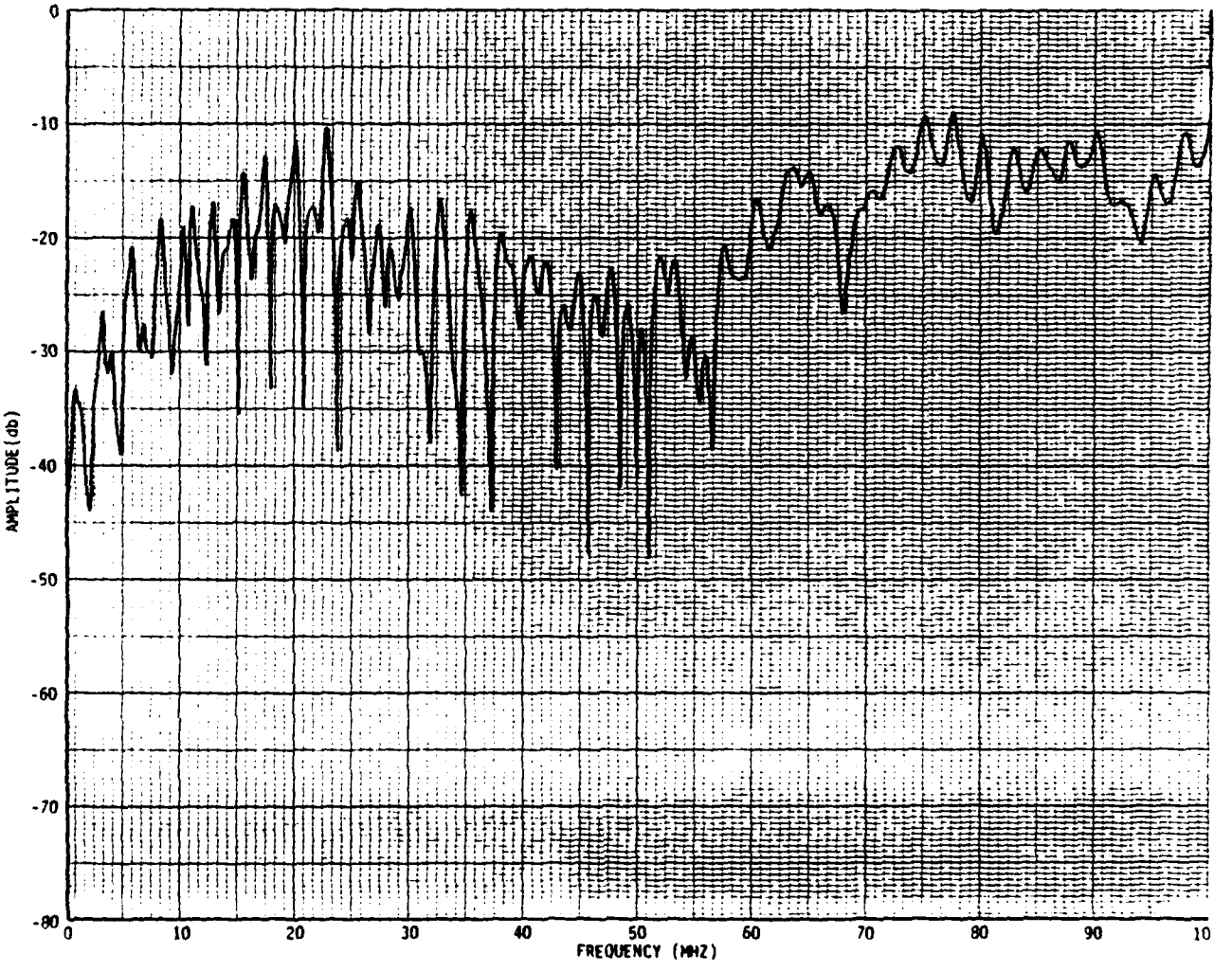


**Figure 4.11(A). B 1-100 MHz at Position RR2, balun feed**

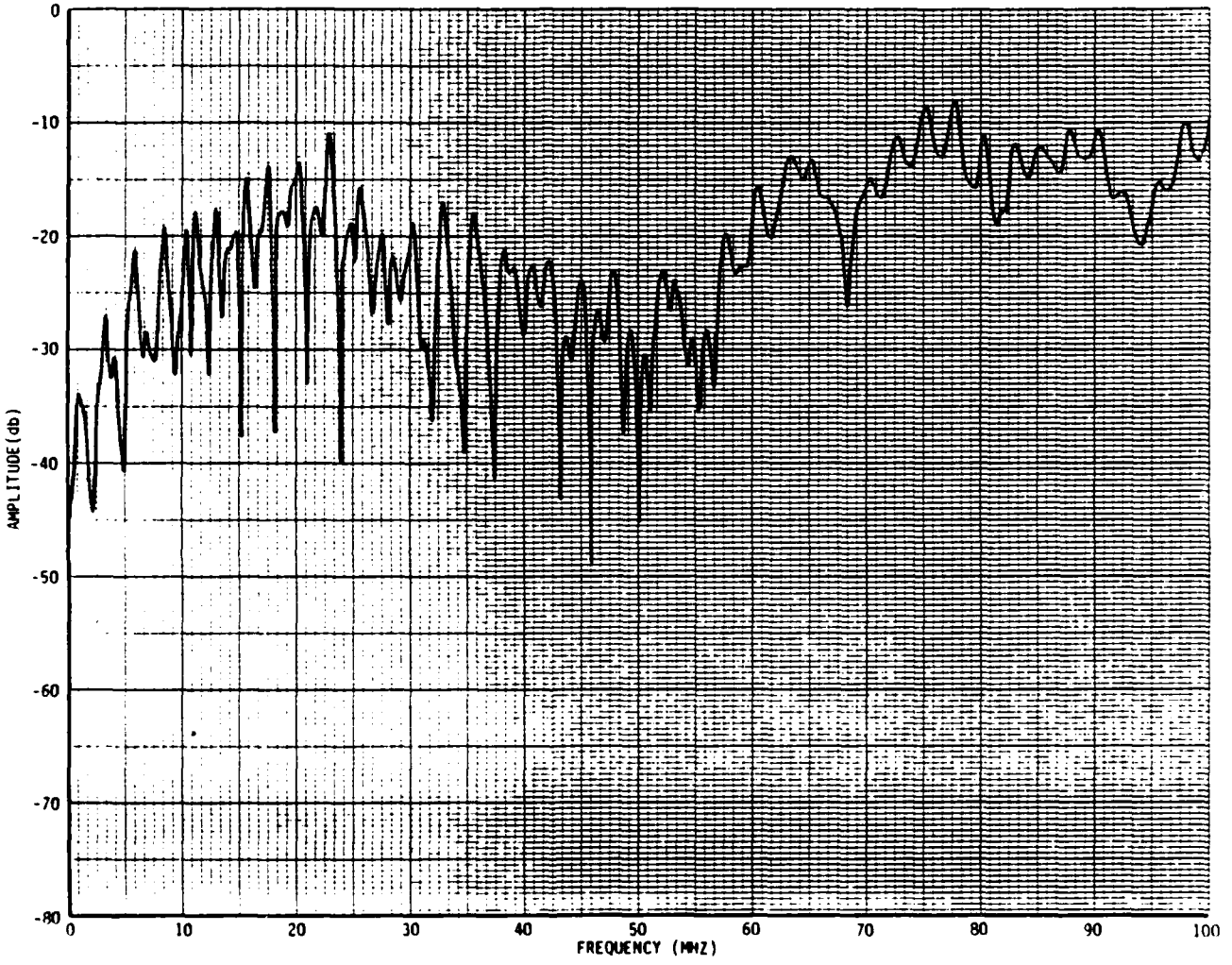


**Figure 4.11(B). B 1-100 MHz at Position RR2, balun feed**

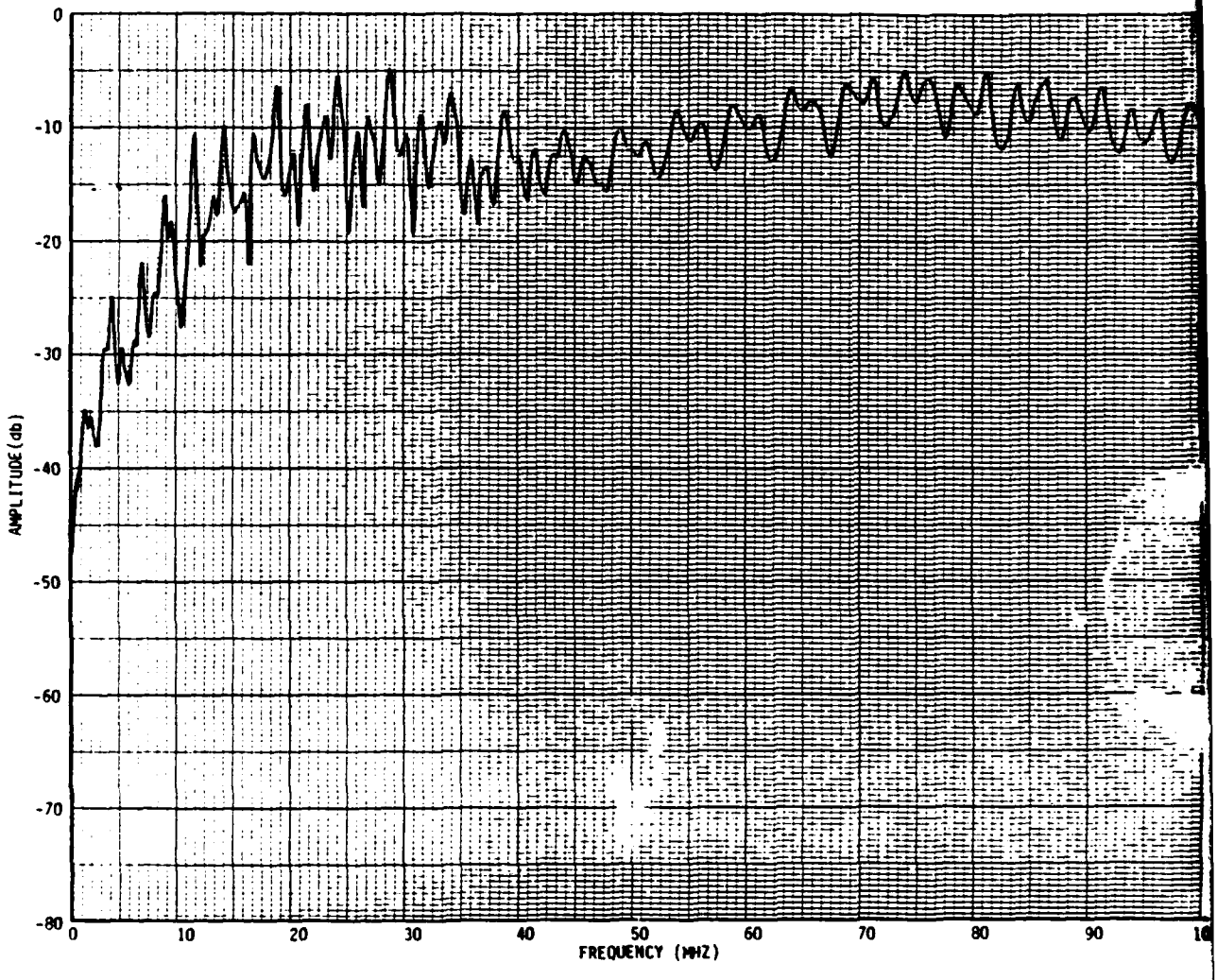


**Figure 4.12. B 1-100 MHz at Position RL3, balun feed**

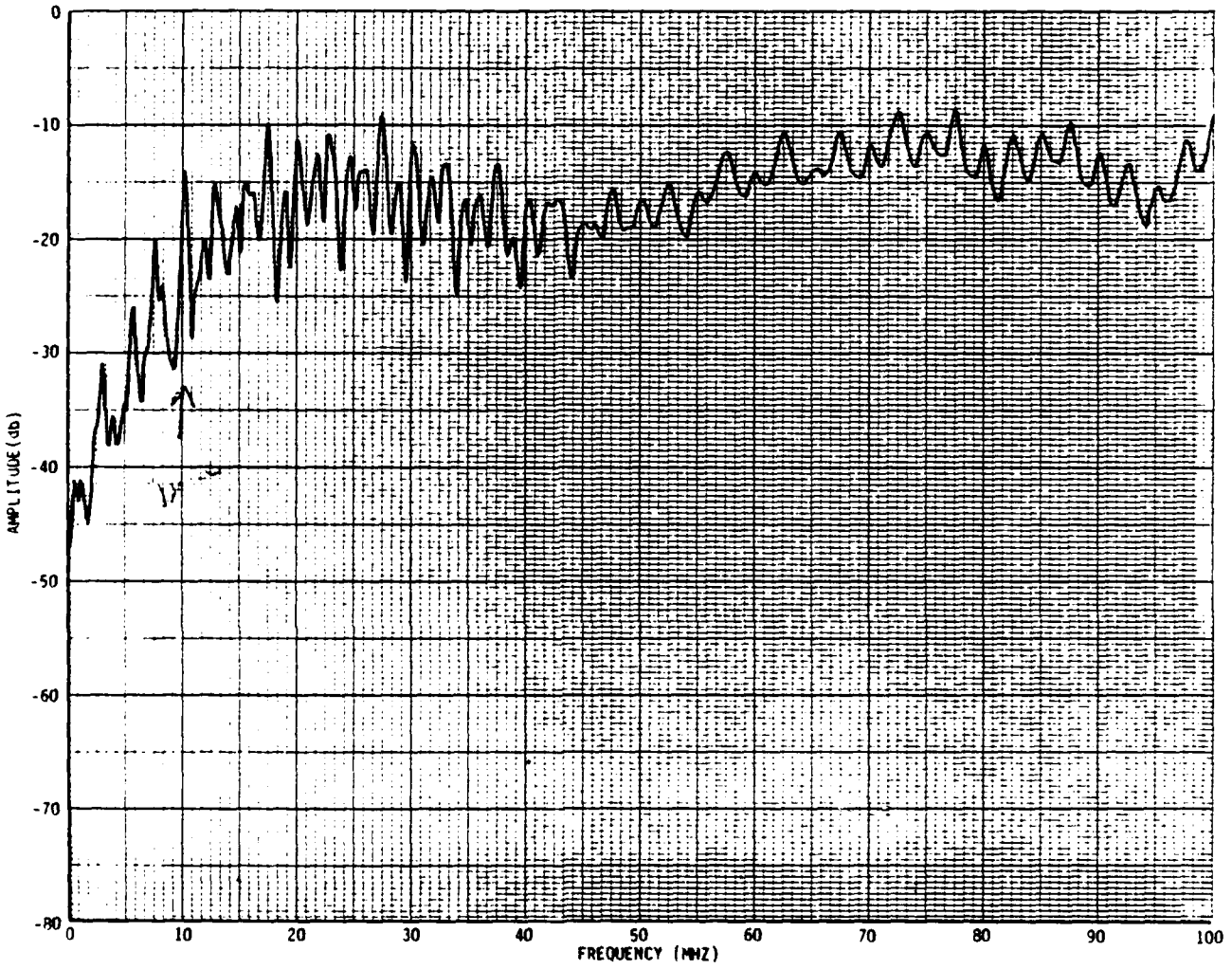


**Figure 4.13. B 1-100 MHz at Position RR3, balun feed**

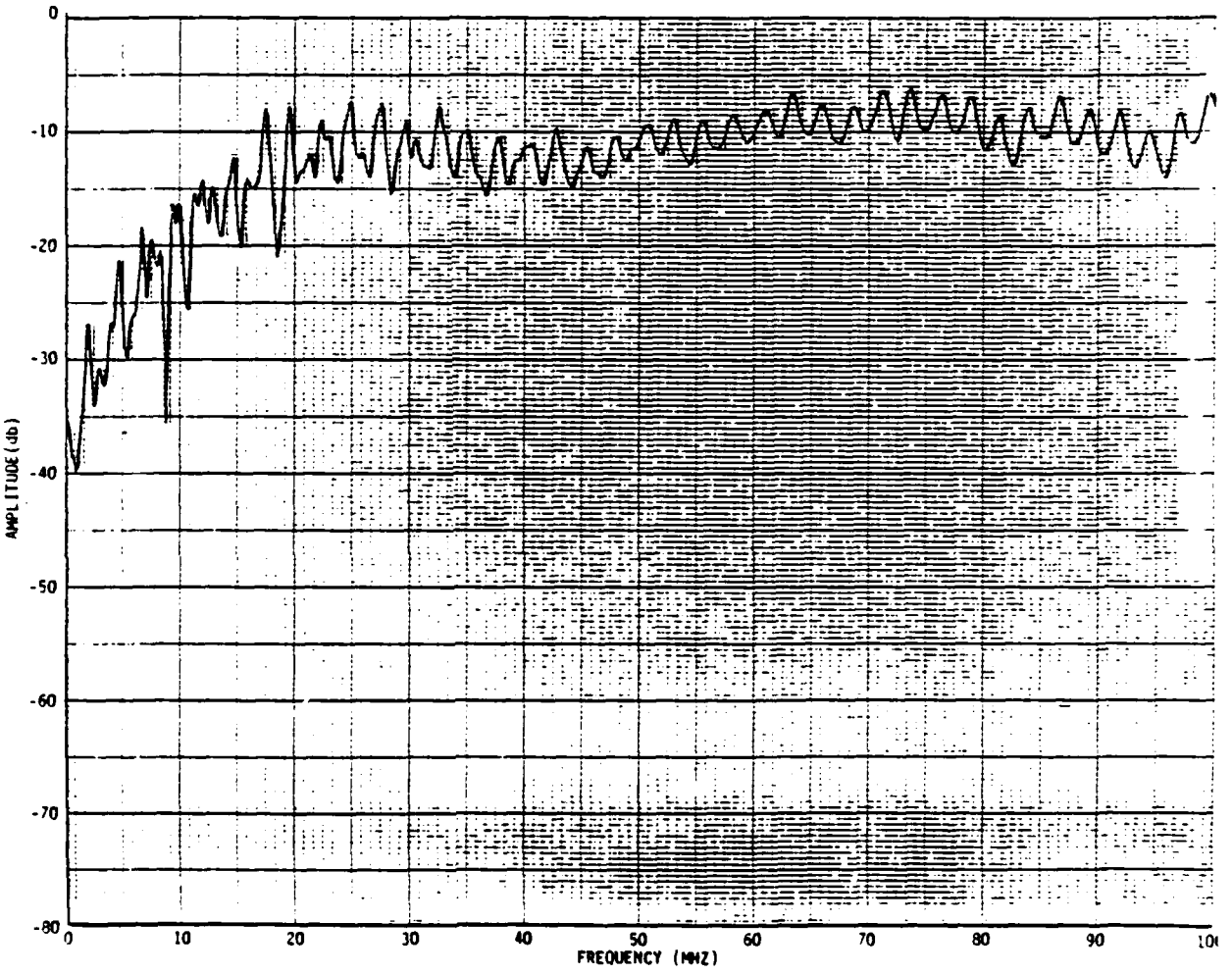


**Figure 4.14. B 1-100 MHz at Position RL4, balun feed**

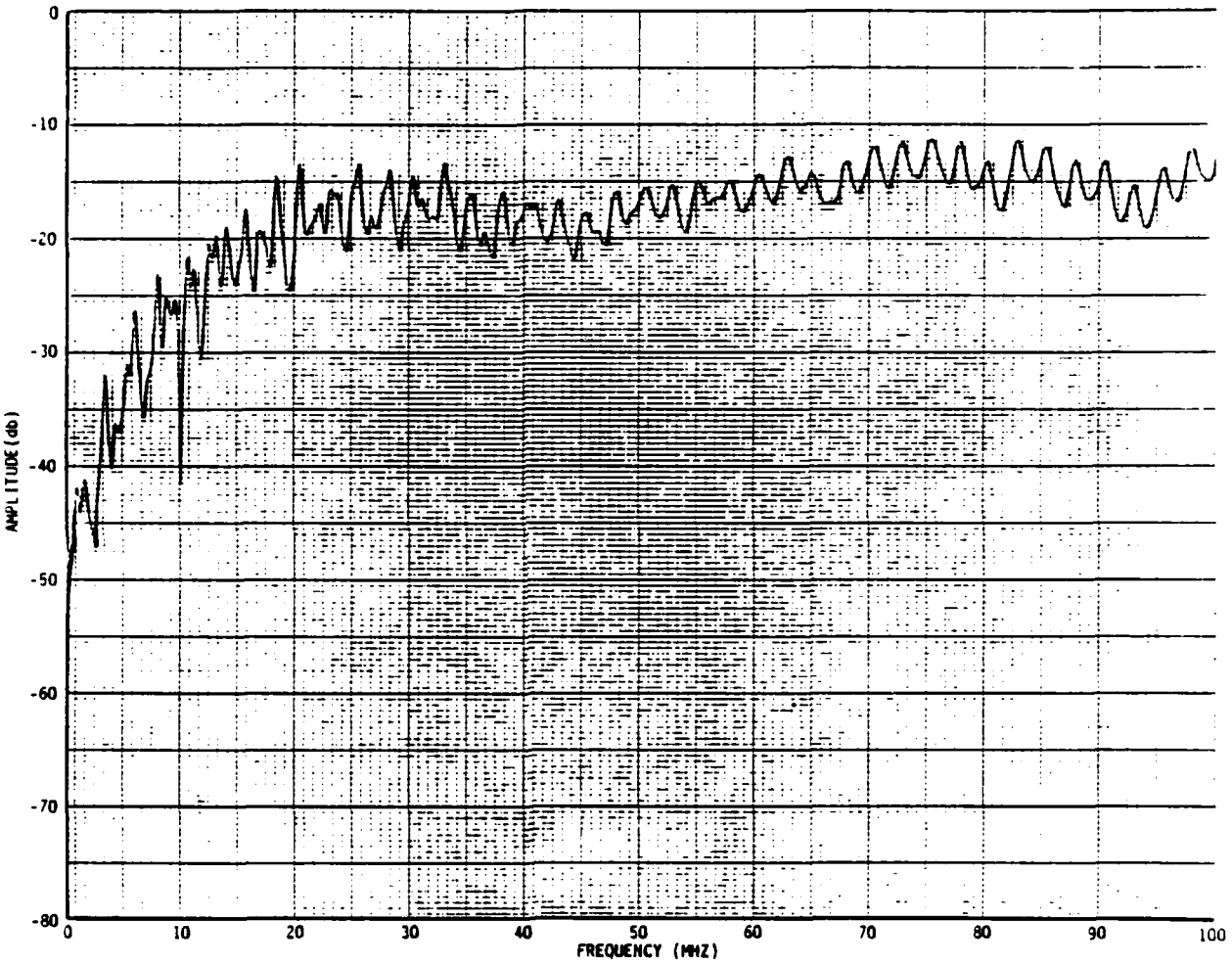


**Figure 4.15. B 1-100 MHz at Position RR4, balun feed**

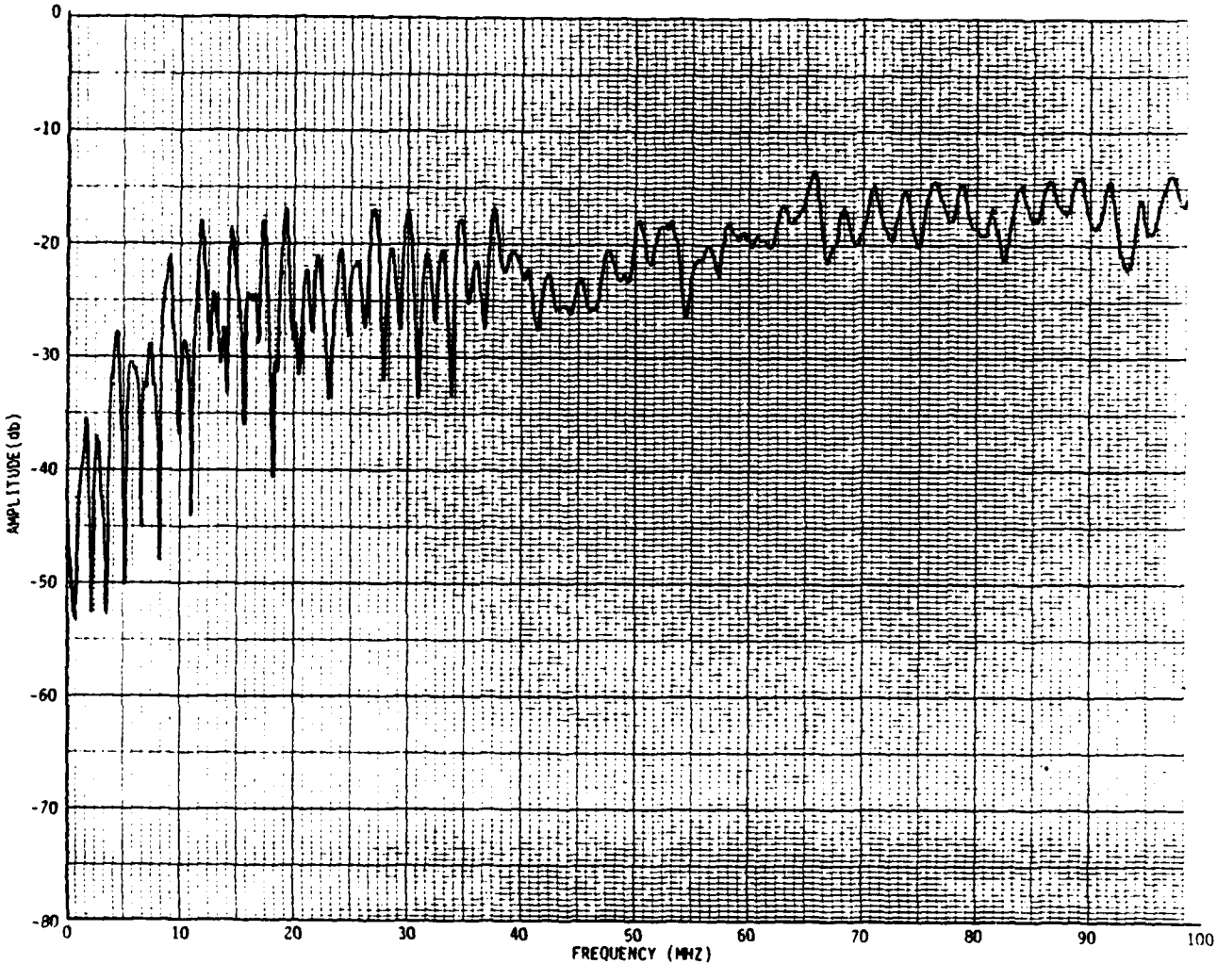


**Figure 4.16. B 1-100 MHz at Position RL5, balun feed**

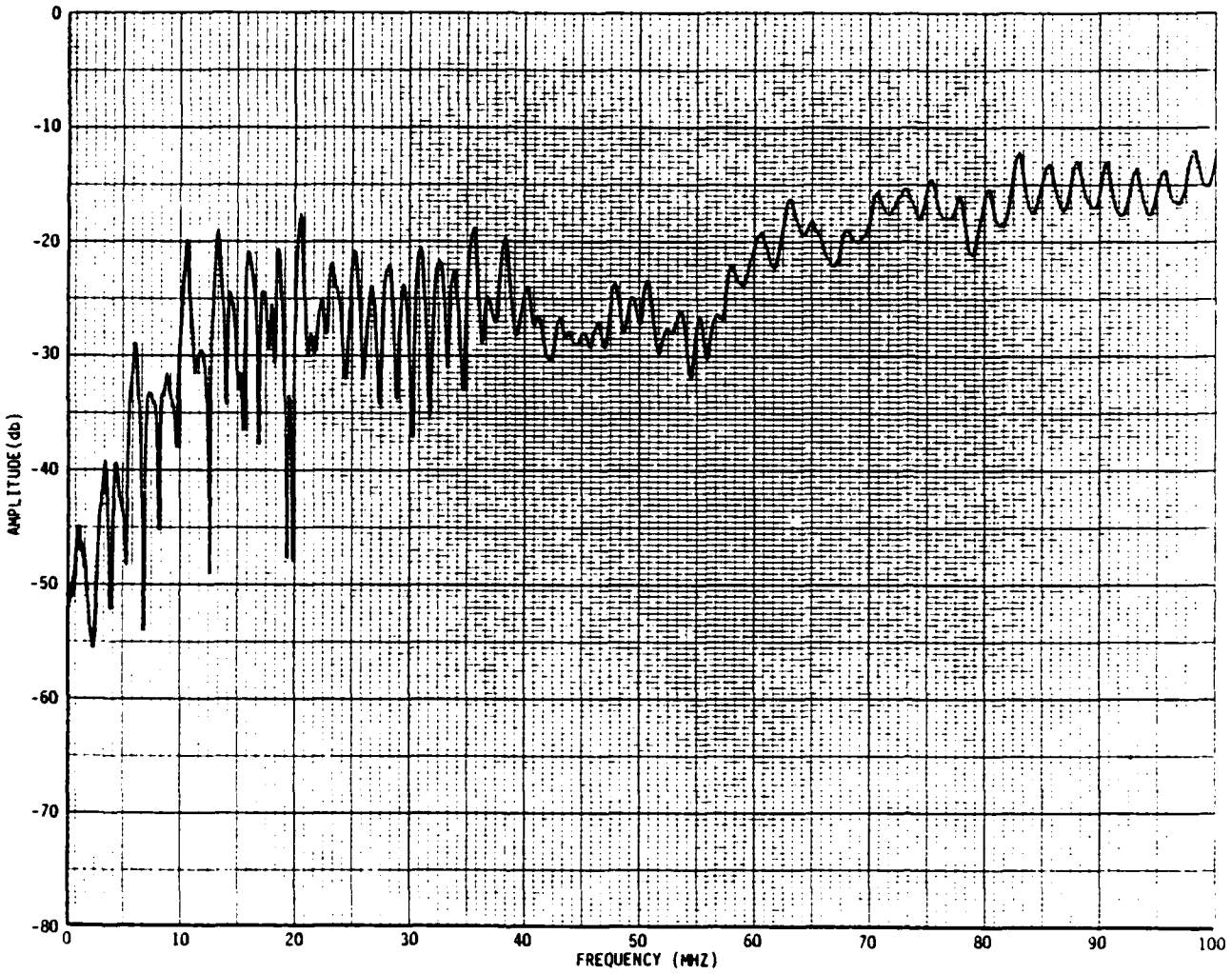


**Figure 4.17. B 1-100 MHz at Position RR5, balun feed**

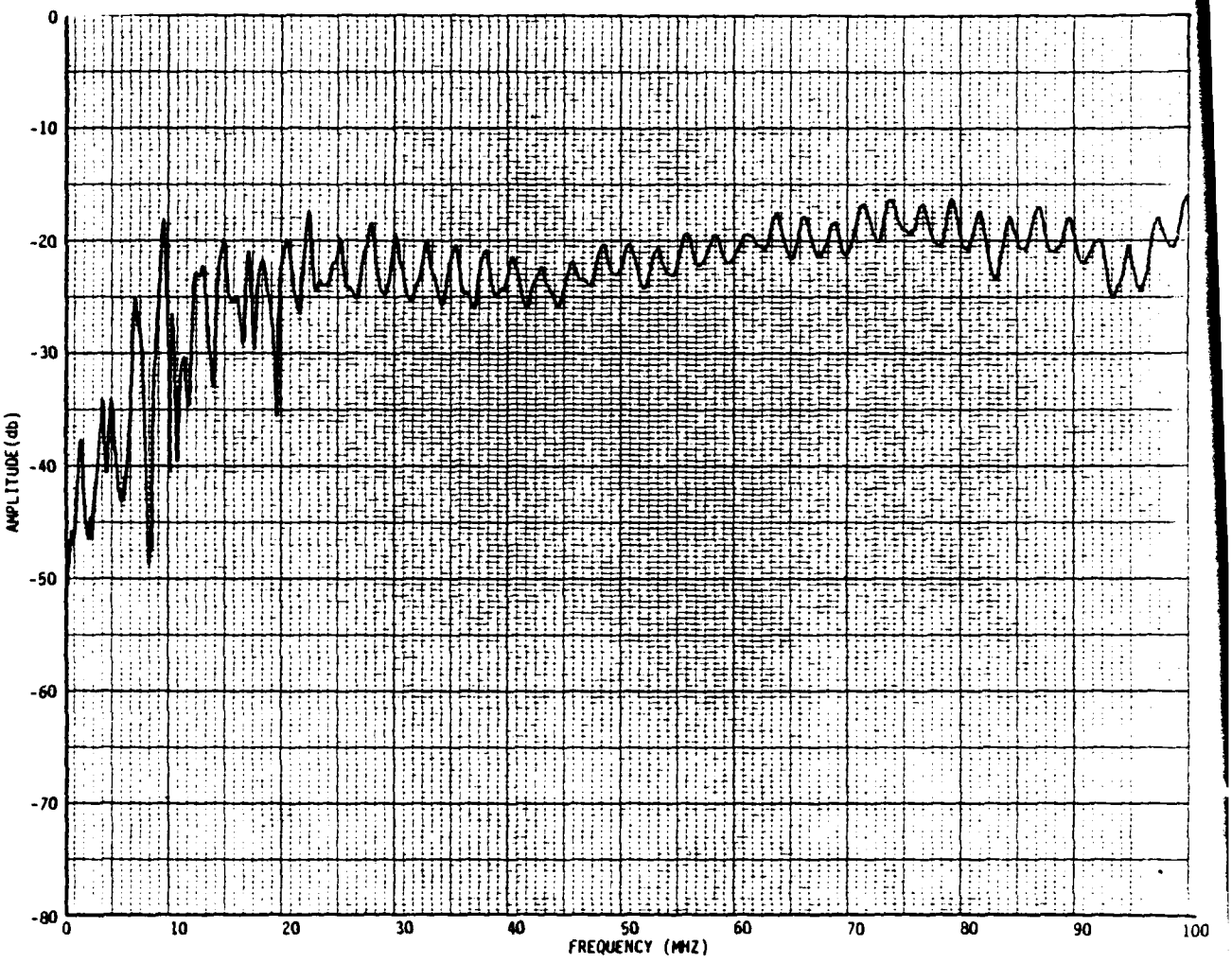


**Figure 4.18. B 1-100 MHz at Position RL6, balun feed**

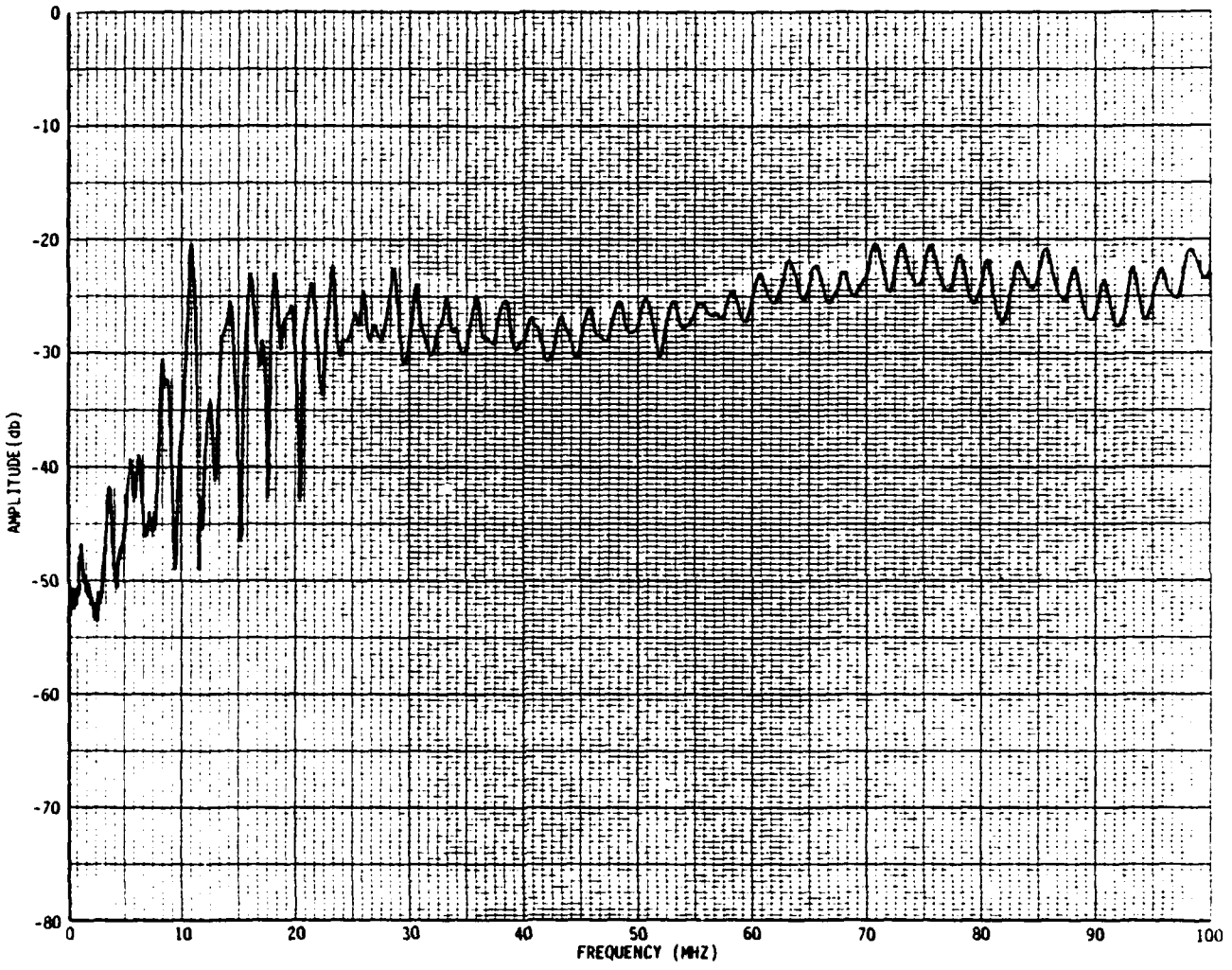


**Figure 4.19. B 1-100 MHz at Position RR6, balun feed**

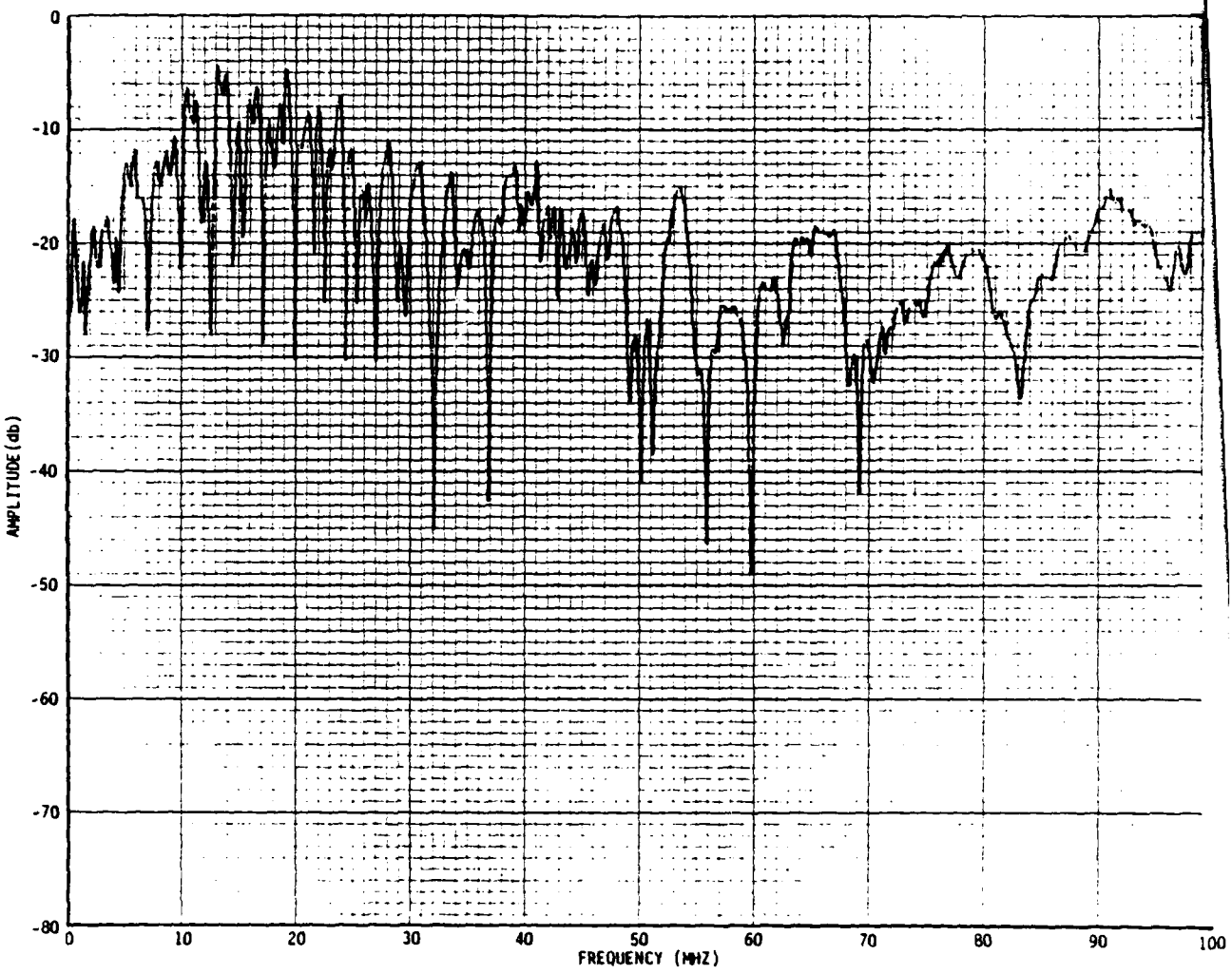


**Figure 4.20. B 1-100 MHz at Position RL2, end feed**

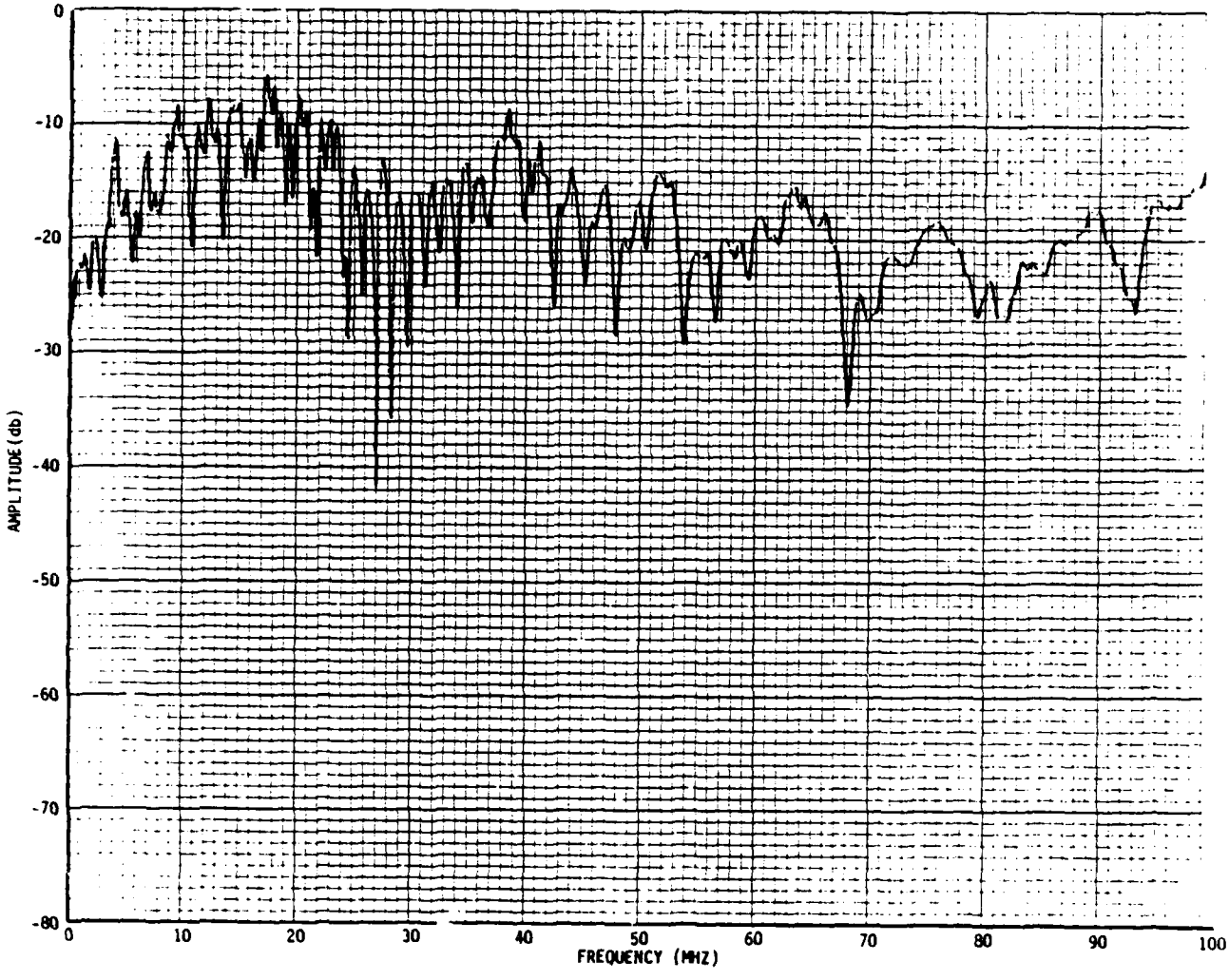


**Figure 4.21. B 1-100 MHz at Position RR2, end feed**

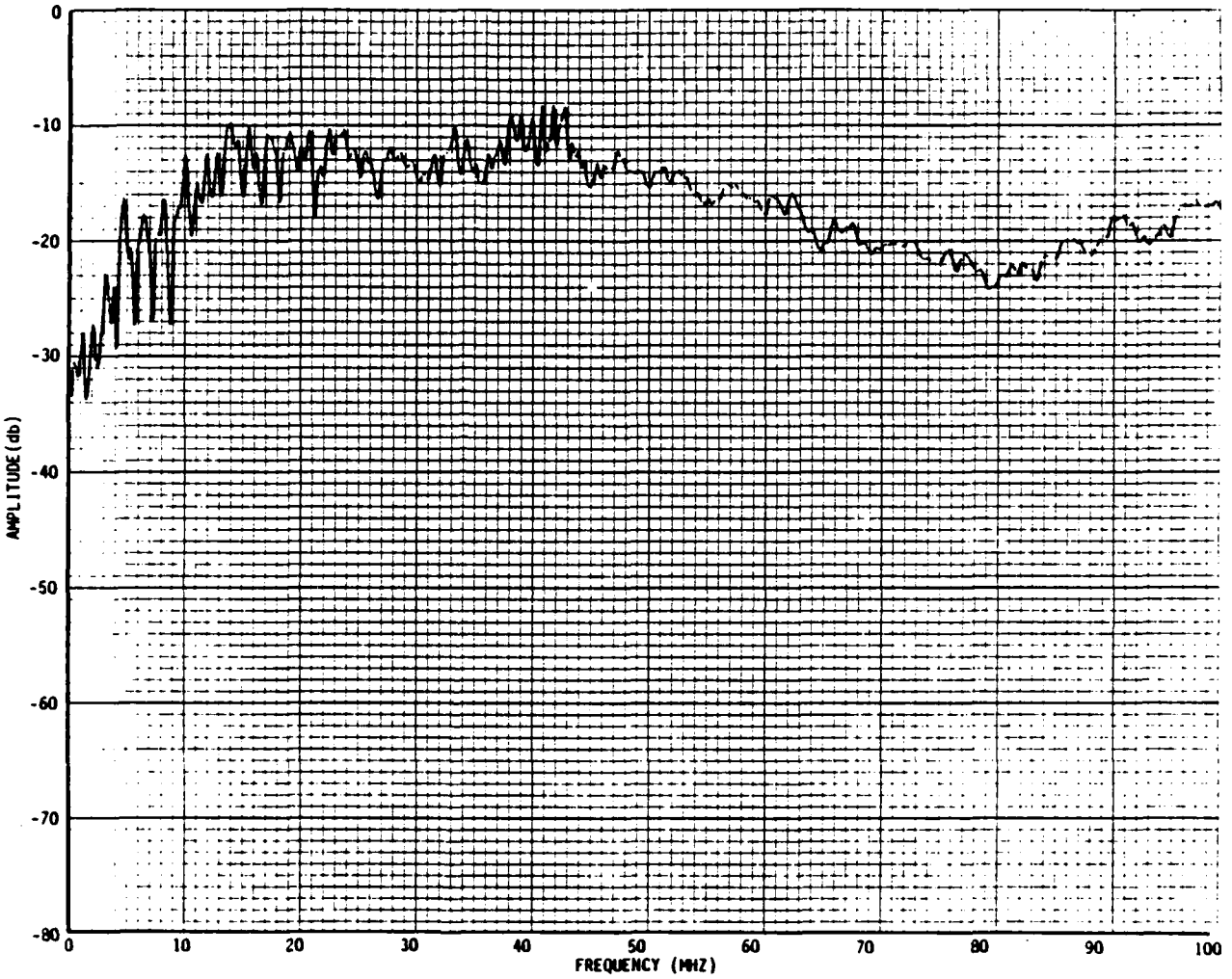


**Figure 4.22. B 1-100 MHz at Position RL4, end feed**

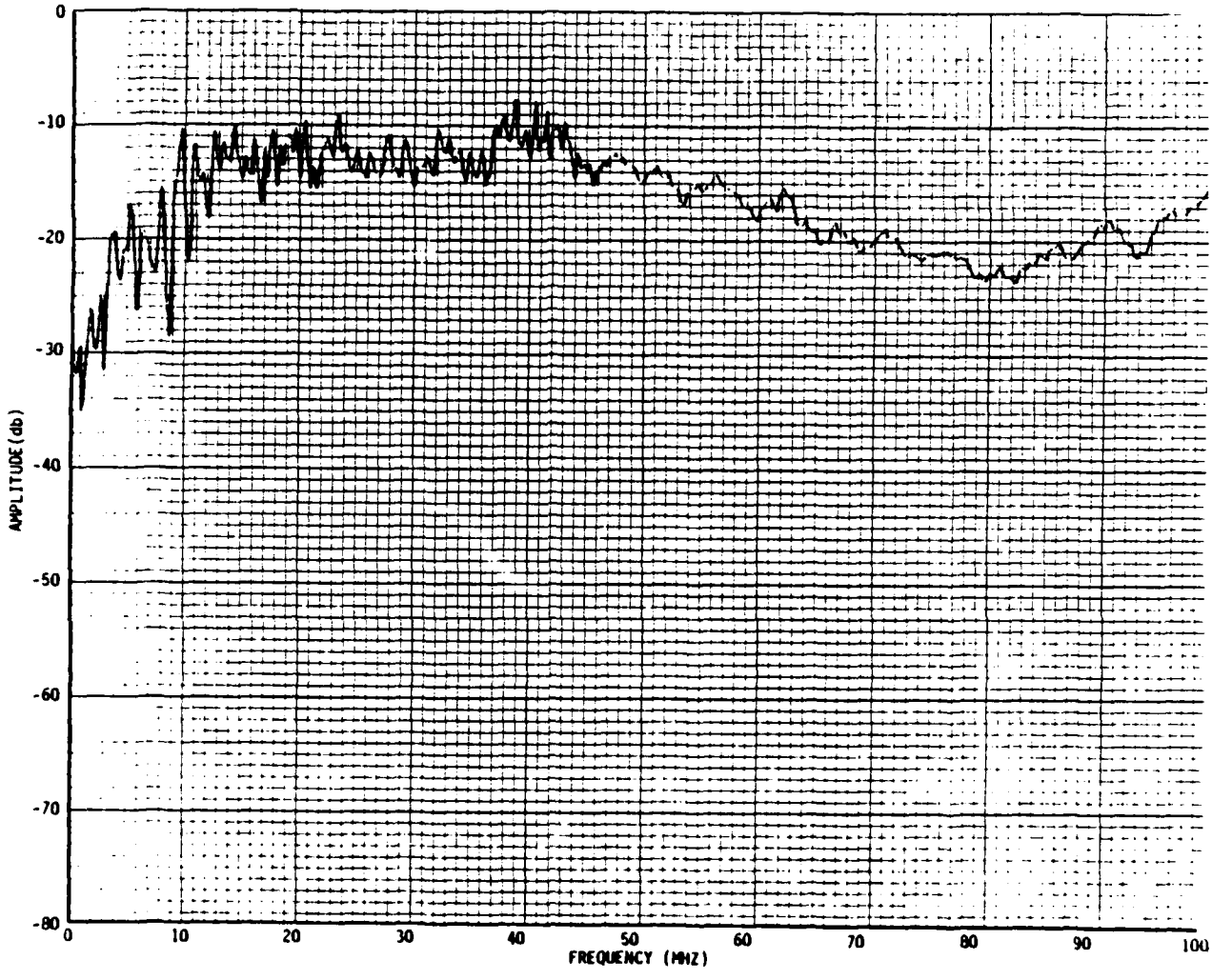


**Figure 4.23. B 1-100 MHz at Position RR4, end feed**

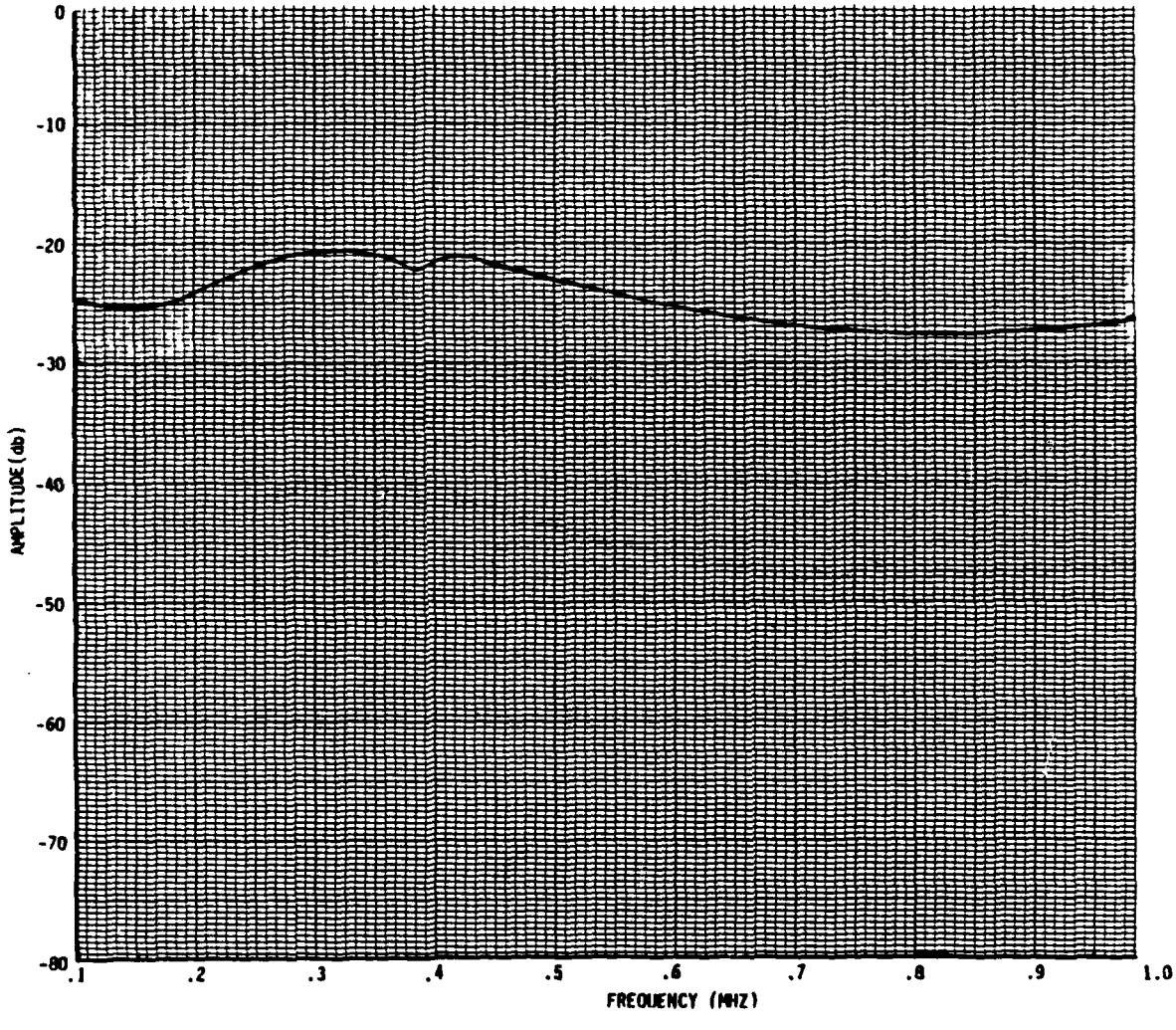


**Figure 4.24. B 100 kHz - 1 MHz at Position R, balun feed**

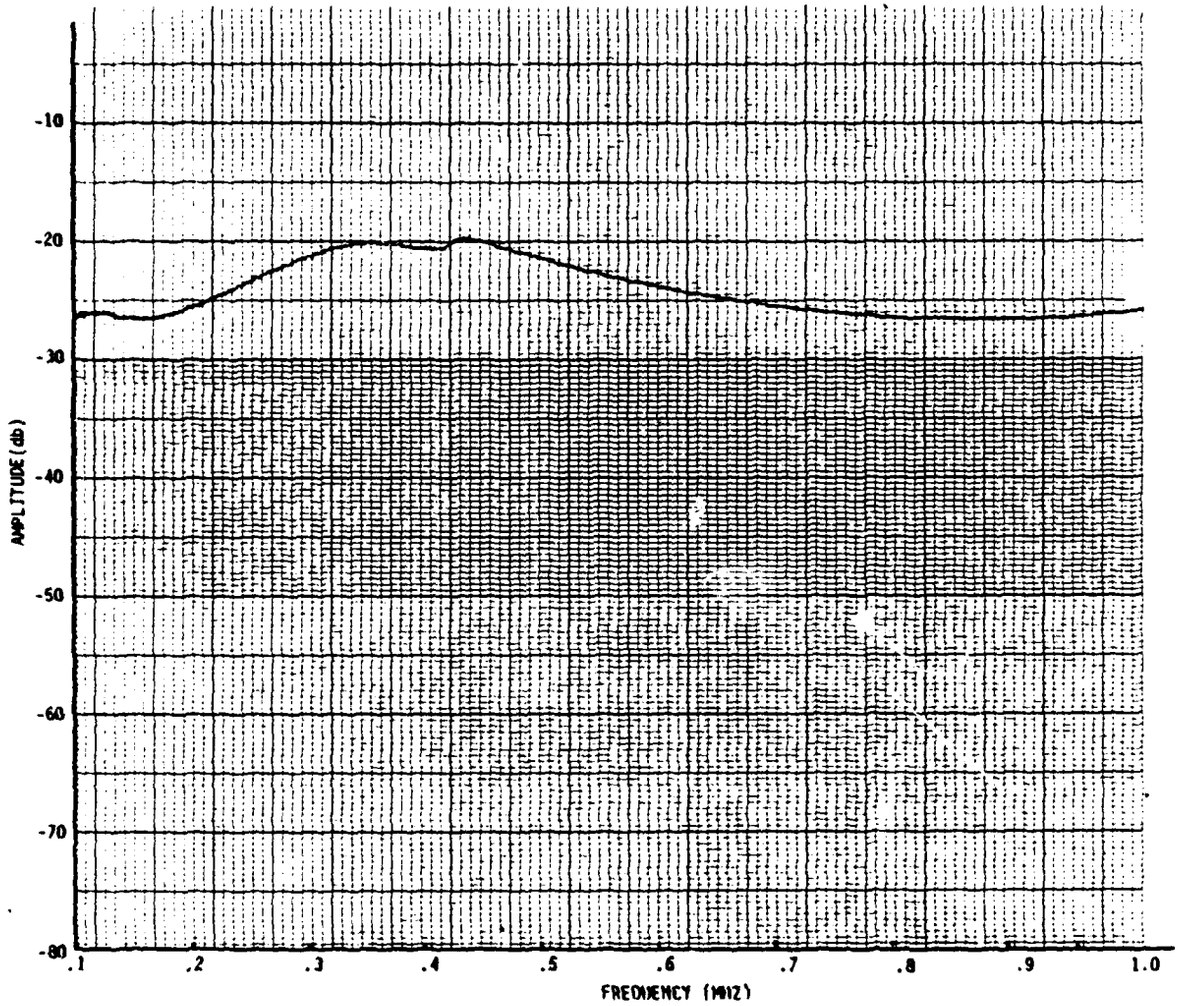


**Figure 4.25.** B 100 kHz - 1 MHz at Position RL1, balun feed

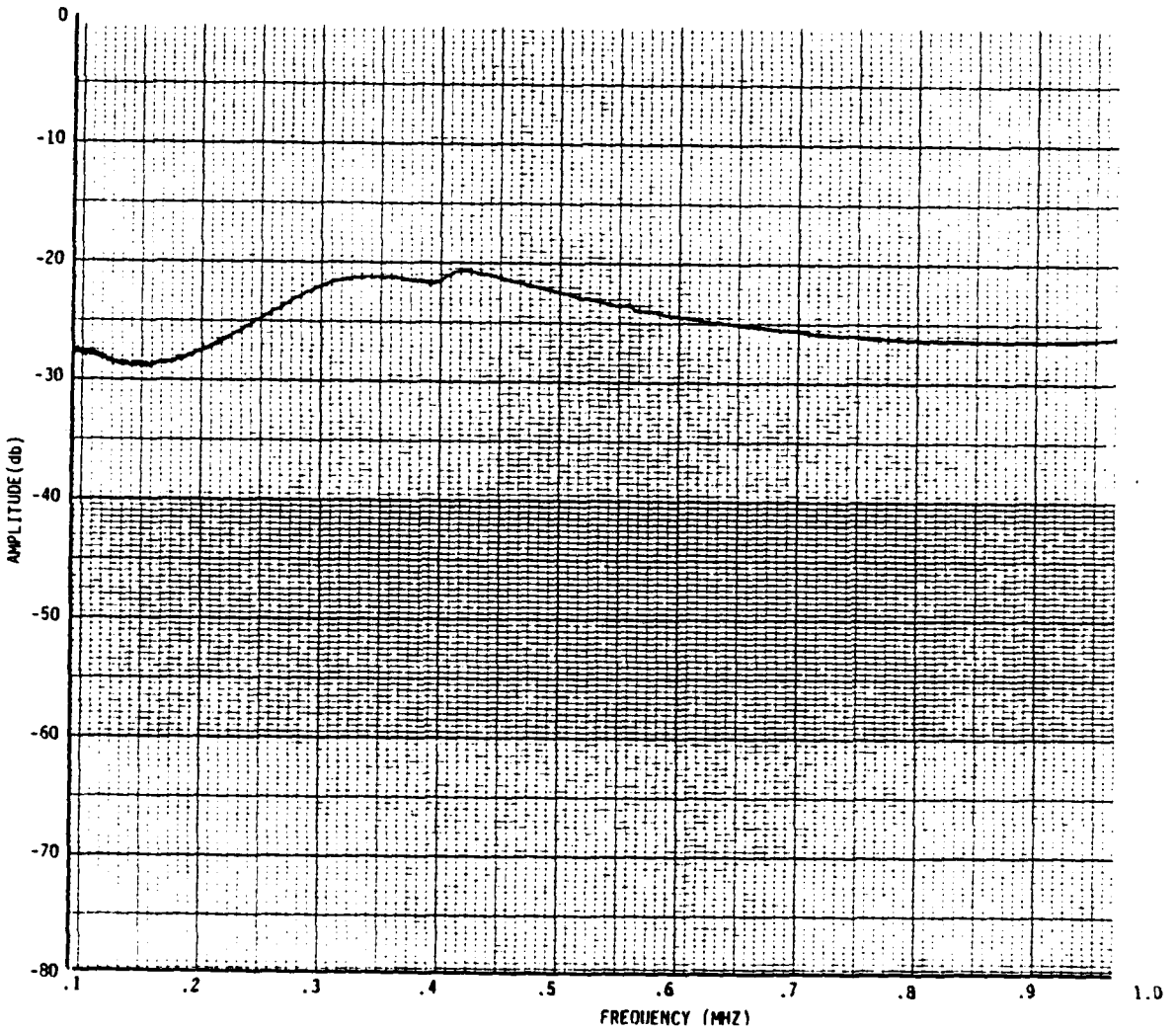


Figure 4.26. B 100 kHz - 1 MHz at Position RL2, balun feed

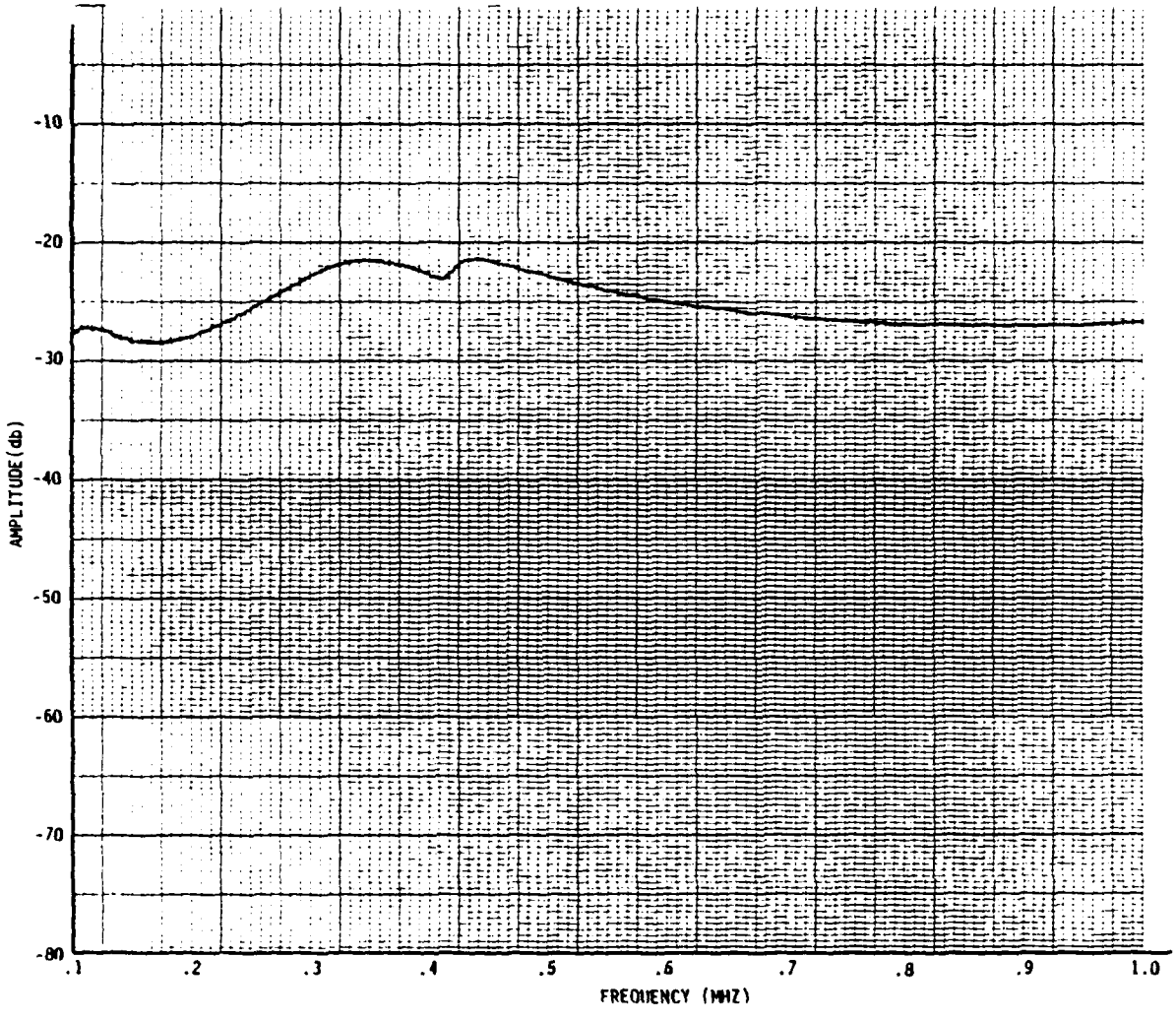


**Figure 4.27. B 100 kHz - 1 MHz at Position RR2, balun feed**

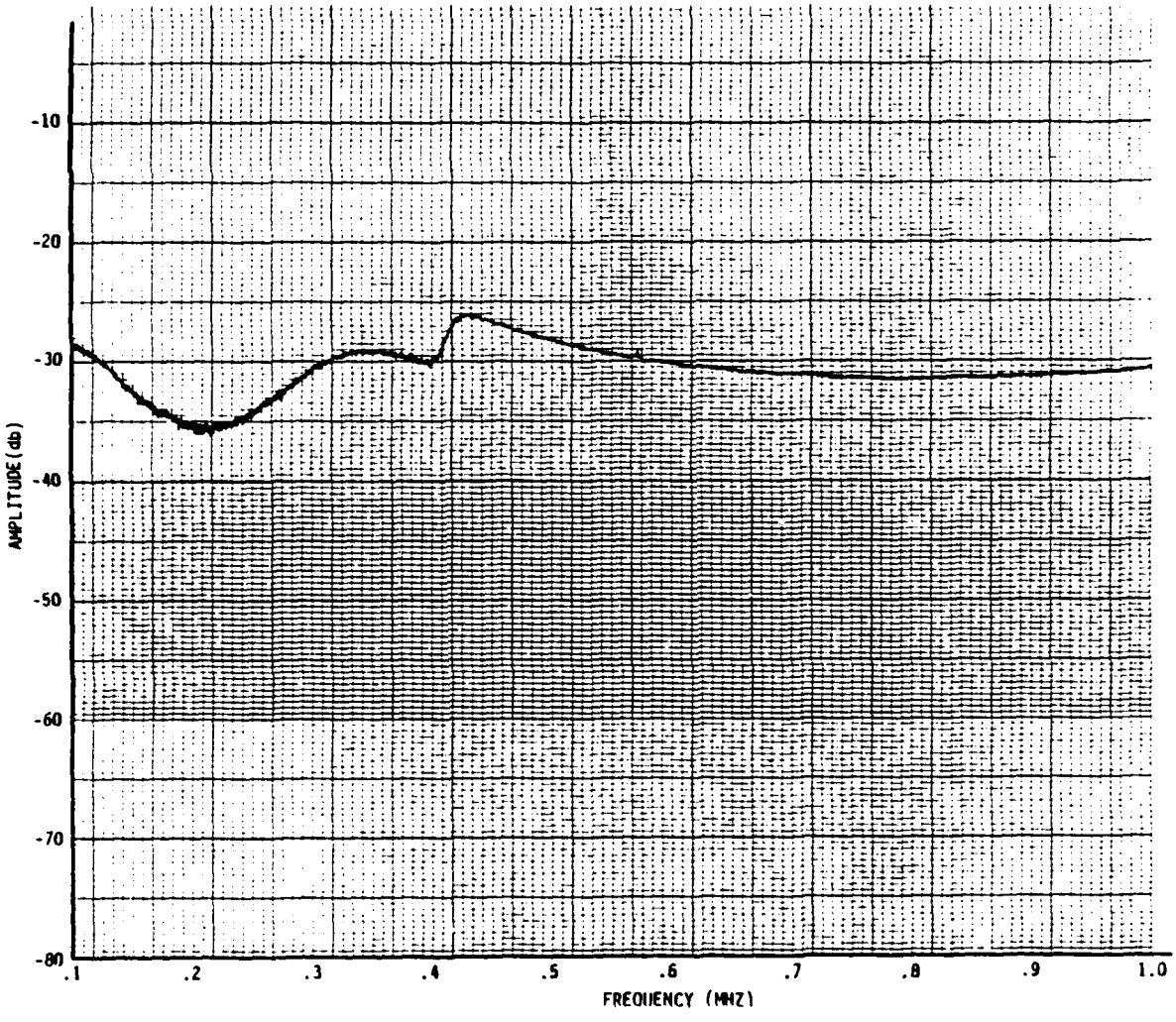


**Figure 4.28. B 100 kHz - 1 MHz at Position RL3, balun feed**

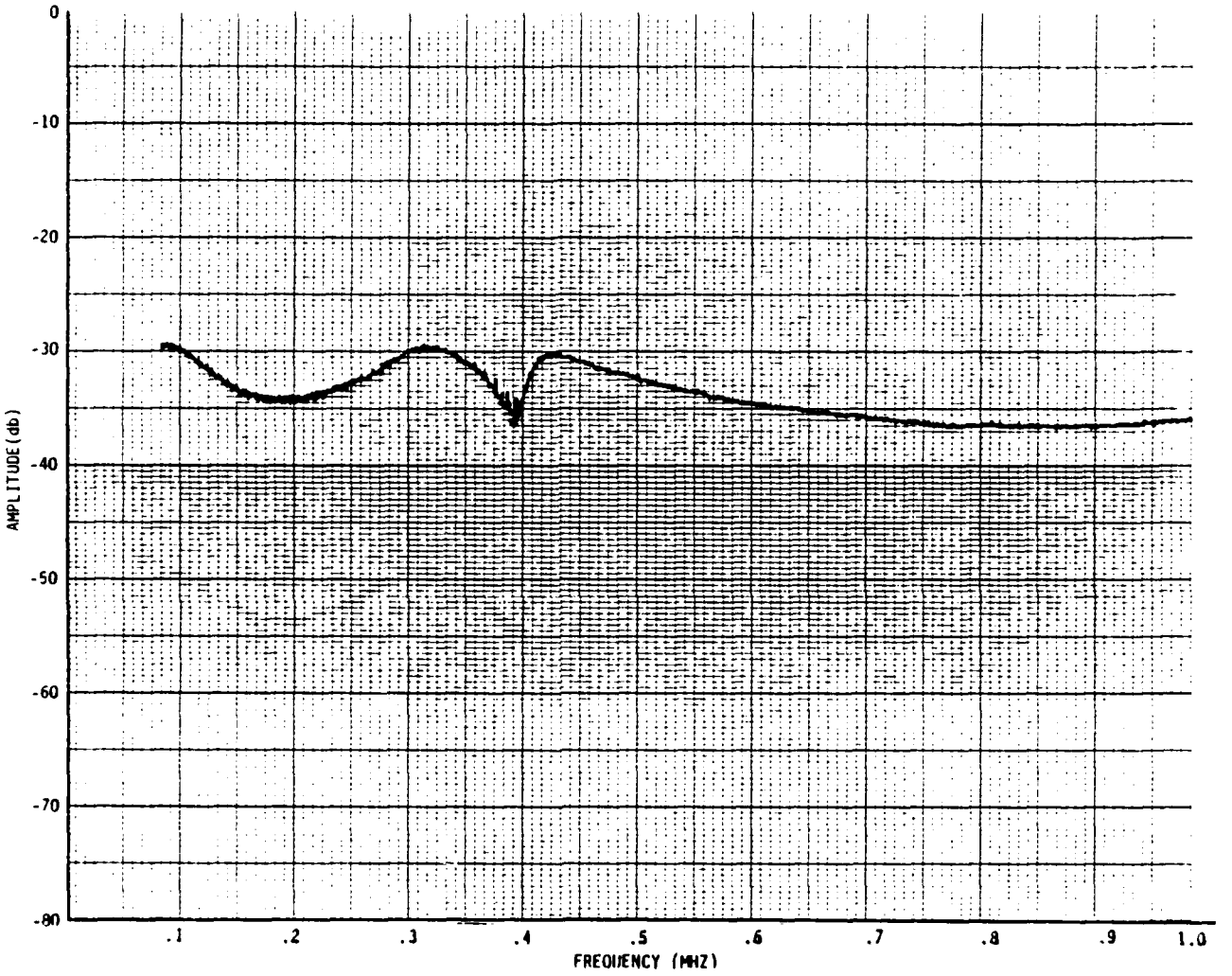


**Figure 4.29. B 100 kHz - 1 MHz at Position RL4, balun feed**

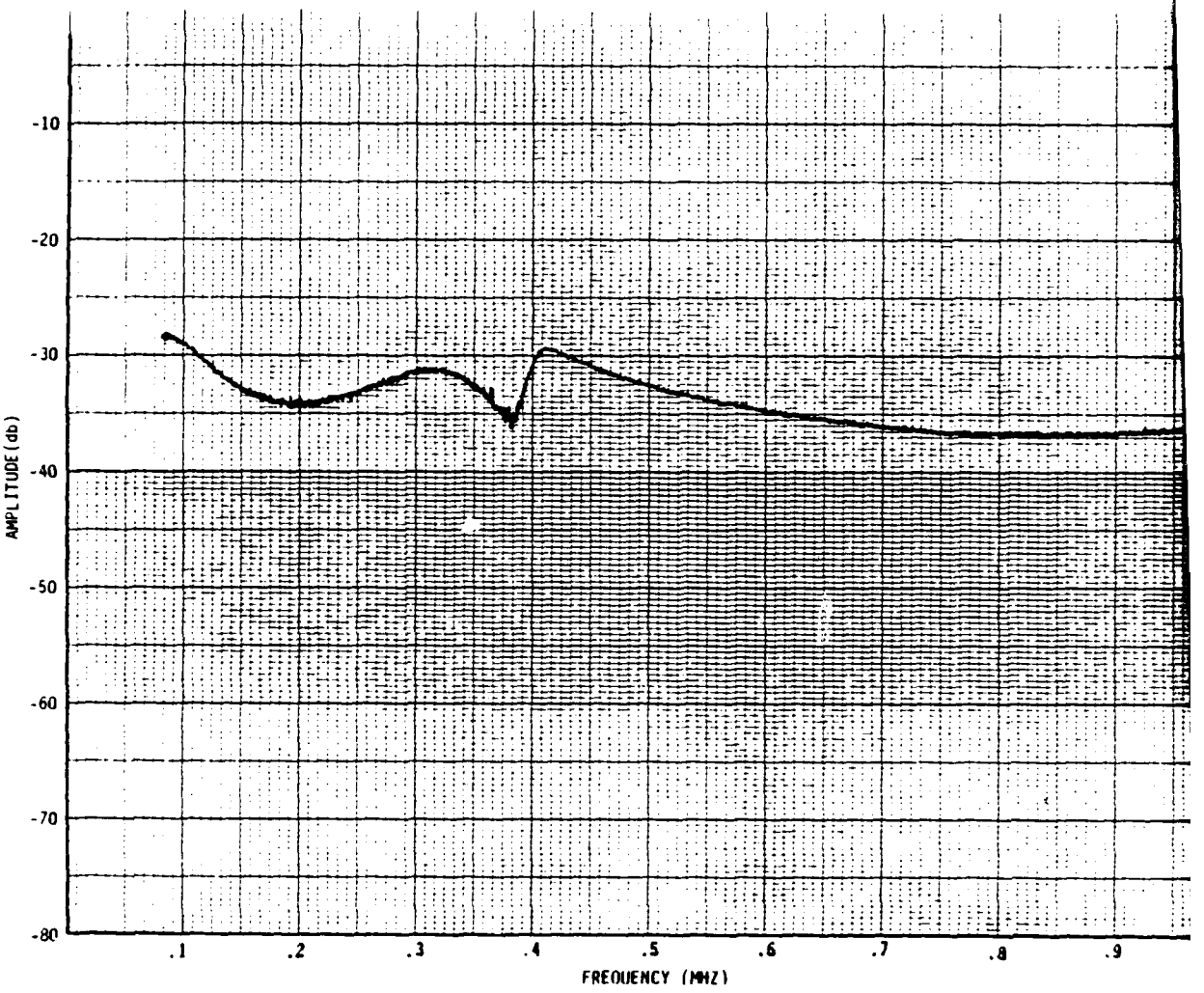


Figure 4.30. B 100 kHz - 1 MHz at Position RR4, balun feed

# APPENDIX A

# ANTENNA DRAWINGS

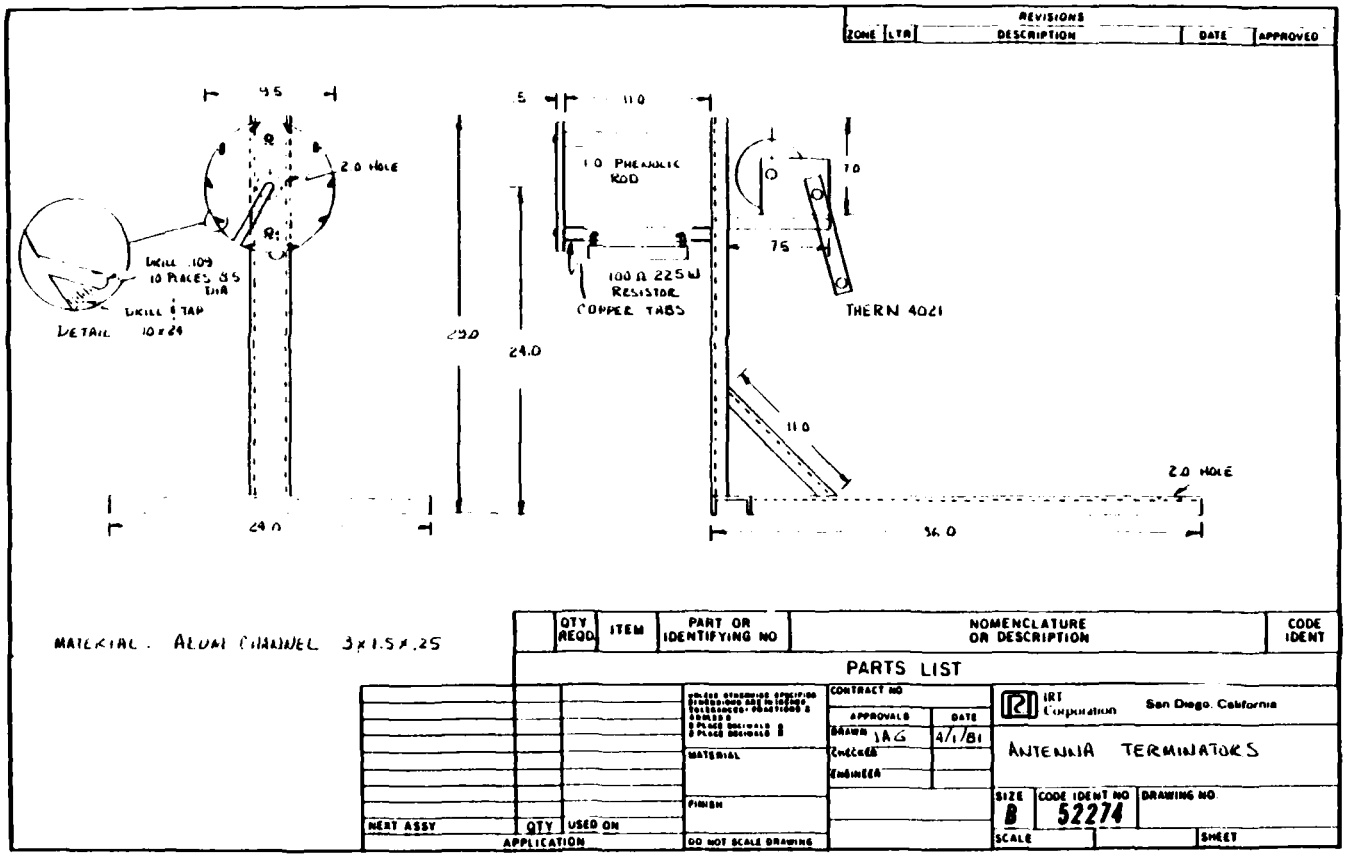


**Figure A.1. Antenna Terminator Assembly**

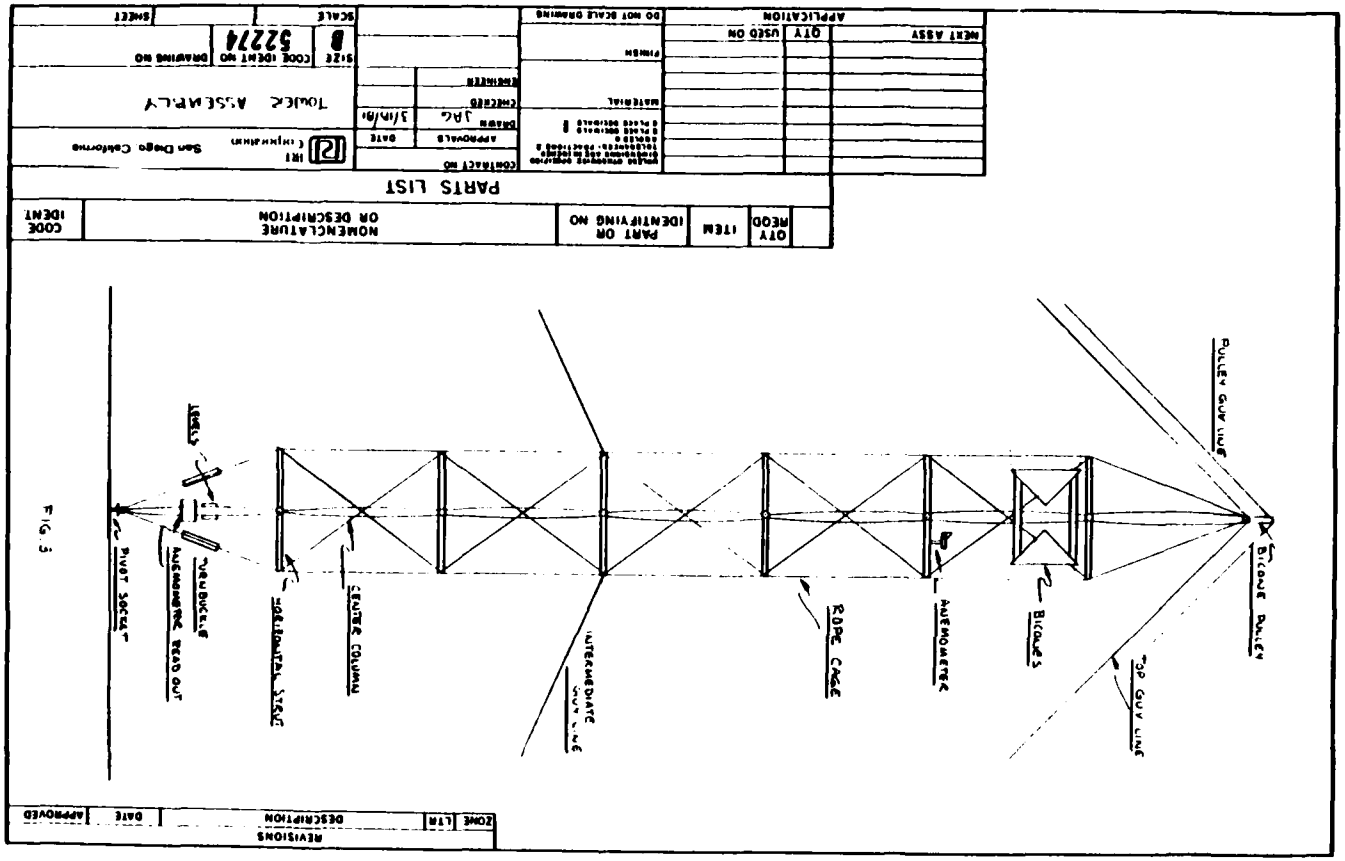


Fig. 3



**Figure A.2. General Dielectric Tower Assembly with Bicones shown in place.**

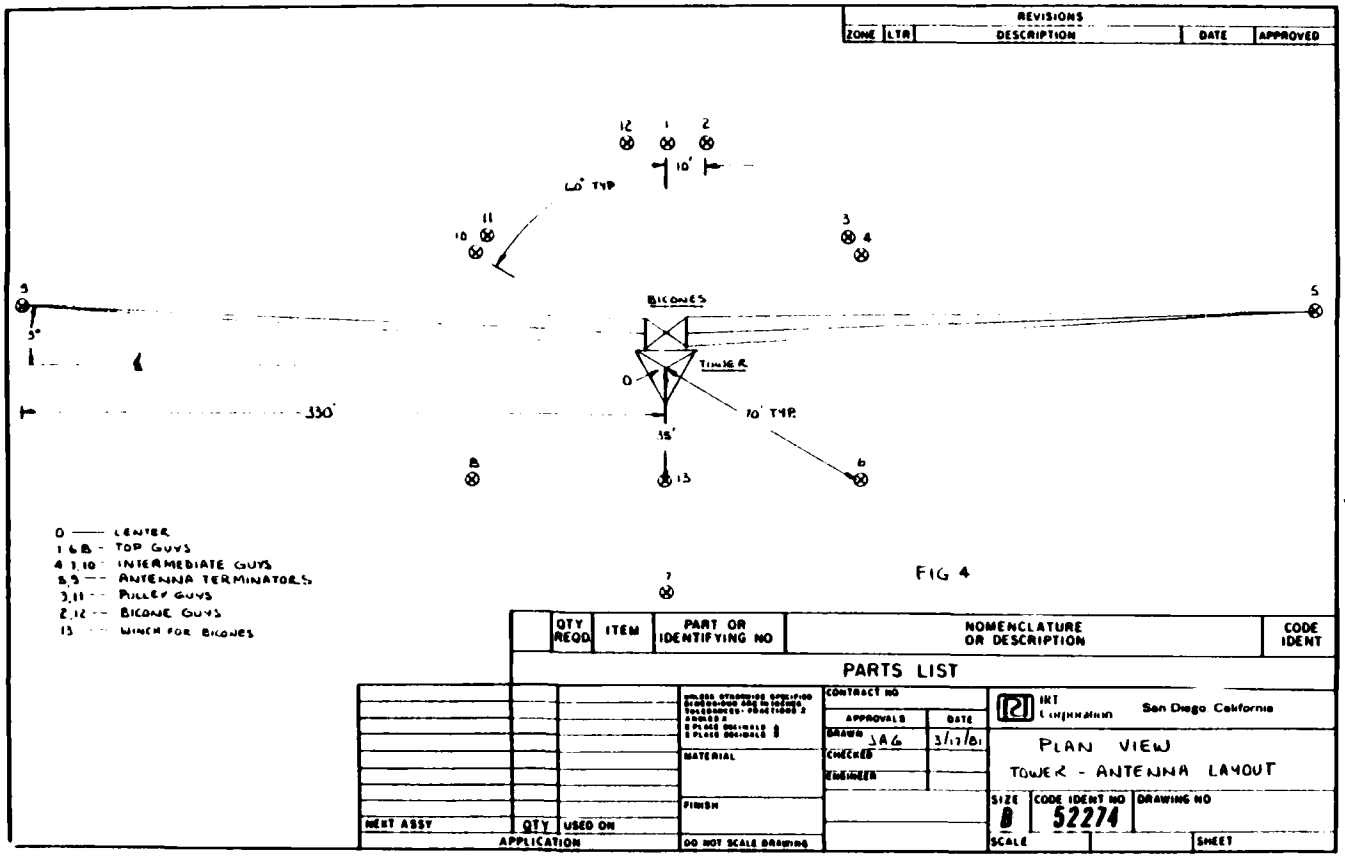


**Figure A.3. Antenna/Antenna Tower and Support Equipment Layout.**

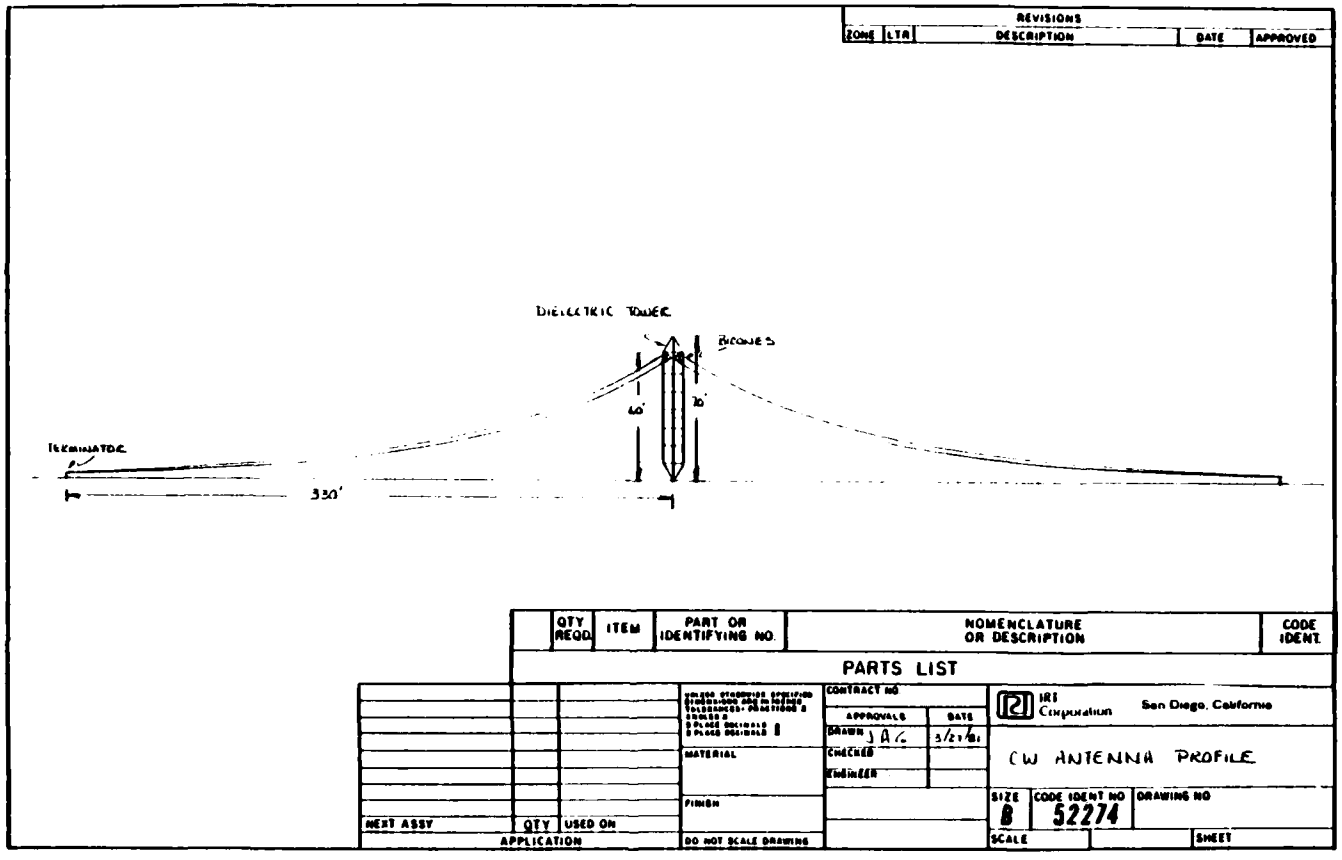


**Figure A.4. CW Antenna and Dielectric Tower Profile in fully erected position.**

## APPENDIX B

## ANALYSIS OF DIELECTRIC TOWER

This Appendix includes an analysis of the dielectric tower performed by ABAM Engineering, Incorporated of Tacoma, Washington. The analysis was made on the tower as originally fielded and tested. The results of the analysis and testing showed that some modifications to the design were necessary in order to give the tower a sufficient design safety margin. The modifications suggested by ABAM were made to the tower, and the final fielded version performed and has continued to perform quite admirably.

### METHOD OF ANALYSIS

No drawings exist for the tower. Tower geometry, member sizes and materials are assumed, based on information obtained over the telephone from Tom Buckman and Larry Bosch. Physical properties of the various materials are not documented. Therefore, reasonable properties representative of such materials are assumed.

Simplifying assumptions are made to minimize the time and cost of the analysis. In some cases, the structure is first assumed to be a plane truss and then correction factors are introduced to account for the third dimension. Reasonable assumptions, such as assuming equal and opposite stresses in a pair of diagonals, are used to make the structure determinant for purposes of analyses. Alternatively, some analyses are made with sufficient members assumed slack, to make the structure determinant.

The analysis is confined to short-term behavior under static loads, with wind load being taken as a static load. No attempt has been made to evaluate the long-term behavior of the materials under exposure to the elements. Also, no analysis of the joints and connections was made, as sufficient information on the cements and other materials is not available.

### SAFETY FACTORS

The Electronic Industry's Association Standard RS-222-A, Structural Standards for Steel Antenna Towers and Antenna Supporting Structures, refers to AISC specifications which give allowable stresses producing a safety factor of about 1.7. The safety factor for guys is given as 2.5 in the EIA standard. Safety factors for other materials are not spelled out.

It would be reasonable to assume that fiberglass materials should be utilized with a somewhat higher factor of safety than steel because of their lack of ductility. We suggest a minimum safety factor of 2.0 for the tower elements. This includes the mylar ropes used in the tower construction itself. The guys, however, which have unknown stresses from vibrations, etc., should have a minimum 2.5 safety factor as called for in the standard.

## BEHAVIOR AS PREVIOUSLY ERECTED

The tower is composed of four main structural elements: the central spine, radians, corner cables, and diagonal and belt cables. The estimated strengths of these elements as controlled by either buckling or breaking is as follows:

- Spine 1,350 lbs.
- Radian 1,390 lbs.
- Corner Cables 3,000 lbs.
- Diagonals & Belts 1,300 lbs.

See Pages 1 and 2 of calculations.

Analysis under various loading conditions indicates that the stress in the radians, diagonals and belts is generally low, and that controlling stress conditions are those in the spine and corner cables. Since the strength of each corner cable is twice that of the spine, and there are a total of three corner cables, controlling strength conditions are almost always governed by the strength of the spine as controlled by buckling over its 10-ft. length. When the tower is subjected to an axial load, i.e., a load aligned with the vertical axis of the tower, the great bulk of the load goes straight down the spine. The corner cables must have some pretension to stabilize the spine and this pretension will be slightly relaxed, with about 3 percent of the load going to relax pretension in each of the corners and 90 percent of the axial load going down the spine. See calculations, page 3.

In addition to the possibility of buckling of individual 10-ft. spine elements, there is also a possibility of overall buckling of the tower. If the pretension is sufficient to keep the corner cables taut during the application of axial load, the overall buckling strength of the tower is computed at 1,900 lbs. (See Page 4 of the calculations.) This is in excess of the 1,350-lbs. strength of the individual spine elements, and thus, the lower strength would control. However, if the pretension is insufficient to keep the corner cables taut, the stiffness of the tower is reduced by a factor of three when one corner

cable goes slack, reducing the overall buckling load of the tower to about 600 lbs. See Page 5 of the calculations.

When the axial load imposed on the tower is close to, but less than, the buckling load, the tower will exhibit a very flexible behavior with very small lateral (wind) loads producing very large deflections, as the tower would be close to instability under these conditions. We believe this is the primary cause of the difference in behavior when erected in North Dakota and New Mexico. In North Dakota, the tower was secured by three hand-held guys. Thus, the tension in the guys was limited. When erected in New Mexico, six guys were used, which were attached to tie-downs and tightened. If the tension in the guys were a little over 100 lbs. each, the vertical component of the six guys would approach 600 lbs. Since the corners were only pretensioned to about 50 lbs. each, it would take a relatively minor wind load to cause a corner to go slack under the high vertical load and the unstable condition would ensue.

Wind loads were computed using the EIA standards and are shown on calculation Page 6. Calculation Sheets 7 and 8 show stresses in terms of a unit wind load, P, for a system with pretension and for a system in which the corner cables are slack. If we assume that a corner cable goes slack, as the ultimate strength is approached, the compression in the core will be 24 P, as shown on Sheet 8. If we take 1,350 lbs. as the breaking buckling safety, the allowable load, P, at each node would be 28 lbs. Referring to Sheet 6 of the calculations, this would correspond to a wind velocity somewhat over 30 mph. However, the guys at the top of the tower will produce some vertical load which will reduce the load capacity in the spine available to resist wind load. We thus conclude that the safe wind load for a tower without intermediate guys will be about 30 mph, and the failure load would be roughly 45 mph. It should be noted that these allowable wind velocities are for the condition in which there are very little vertical load at the top of the tower. The effect of significant pretension in the guys can reduce the allowable wind velocity, as was described earlier. Also, the presence of the antenna system and its accessories will greatly affect these results as is discussed later.

## LOADS FROM ANTENNA

Although the antenna system appears to be quite light, the loads from the antenna have considerable structural effect on the tower. The dead weight of the bicones and antenna system is given as 150 lbs. in Tom Buckman's letter of March 28. Additionally, there is a vertical component of cable tension at each anchor point which we estimate

to be about 25 lbs. at each end. This creates an applied downward vertical load of 200 lbs. at the top of the tower, but the bicones and antenna are supported by a line going over a pulley at the top of the tower and then tied off at the tower base. This effectively doubles the vertical dead load applied at the top of the tower to 400 lbs.

The wind loads on the bicones and antenna system are considerable. In a 50 mph wind, the wind load on the bicones and antenna is computed at 371 lbs. applied at the top of the tower. Additionally, there is a 42-lbs. horizontal load from wind on the guys and additional loads from wind on the tower. (See Sheet 6.)

The wind pressure on the antenna wires creates additional tension in the wires estimated at over 2,000 lbs. total for the ten wires. See Calculation Sheet 11. This additional tension produces a substantial downward load on the top of the tower, estimated at 930 lbs.

## RECOMMENDATIONS FOR RE-ERECTING THE TOWER

Figure 1 shows the recommended configuration for re-erecting the tower to resist 50 mph winds with the antenna in place. We recommend using six guys attached to the top of the tower with the guy anchors being 80 feet from the base of the tower. Additionally, we recommend attaching three guys at the 30-ft. level. The layout of the guys and anchors with respect to the location of the antenna wires should be as shown in Figure 1. We recommend pretensioning the guys to a load of 100 lbs. per guy. This will allow some guys to go slack under the maximum wind load. However, we feel this is preferable to the use of a higher pretension in the guys, which would add to the loads on the tower.

Calculation Sheet 9 gives the load on the re-erected tower under the 50 mph wind. The vertical loads are considerable, amounting to approaximately one ton. The dead weight of the materials is little over 10% of this amount, but the loads due to pretension and wind on the antenna system produce in the high loads.

We recommend pretensioning the corner cables to 150 lbs. each to prevent their going slack under wind load conditions, which would reduce the buckling strength as previously noted. To satisfy these loads with a safety factor of 2.0, the spine elements should have an ultimate strength of about 500 lbs., which is roughly four times that of the present spine elements. Thus, new spine elements will be required to meet the conditions of 50 mph wind with antenna in place. As shown on Page 12, this could be done with a captive column using 3/8 corner rods in a triangular configuration with an

overall dimension of six inches. The other elements of the tower are adequate for the new loadings, however, an additional "belt" cable would be desirable at the 30-ft. elevation where the intermediate guys are attached.

## SUMMARY

The tower may be used in winds up to 50 mph provided stronger spine elements are used, and it is guyed as shown in Figure 1. The need for modification of the spine elements results primarily from the large loads which are applied at the top of the tower due to wind effects on the long antenna wires. The appearance of the modified spine elements will be little different from the previous elements. Although the weight of the tower will be increased somewhat, it will still be an extremely light structure.

PROJECT IRT TOWER SHEET NO. ___ OF ___

DES.

SUBJECT RECOMMENDED INSTALLATION JOB NO. 5/22/80

DATE

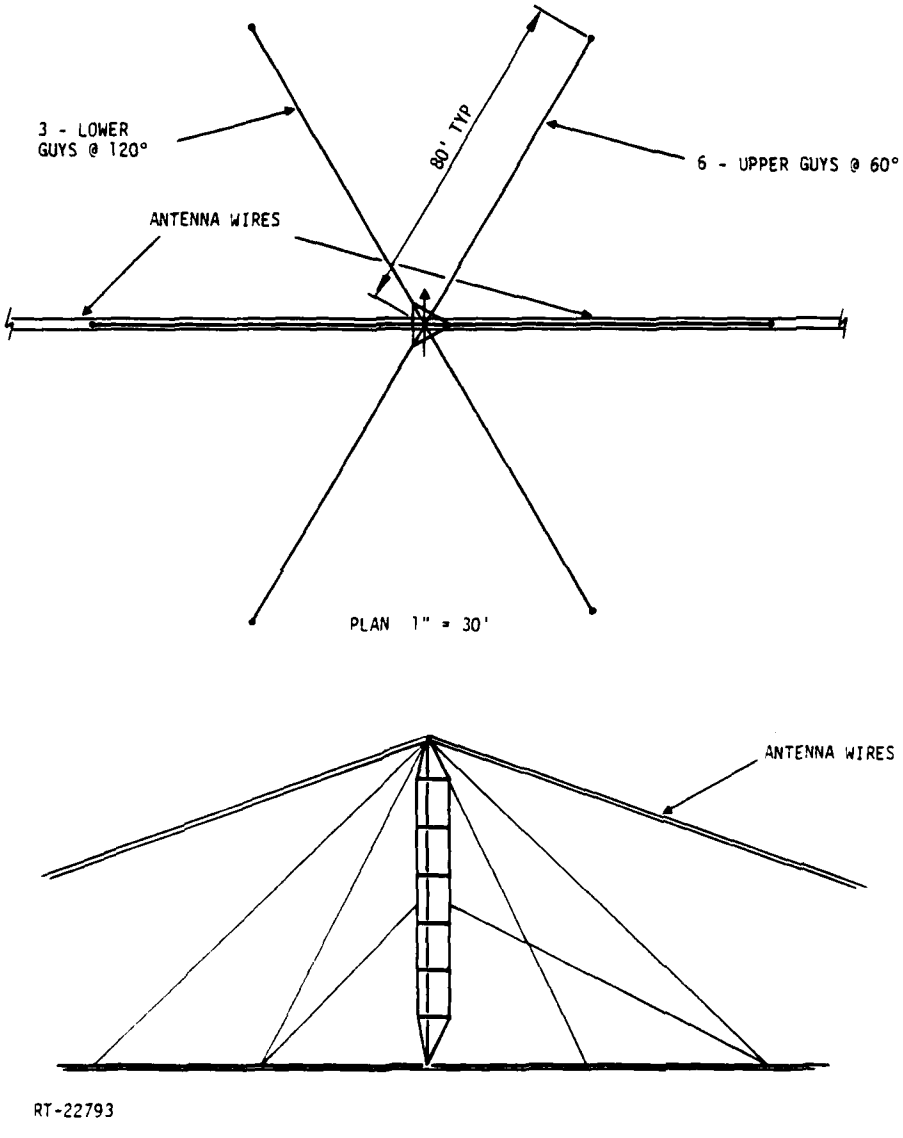


**Figure** 1.

PROJECT IRT TOWER SHEET NO. 1 OF 13

DES.

SUBJECT MEMBER PROPERTIES JOB NO. 4/15/80

DATE

## SPINE

- 10-ft. long captive column, tapered
- 3-1/4 in. fiberglas columns

$A = .049\ in^2$ (ea.)

$f_c = 50{,}000$ psi (assumed)

$E = 6{,}000{,}000$ psi (assumed)

$$I = 2 \times .049 \times \left(\frac{3.75}{2}\right)^2 = .345\ in^4$$

$P_{cr} = \Pi^2 EI/L^2 = 1417$ lbs.

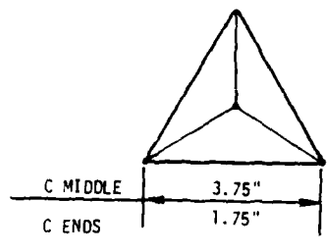


- Assume 5% reduction due to taper and shear flexibility

$P_{cr}$ = 1346 lbs. = Compressive strength of spine element, as governed by buckling

$AE = 3 \times .049\ in^2 \times 6{,}000{,}000 - 882{,}000$ lbs

$f = 1346/3 \times .045 = 9150$ psi

## RADIAN

- 5-ft. long square captive column
- 4-3/16 in. fiberglas columns

$A = .0276\ in^2$

$f_c = 50{,}000$ (assumed)

$E = 6{,}000{,}000$ (assumed)

$$I = 4 \times .0276 \times \left(\frac{1.75}{2}\right)^2 = .0846\ in^4$$

$P_{cr} = \Pi^2 EI/L^2 = 1391$ lbs.

$AE = 4 \times .0276 \times 6{,}000{,}000 = 662{,}000$ lbs.

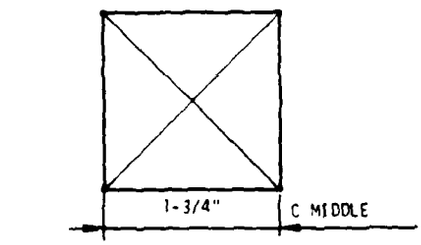


RT-22804

## CORNER CABLES

From U.S. Plastic Rope Catalog:

- 3/8-in. Mylar rope
- Strength = 3000 lbs. (breaking)
- AE = 2800 lbs./.0883 elongation = 31,700 lbs.

## DIAGONALS & BELTS

- 1/4-in. Mylar rope. Use $(1/4/3/8)^2$ of props for 3/8-in. rope
- Strength = 1333 lbs.
- AE = 14,100 lbs.

PROJECT IRT TOWER SHEET NO. 3 OF 13

DES.

SUBJECT AXIAL LOAD JOB NO.

DATE

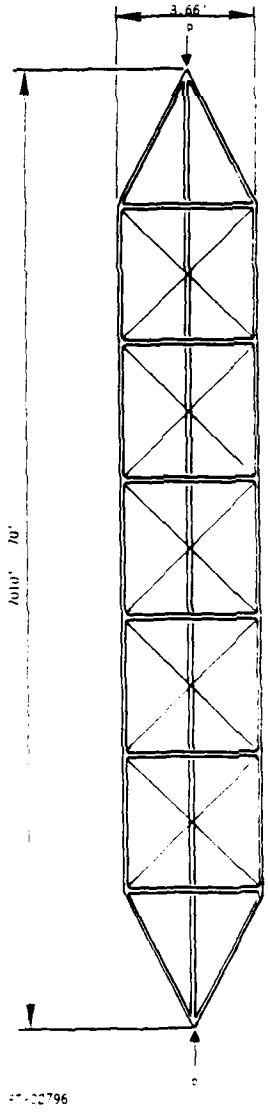


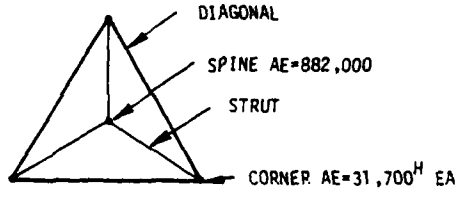


For a pretensioned system, assume spine & corners share load in proportion to AE.

$$\Sigma AE\text{'s} = 882{,}000 \text{ lbs.} + 3(31{,}700)^4 = 997{,}100$$

- Spine = 882,000/977,000 = 90.3%
- Corners = 31,700/977,000 = 3.2% (ea.)

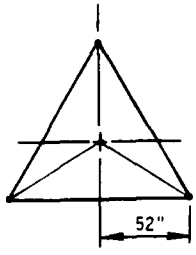


## ASSUME CORNER CABLES ARE TAUT.

3/8-in. Mylar rope

$AE = 31{,}700$ lbs.

$EI = 2 \times AE \times 52^2 = 1.71 \times 10^8$ lbs. $in^2$

$P_{euler} = \Pi^2 EI/L^2 = \Pi^2 \times 1.71 \times 10^8$ lbs. $in^2/840^2$ $in^2$

$P_e = 2398$ lbs

## EFFECT OF SHEAR FLEXIBILITY

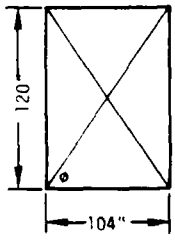


ϕ = 49.09°

RT-22803

Refer to Timoshenko, Strength of Materials, Part 2, pages 174-175

For X-bracing, there are two diagonals and no stress in belts. Thus, Equation 147 becomes:

$$P_{cr} = \frac{P_e}{1 + P_e} \left( \frac{1}{\sin\phi\cos^2\phi} \right) 2\,EA_d$$

$EA_d = 14{,}100$ lbs.

$$P_{cr} = \frac{2398 \text{ lbs.}}{1 + 2398 \text{ lbs.}/9141 \text{ lbs.}}$$

$P_{cr} = 1900$ lbs.

But: strength will be controlled by buckling of individual 10-ft. spine elements.

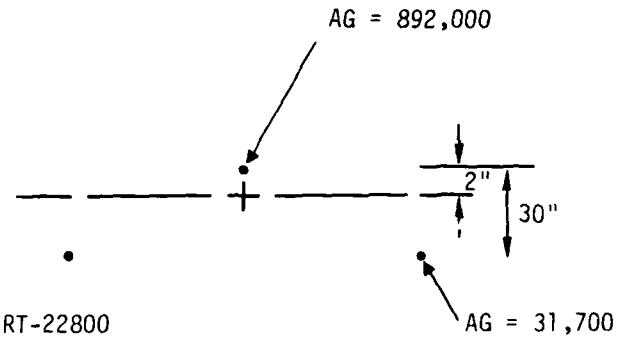


**WHAT IF A CORNER CABLE IS SLACK?**

$$C.G. = \frac{31{,}700 \times 2 \times 30 \text{ in.}}{882{,}000 + 31{,}700 \times 2} = 2.01 \text{ in.}$$

$$EI = 882{,}000 \times 2^2 + 2 \times 31{,}700 \times 28^2$$

$$EI = 5.32 \times 10^7$$

= 31% of EI with taut corner!

Assume $P_{cr}$ = 31% (1900 lbs.) = 590 lbs.

**COMPUTE WIND LOADS TRIBUTARY TO A NODE**
(Nodes spaced at 10 ft.)

Reference: EA1 Standard RS-222-A

$P = .004\ V^2$ for flat surfaces

For cylinders, use 2/3 area

**TABULATE AREAS/10-ft. SECTION:**

| | | |
|---|---|---|
| Spine: 3.33-in. AVE/12 x 10 ft. | = | 2.78 SF |
| Radians: 1.83-in. AVE/12 x 8.66 ft. | = | 1.32 |
| Corners: 3e 3/8 in./12 x 2/3 x 10 ft. | = | .63 |
| Diagonals: 6e 1/4-in./12 x 2/3 x 12 ft. | = | 1.00 |
| Belt: 1/4 in./12 x 2/3 x 8.66 ft. | = | .12 |

TOTAL PROJECTED AREA = 5.84 SF/10-ft. SECTION

**COMPUTE WIND LOADS (c each node):**

$P = .004\ V^2$ (area)

| V | P/NODE |
|---|---|
| 20 mph | 9* |
| 30 mph | 21* |
| 40 mph | 37* |
| 50 mph | 58* |

**WIND ON BICONES PLUS ANTENNA**

Bicones approximately 10 SF (transverse)

1/2 of 2 x 10-5/32 in. guys = $2 \times 10 \times \frac{5}{32} \times \frac{1}{12} \times 350$ ft. $\times\ 1/2 = 45.6$ SF

$\Sigma = 55.6$ SF x 2/3* = 37.1 SF

P c 50 mph = 371 lbs.

**WIND ON GUYS**

6 e 1/4 in. approximately 100-ft. long

1/2 x 6 x 1/4 x 1/12 x 100 x 2/3 = 4.2 SF

P c 50 mph = 42 lbs.

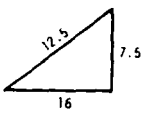


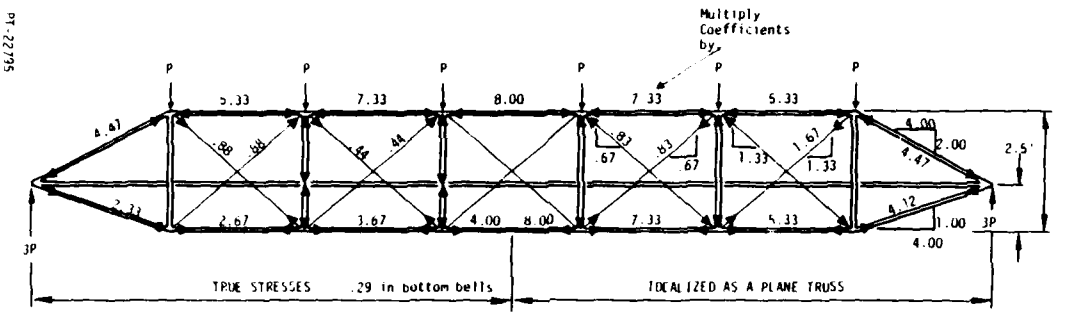


MIDSPAN MOMENT = 3P x 20 ft. = 60P

CHORD FORCES = 60P/7.5 ft. = 8P

ASSUME DIAGONALS SHARE THE SHEAR EQUALLY

**CONVERSION TO TRUE STRESS:**

Bottom chord: 0.5 (ea. of 2)

Diagonals: $1/2 \quad \frac{\sqrt{12.5^2 + 4.33^2}}{12.5} = .529$

End Diag.: $1/2 \quad \frac{\sqrt{10^2 + 2.5^2 + 4.33^2}}{\sqrt{10^2 + 2.5^2}} = .542$

PROJECT IRT TOWER

SHEET NO. 8 OF 13

SUBJECT WIND STRESSES

DES.

JOB NO.

DATE

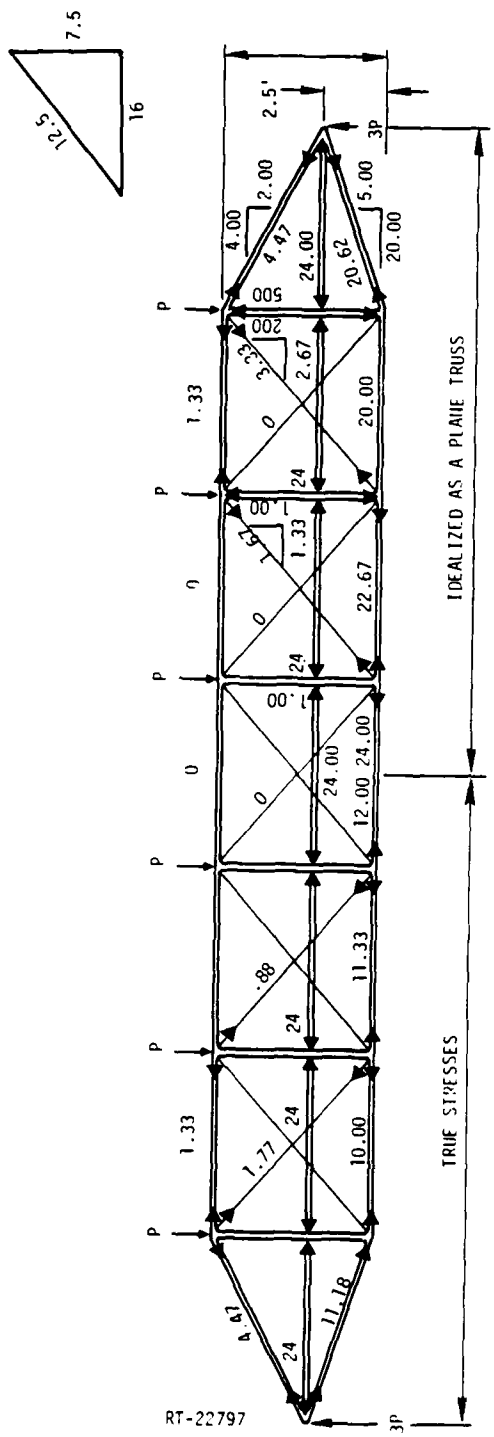

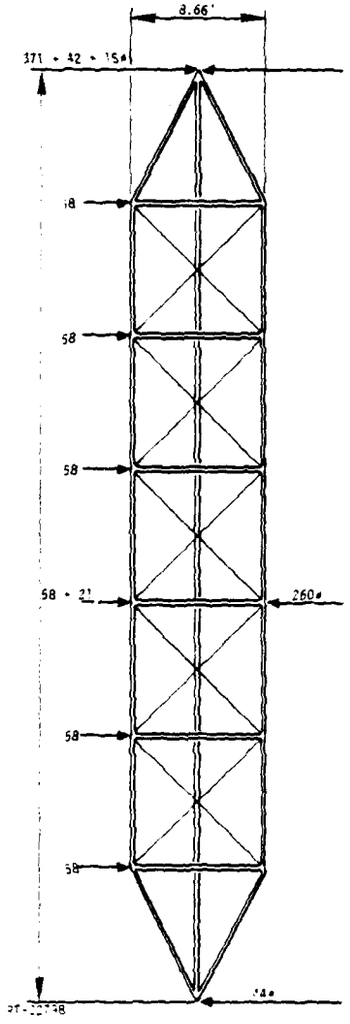


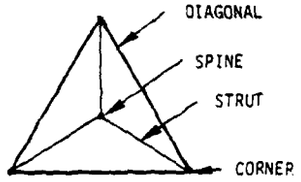


**TABULATE VERTICAL LOADS:**

| AT TOP: | Vertical Component |
|---|---|
| Antenna load | 400 lbs. |
| Increase in antenna tension due to wind | 930 lbs. |
| Guy tension - wind | 493 lbs. |
| Pretension in guys under antenna | 131 lbs. |
| Load @ top: | 1954 lbs. |
| AT 30-ft. HEIGHT: | |
| Guy tension - wind | 111 lbs. |
| Pretension in one guy | 35 lbs. |
| Taper cut | 70 lbs. |
| Total load: | 2170 lbs. |

PROJECT IRT TOWER

SUBJECT RECOMMENDED INSTALLATION

SHEET NO. 10 OF 13

DES. REM

JOB NO.

DATE 5/22/80

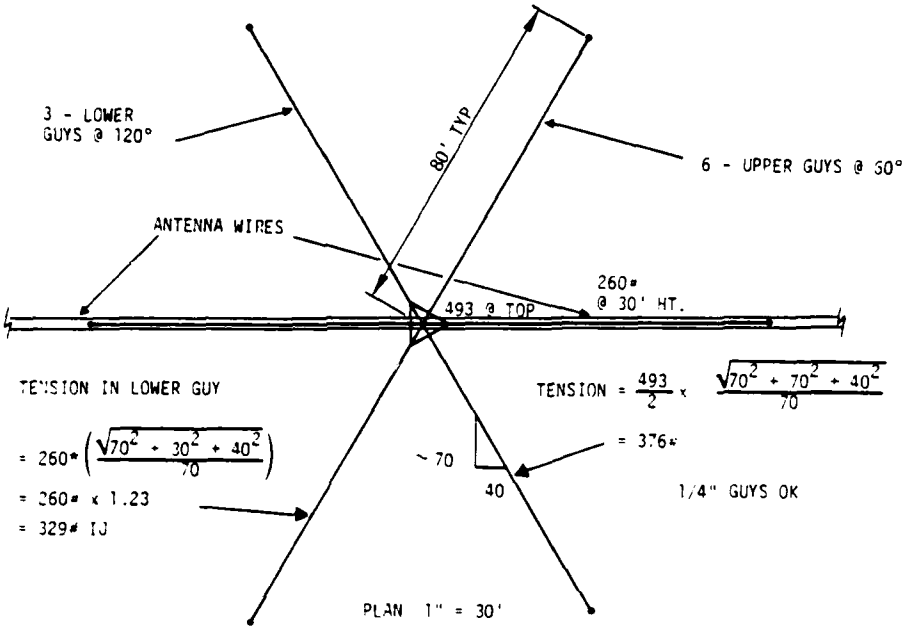


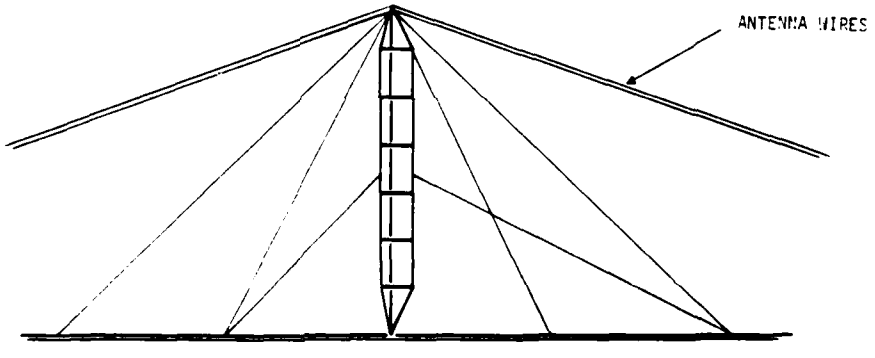


RT-22794

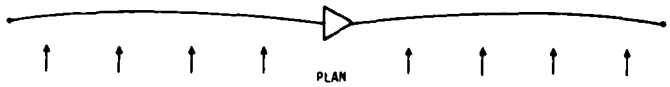


RT-22802

**WIND LOAD ON ANTENNA WIRES =**

10 wires x 5/32 in. x 1/12 ft. x 2/3 (circular) x 10 psi = .87 lbs./ft.

$$M = \frac{WL^2}{8} = .87 \times 350^2/8 = 13{,}292 \text{ ft.}$$

Assume sag = 6 ft.

T = M/6 ft. = 2215 lbs. = 221 lbs./wire = 221/.0192 = 11,500 psi

**CHECK SAG:**

Vertical component = 2215 x .21 x 2 sides = 930 lbs.

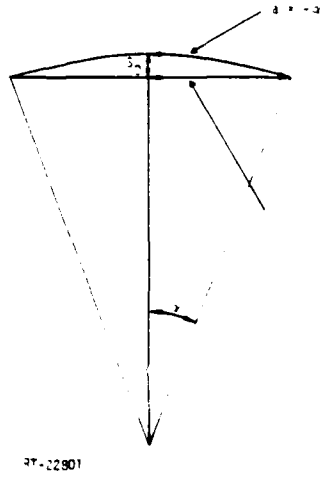

RT-22801

$$\Delta = L_a - L_c = R(\alpha - \sin\alpha)$$

$$\geq R(\alpha - (\alpha - \alpha^3/3^1 + \alpha^5/5^1 \ldots))$$

$$\geq R(\alpha^3/6)$$

but R = $175/\alpha$

$$\Delta = 175/6\,\alpha^2$$

but $\Delta$ = 175 ft. (f/E) = $175 \times \frac{11{,}500}{30{,}000{,}000}$ = .067 ft.

$$\alpha^2 = .067 \times 6/175$$

$$\alpha = .048$$

$$R = 175/.048 = 3649 \text{ ft.}$$

$$S = \frac{L^2}{8R} = \frac{350^2}{8R} = 4.2 \text{ ft.}$$

With inital sag, 6 ft. total sag is reasonable.

## BENDING DUE TO WIND

For intermediate guys, stresses are approximately 1/4 of those for 70-ft. span. Assume pretension to prevent slack corners.

From P.7, maximum corner stress = 1/4(8P) = 2P = 2(58) = 116 lbs.

Assume 150 lbs. pretension/corner

## OVERALL BUCKLING

For 40-ft. unsupported length, $P_e = (70/40)^2$ x for 70-ft. length

$$P_e = (7/4)^2(2398) = 7344 \text{ lbs.}$$

$$P_{cr} = \frac{7344}{1 + 7344/9141}$$ (see page 4)

$$P_{cr} = 4072 \text{ lbs.}$$

$P_c$ top = 1954 lbs.

F.S. = 2.08 ok

## BUCKLING OF NEW 10-ft. SPINE ELEMENT

Try 3/8-in. rods @ 6 in. O to O.

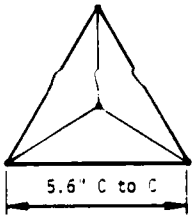


A = .1104

I = $2(.1104)(2.7)^2$ = 1.61 $in^4$ = 4.67 x BXT 6 ft.

$P_{cr}$ = 4.67 x 1346 = 6280 lbs.

P = 2170 lbs. + 600 lbs. due to pretension of corners & diagonals

= 2760 lbs.

F.S. = 2.28 ok

or 5/16-in. rods @ 6-1/2 in. O to O

BT-22305

## APPENDIX C

## PxM ANTENNA ANALYSIS

Fields associated with a Z-directed current element of electric moment $I\ell$ and a current loop which produces a Z-directed magnetic dipole of magnetic moment IS are given by:

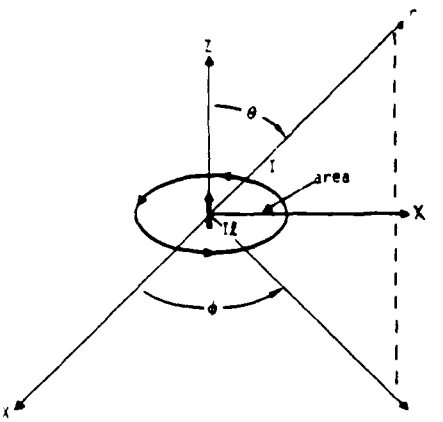


RT-21773

**Figure C-1. A Z-directed electric dipole and a current loop which produces a Z-directed magnetic dipole**

ELECTRIC DIPOLE

$$E_r = \frac{I\ell}{2\pi} e^{-jkr}\left(\frac{\eta}{r^2} + \frac{1}{j\omega\epsilon r^3}\right)\cos\theta$$

$$E_\theta = \frac{I\ell}{4\pi} e^{-jkr}\left(\frac{j\omega\mu}{r} + \frac{\eta}{r^2} + \frac{1}{j\omega\epsilon r^3}\right)\sin\theta$$

$$H_\phi = \frac{I\ell}{4\pi} e^{-jkr}\left(\frac{jk}{r} + \frac{1}{r^2}\right)\sin\theta$$

MAGNETIC DIPOLE

$$H_r = \frac{IS}{2\pi} e^{-jkr}\left(\frac{jk}{r^2} + \frac{1}{r^3}\right)\cos\theta$$

$$H_\theta = \frac{IS}{4\pi} e^{-jkr}\left(\frac{-k^2}{r} + \frac{jk}{r^2} + \frac{1}{r^3}\right)\sin\theta$$

(C.1)

$$E_\phi = \frac{\eta IS}{4\pi} e^{-jkr}\left(\frac{k^2}{r} + \frac{1}{r^2}\right)\sin\theta$$

The magnetic and electric dipole moments can be defined as follows:

$$P_e = \frac{I\ell}{j\omega} \quad \text{and} \quad P_m = \frac{K\ell}{j\omega} \tag{C.2}$$

In order for the current loop to produce the same magnitude fields as a magnetic dipole

$$\frac{K\ell}{j\omega} = \mu IS$$

substituting these expressions into equations C1 gives

ELECTRIC DIOPOLE

$$E_r = \frac{P_e}{2\pi\epsilon} e^{-jkr}\left(\frac{jk}{r^2} + \frac{1}{r^3}\right)\cos\theta$$

$$E_\theta = \frac{P_e}{4\pi\epsilon} e^{-jkr}\left(\frac{-k^2}{r} + \frac{jk}{r^2} + \frac{1}{r^3}\right)\sin\theta$$

$$H_\phi = \frac{cP_e}{4\pi} e^{-jkr}\left(\frac{-k^2}{r} + \frac{jk}{r^2}\right)\sin\theta$$

MAGNETIC DIOPOLE

$$H_r = \frac{P_m}{2\pi\mu} e^{-jkr}\left(\frac{jk}{r^2} + \frac{1}{r^3}\right)\cos\theta$$

$$H_\theta = \frac{PM}{4\pi\mu} e^{-jkr}\left(\frac{-k^2}{r} + \frac{jk}{r^2} + \frac{1}{r^3}\right)\sin\theta$$

$$E_\phi = \frac{cPM}{4\pi} e^{-jkr}\left(\frac{k^2}{r} + \frac{-jk}{r^2}\right)\sin\theta$$

(C.3)

By defining two coordinate system, primed and double-primed, one can take a Z'-directed magnetic dipole (M) and a Z" electric dipole (P) oriented in such a way as to produce TEM fields along the axis defined by PxM when $P_m = yP_e$ (Figure C-2).

If one now takes and locates the electric and magnetic dipoles over an ideal ground plane which is the x-z plane of an unprimed coordinate system, the associated fields can be solved for by using image theory. This situation is depicted in Figure C-3.

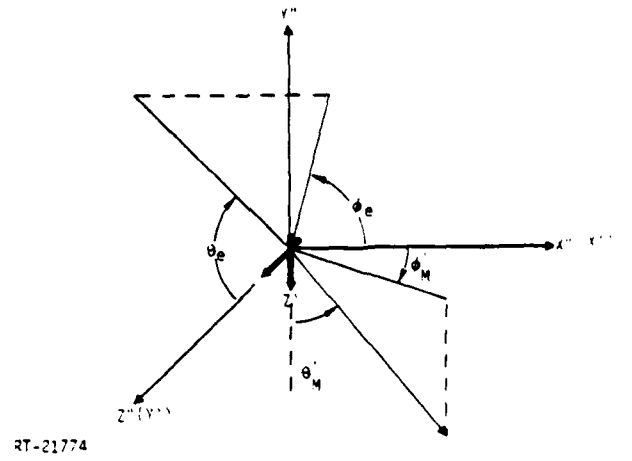


Figure C-2. Z-directed electric and magnetic dipoles in primed and double-primed coordinate system, respectively

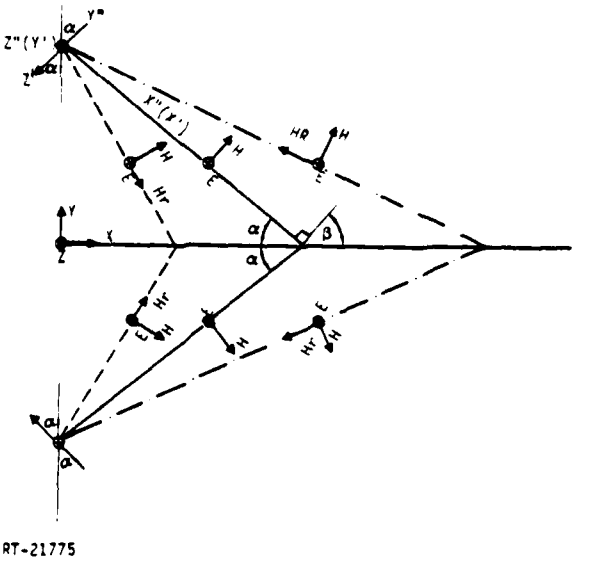


Figure C-3. Side view of electric and magnetic dipoles over an ideal ground plane with the magnetic dipole oriented so that the TEM axis intersects the ground plane

Figure C-4 shows the same situation from a different perspective.

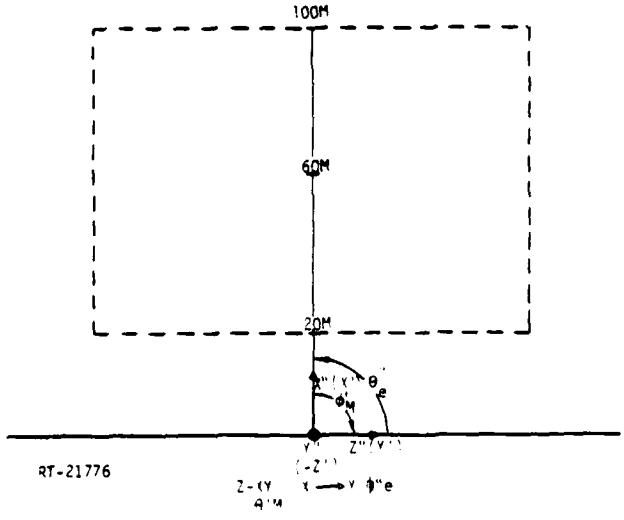


**Figure C-4. Top view of primed and double-primed coordinate system showing relationship to simulation area (represented by dashed lines)**

The relationships between spherical and rectangular coordinates for magnetic dipole and electric dipole H field components are

$$\begin{aligned} H_x'' &= (\sin\theta_m\cos\phi_m)Hr' + (\cos\theta_m\cos\phi_m)H_\theta' + (-\sin\phi_e)H_\phi'' \\ H_y'' &= (-\cos\theta_m)H_r' + (\sin\theta_m)H_\theta' + (\cos\phi_e)H_\phi'' \\ H_z'' &= (\sin\theta_m\sin\phi_m)H_r' + (\cos\theta_m\sin\phi_m)H_\theta'' \ . \end{aligned} \tag{C.4}$$

With the angle relationships between electric and magnetic dipole coordinates

$$\begin{aligned} \phi_e &= \theta_m - 90^o & \theta_m &= \phi_e + 90^0 \\ \theta_e &= (90^o - \phi_m) & \phi_m &= 90^o - \theta_e \end{aligned} \tag{C.5}$$

where the subscript e refers to the electric dipole (double-primed) and the subscript m refers to the magnetic dipole (primed) coordinates.

$$\sin\theta_m = \cos\phi_e \quad \cos\phi_m = +\sin\theta_e \quad \sin\phi_m = \cos\theta_e \quad \cos\theta_m = -\sin\phi_e \tag{C.6}$$

one can express the relationship in electric dipole angles

$$H_x'' = (+\cos\phi_e \sin\theta_e)H_r' + (-\sin\phi_e \sin\theta_e)H_\theta' + (-\sin\phi_e)H\phi'$$
$$H_y'' = (\sin\phi_e)H_r' + (\cos\phi_e)H_\theta' + (\cos\phi_e)H_\phi' \qquad (C.7)$$
$$H_z'' = (\cos\phi_e \cos\theta_e)H_r' + (-\sin\phi_e \cos\theta_e)H_\theta' \ .$$

A low frequency approximation is obtained when $kr \ll 1$ which implies that only the $1/r^3$ terms are significant contributers. Thus, only $H_r'$ and $H_\theta'$ contribute.

$$H_x'' = (+\cos\phi_e \sin\theta_e)H_r' (-\sin\phi_e \sin\theta_e)H_\theta$$
$$H_y'' = (\sin\phi_e)H_r' + (\cos\phi_e)H_\theta \qquad (C.8)$$
$$H_z'' = (\cos\phi_e \cos\theta_e)H_r' + (-\sin\phi_e \cos\theta_e)H_\theta \ .$$

In a similar way, a high frequency approximation is obtained when $kr$ 1 which implies that only $1/r$ terms are significant. Thus $H_\theta'$ and $H_\phi''$ contribute.

$$H_x'' = (-\sin\phi_e \sin\theta_e)H_\theta' - (\sin\phi_e)H_\phi''$$
$$H_y'' = \cos\phi_e H_\theta' + \cos\phi_e H_\phi'' \qquad (C.9)$$
$$H_z'' = -\sin\phi_e \cos\theta_e H_\theta' \ .$$

In order to calculate the low frequency H field, one substitutes from (C.3) into (C.8) using the relationship in (C.6).

The expression (C.10) has been normalized by setup

$$\frac{nP_e}{2\pi\mu} = 1$$

$$H_x'' = \frac{1}{r^3}(-\cos\phi_e \sin\theta_e \sin\phi_e - \sin\phi_e \sin\theta_e \cos\phi_e) = \frac{-1}{r^3}(\sin\theta_e)\sin^2\phi_e$$

$$H_y'' = \frac{1}{r^3}(-\sin^2\phi_e + \cos^2\phi_e) = \frac{1}{r^3}\cos^2\phi_e \qquad (C.10)$$

$$H_z'' = \frac{1}{r^3}(-\cos\phi_e \cos\theta_e \sin\phi_e - \cos\phi_e \sin\theta_e \cos\phi_e) = \frac{-1}{r^3}(\cos\theta_e)\sin^2\phi_e$$

Finally, conversion from the double-primed to the unprimed coordinates can be accomplished with the following relationships

$$\begin{aligned} H_x &= \cos\alpha H_x'' + \sin\alpha H_y'' \\ H_y &= \sin\alpha H_x'' + \cos\alpha H_y'' \\ H_z &= H_z'' \end{aligned} \tag{C.11}$$

When evaluating the total H field at the surface of the ideal ground plane, the following expression applies

$$\begin{aligned} H_{xT} &= 2H_x \\ H_{yT} &= 0 \\ H_{zT} &= 2H_z \end{aligned} \tag{C.12}$$

In a similar way, the high frequency fields can be evaluated by substituting from (C.3) and (C.6) into (C.9). The phase term $e^{-jkr}$ is suppressed since the interest is in peak values. Thus from (C.3)

$$H_\phi'' = \frac{-cP_e k^2}{4\pi} \frac{1}{r} \sin\theta_e \qquad H\theta' = \frac{-P_m k^2}{4\pi\mu} \sin \frac{1}{r}\, m \tag{C.13}$$

noting that

$$c = \frac{1}{\sqrt{\pi\epsilon}} \qquad K = \omega\sqrt{\mu\epsilon}$$

and normalizing as before with

$$\frac{nP_e}{2\pi\mu} = 1$$

one obtains

$$H_\phi'' = \frac{-\omega^2}{2C^2 r} \sin\theta_e \qquad H_\theta' = \frac{-\omega^2}{C^2 r} \sin\theta_m \tag{C.14}$$

AD-A131 291 CW (CONTINUOUS WAVE) ANTENNA DESIGN AND TESTING(U) IRT 2/2
CORP SAN DIEGO CA T BUCKMAN ET AL. 01 AUG 82 DNA-6188F
DNA001-79-C-0210

UNCLASSIFIED F/G 9/5 NL

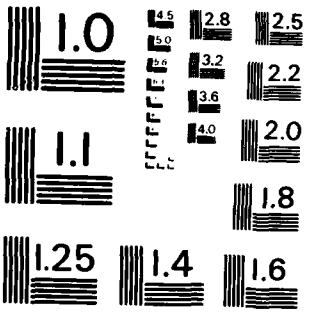


MICROCOPY RESOLUTION TEST CHART
NATIONAL BUREAU OF STANDARDS - 1963 - A

now using (C.6) and (C.9)

$$H_x'' = \frac{\omega^2}{c^2 r} (\sin\phi_e \sin\theta_e \cos\phi_e + \sin\phi_e \sin\theta_e)$$

$$H_y'' = \frac{-\omega^2}{2c^2 r} (\cos\phi_e \cos\phi_e + \cos\phi_e \sin\theta_e) \qquad \text{(C.15)}$$

$$H_z'' = \frac{\omega^2}{c^2 r} (\sin\phi_e \cos\theta_e \cos\phi_e)$$

Conversion and to total H field can be accomplished with (C.11) and (C.12).

An expression for the total incident E field on the TEM axis can be obtained by noting that $E_\phi'$ combines with $E_\theta''$ in the following manner

$$E_\theta'' = \frac{P_e}{4\pi\epsilon}\left(\frac{-k^2}{r} + \frac{1}{r^3} + \frac{jk}{r^2}\right) - \frac{cnP_e}{4\pi}\left(\frac{k^2}{r} - \frac{jk}{r^2}\right) \qquad \text{(C.16)}$$

$$E_\theta'' = \frac{nP_e}{4\pi}\left[\left(\frac{c}{r^3} - \frac{2\omega^2}{cr}\right) + \frac{j2\omega}{r^2}\right]$$

## APPENDIX D

### A SIMPLIFIED ANALYSIS OF LOW FREQUENCY H-FIELD

This Appendix includes a simplified analysis of the low-frequency H-field associated with a hybrid-type antenna. This analysis is conducted only for the Hz component in the y-z plane (Figure D-1).

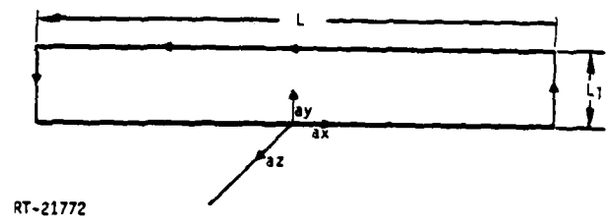


**Figure D-1. Assumed geometry for current filament model of hybrid-type antenna**

The appropriate nonzero magnetic vector potential component is

$$A_x = \frac{I}{4\pi} \int_{+\frac{1}{2}}^{-\frac{1}{2}} \frac{I}{|r-r'|} e^{-jk|r-r'|} dr'$$

Assuming $e^{-jk|r-r'|} \approx 1$ for the quasi-static case and with r in the y-z plane being

$$r = y\hat{a}_y + Z\hat{a}_z$$

and r' being

$$r = \chi\hat{a}_x + L_1\hat{a}_y$$

$$Ax = \frac{I}{4\pi} \int_{+½}^{-½} \frac{dx'}{\nu\chi^2 + (y-L_1)^2 + Z^2}$$

thus,

$$Ax = \frac{I}{4\pi} \left| n(\chi + \sqrt{^2 + (y-L_1)^2 + Z^2} \right|_{½}^{-½}$$

substituting in the limits and noting that

$$H_z = -\frac{\partial A_x}{\partial y}$$

$$H_z = \frac{I}{2\pi} \left[ \frac{(y-L_1)}{(-\frac{L}{2} + \sqrt{\frac{L^2}{4} + L_1^2 + Z^2})(\sqrt{\frac{L^2}{4} + L_1^2 + Z^2})} - \right.$$

$$\left. \frac{(y-L_1)}{(\frac{L}{2} + \sqrt{\frac{L^2}{4} + L_1^2 + Z^2})(\sqrt{\frac{L^2}{4} + L_1^2 + Z^2})} \right]$$

Evaluating the above expression in the z-x plane which is assumed to be an ideal conductor yields, with some rearranging, the final expression

$$H_z = \frac{I}{\pi} \left[ \frac{L_1 L \sqrt{\frac{L^2}{4} + L_1^2 + Z^2}}{(\frac{L^2}{4} + L_1^2 + Z^2)^2 - \frac{L}{2}^2 (\frac{L^2}{4} + l_1^2 + Z^2)} \right]$$

# DISTRIBUTION LIST

## DEPARTMENT OF DEFENSE

Defense Communications Engr Ctr
ATTN: Code R720, C. Stansberry

Defense Nuclear Agcy
ATTN: RAEE
4 cy ATTN: TITL

Defense Tech Info Ctr
12 cy ATTN: DD

Field Command
Defense Nuclear Agcy
ATTN: FCTT, G. Ganong
ATTN: FCTT, W. Summa
ATTN: FCTXE
ATTN: FCPR
ATTN: FCLMC, H. Putnam

## DEPARTMENT OF THE ARMY

Harry Diamond Labs
ATTN: DELHD-NW-EE, 21500
ATTN: DELHD-NW-EB, 21200
ATTN: DELHD-NW-ED, 21400
ATTN: DELHD-NW-E, 21000
ATTN: DELHD-R, 22000
ATTN: DELHD-NW, J. Bombardt, 20000
ATTN: DELHD-TA-L, 81100
ATTN: DELHD-TF
ATTN: DELHD-NW-EA, 21100
ATTN: DELHD-NW-EC, 21300
ATTN: DELHD-TD, 00102
ATTN: DELHD-NW-P, 20240
2 cy ATTN: DELHD-NW-RC, 22300

## DEPARTMENT OF THE NAVY

Naval Surface Wpns Ctr
ATTN: Code F30
ATTN: Code F32, E. Rathbun

## DEPARTMENT OF THE AIR FORCE

Air Force Wpns Lab
ATTN: NTYEE, C. Baum
ATTN: CA
ATTN: NXS
ATTN: NTYEP, W. Page
ATTN: NT
ATTN: SUL

## DEPARTMENT OF DEFENSE CONTRACTORS

Boeing Co
ATTN: Kent Tech Library
ATTN: D. Kemle
ATTN: B. Hanrahan

EG&G Wash Analytical Svcs Ctr, Inc
ATTN: C. Giles

IIT Rsch Institute
ATTN: J. Bridges
ATTN: I. Mindel

IRT Corp
2 cy ATTN: B. Williams
ATTN: N. Rudie
2 cy ATTN: R. Stewart
2 cy ATTN: T. Buckman

Kaman Tempo
ATTN: DASIAC

Pacific-Sierra Rsch Corp
ATTN: H. Brode, Chairman SAGE

R&D Assoc
ATTN: Doc Con
ATTN: W. Karzas
ATTN: P. Haas

Rockwell International Corp
ATTN: D/243-068, 031-CA31
ATTN: V. Michel
ATTN: J. Erb

SRI International
ATTN: A. Whitson
ATTN: E. Vance

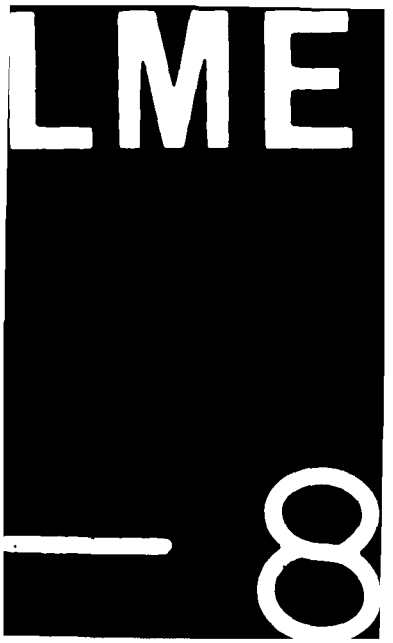
LME
8